IMPROVING MULTIPLEXED RNA DETECTION ASSAYS BY INTERFACING ENZYMATIC AMPLIFICATION STRATEGIES WITH SILICON PHOTONIC MICRORING RESONATORS

BY

RICHARD MARTIN GRAYBILL

DISSERTATION

Submitted in partial fulfillment of the requirements
for the degree of Doctor of Philosophy in Chemistry
in the Graduate College of the
University of Illinois at Urbana-Champaign, 2017

Urbana, Illinois

Doctoral Committee:

Professor Ryan C. Bailey, Chair
Professor Jonathan V. Sweedler
Associate Professor Douglas A. Mitchell
Associate Professor Timothy M. Fan

ABSTRACT:

The ability to make multiplexed measurements has significantly improved our understanding of disease onset and progression. This newfound understanding has the potential to transform clinical diagnostics. Also known as personalized medicine, diagnostic decisions are improved by relying on a detailed knowledge of an individual's biochemical signature. While routine clinical tests detect one biomarker at a time, new technologies are needed that enable the analysis of multiple targets per clinical sample.

This doctoral dissertation presents a platform that can complete these goals by developing assays that combing enzymatic processing steps with silicon photonic microring resonators, a technology pioneered by the Bailey Research Laboratory. While other efforts in lab have been geared to other classes of biomolecules, the developed assays discussed in this dissertation are designed to profile nucleic acid biomarkers in a host of clinically relevant samples. The results from these studies are confirmed using clinical gold standard techniques and compared with findings in the literature to validate the platform.

Chapter 1 discusses how silicon photonic microring resonators fit into the landscape of next-generation multiplexed biomolecular detection platforms while also developing the motivation to use enzymatic processing of nucleic acids to produce ultra-sensitive detection platforms. Chapter 2 gives an exhaustive review of current microRNA (miRNA) detection platforms, both clinical gold standards and emerging technologies. Given the unique detection challenges of microRNAs, this class of RNA molecule was used to develop a detection platform which could then be translated to other RNA molecules. Chapter 3 describes the use of enzymatic processing of miRNA sequences and subsequent on-chip enzymatic signal

enhancement strategy to lower the required input of RNA material to a clinically relevant amount. Chapter 4 outlines further improvements to enzymatic pre-processing of miRNA molecules by interfacing an adapted polymerase chain reaction process with the microring platform to study miRNA expression in glioblastoma patients. It also eliminates the need for on-chip signal amplification. Chapter 5 adapts this workflow and uses it for the detection of long-noncoding RNA (lncRNA) molecules in a previously uncharacterized glioblastoma cell line. Chapter 6 outlines additional research efforts and future directions, which include efforts to build a platform combining enzymatic pre-processing with microring resonator detection and efforts to push into an expanded set of clinical and research applications where low sample inputs and short analysis times are needed.

ACKNOWLEDGEMENTS:

Multiple people deserve thanks for the help they have provided along my journey to obtain a Ph.D. Each of them has helped me overcome numerous hurdles and also been there to celebrate the milestones along the way. My experiences in graduate school would not have been the same without you.

First, I have to thank my advisor, Prof. Ryan Bailey. He has fostered a lab-environment that allowed me to succeed by giving me the freedom to chart my own course on various projects and having a door that was always open whenever questions arose. His mentorship is something I will appreciate long after my days in graduate school are over. Additionally, I would like to thank my doctoral committee members, Professor Tim Fan, Professor Doug Mitchell, and Professor Jonathan Sweedler for their support, mentorship, and conversations over a variety of research collaborations.

Second, I would like to think my fellow lab members in the Bailey Lab, past, present, and honorary: Maria, James, Yi, Heather, Steve, Alex, Jamy, Ellen, Dan, Winnie, Chris, Melinda, Meng, Quique, and Amit. You all helped make those long days and nights in lab worthwhile and enjoyable. It has been a pleasure working with all of you. I would like to especially recognize Chris Para and Maria Cardenosa-Rubio for their help with many of the chapters presented here and the greater efforts of RNA detection in the lab.

My undergraduate research advisors, Drs. John and Sandy Wheeler, have always served as a source of inspiration. You instilled in me scientific curiosity and the perseverance to investigate the unknown. You also gave me the encouragement to always challenge myself and have been a helpful ear as I navigated the decision process of choosing what my next career steps would be.

Lastly, thank you to my family for their love and encouragement, especially my wife Meg. You moved out to Illinois, supported me through all of the late nights and weekends in lab, and weathered a relocation to Michigan alongside me. For that I will always be grateful.

TABLE OF CONTENTS:

Chapter 1

INTRODUCTION TO MULTIPLEXED ANALYSIS AND THE SILICON PHOTONIC MICRORING RESONATOR PLATFORM

1.1 Motivation for Multiplexed Analysis

Personalized, or precision, diagnostics has been fueled by the concept that early detection of disease would benefit patients. This early detection would make tumors easier to resect and treatments more effective. Technological advances enabling the ability to view and understand an individual's biomolecular signatures have revolutionized clinical diagnostics and have begun to make personalized medicine a reality. While the discussion here will be limited to genomics and transcriptomics, the same trends can also be said for protein-based biomarkers as well.[1]

The advent of the polymerase chain reaction in the 1980s gave researchers the ability to analyze genetic differences between multiple samples.[2,3] A couple of years later, scientists took this idea and combined it with the semiconductor industry to create nucleic acid microarrays,[4,5] which, combined with the completion of the Human Genome Project,[6] facilitated gene profiling studies that allowed researchers to compare the genetic differences between healthy individuals with those who developed specific disease states.[7] These discoveries motivated the development of next-generation sequencing technologies, and now we are able to sequence an individual's genome at a cost approaching $1,000.

With the cost of these genetic testing technologies decreasing, the ability to place them in the clinic becomes more and more attainable. However, new technologies are needed to realize the potential of genetic testing in clinical settings. The two clinical gold standards, quantitative polymerase chain reaction (qPCR) and next generation sequencing (NGS), serve two opposite functions. qPCR focuses on the analysis of one target per sample but makes it reasonably easy to analyze the expression of that target from multiple samples. On the other hand, NGS enables the

analysis of all genetic material from a sample, but one cannot analysis multiple patient samples easily. With it becoming clearer that multiplexed panels of 10s-100s of gene targets have the ability to identify predisposition to various disease types[8] and in some instances can better diagnose patients and identify the optimal therapeutic regimens,[9] new technologies are needed the void between the single-plex nature of qPCR and the lower throughput of NGS as shown in Figure 1.1.

1.2 Next Generation Technologies for Meso-plex Diagnostics

Recently, researchers have begun to fill the void by developing meso-plex diagnostic instrumentation. These solutions take form using a variety of transducers to make measurements and have shown moderate success in a host of diseases. In order to be clinically viable, detection platforms must have the following attributes: (1) the ability to profile low sample inputs, (2) good efficiency, (3) easy to use, (4) the ability to multiplex, (5) high degree of reproducibility, and (6) the ability to selectively detect the correct biomolecule.[10] While there are numerous examples in the literature, commonly discussed meso-plex instrumentation can be organized in the following two groupings: solution-phase fluorescent based instrumentation and array based surface-detection methodologies, like nuclear resonance, refractive-index, electrochemistry, etc.

New platforms based on fluorescent transducers take place in many shapes, either focusing on detecting fluorescent beads or fluorescent barcodes functionalized to a recognition biomolecule. In the first case, microparticles are coated with a recognition element, i.e. antibody or complimentary nucleic acid sequence. These coated microparticles are then incubated with a sample of interest and washed. Fluorescent dye functionalized molecules specific to the bound analyte molecules are then added to the sample well and allowed to bind. After another washing

step, this solution is then ready using scanning instrumentation. This technology is being commercialized by Singulex. Initially the scanning instrumentation was similar to that of flow cytometry, but recently they have introduced a second generation technology that can make the measurement straight from the sample well.[11] Additionally, while simple, this technology has limited multiplexing capabilities due to the use of fluorescent dyes. A recent study incorporated multiple excitation lasers to measure the expression of three proteins from a sample volume, but even with this innovation multiplexing capabilities are limited by the spectral overlap of the fluorescent dyes.[12] Figure 1.2 outlines the basic schematic of this technology as well as attempts to multiplex.

A variation to this technique aims to increase multiplexing capabilities and is being commercialized by Luminex. This assay also relies on sandwich assays but increases multiplexing capabilities by using two fluorescent beads. The first bead used to capture the target of interest contains differing concentrations of a fluorescent dye. This bead contains a specific concentration of dye that is related to the capture probe on the surface. Therefore different fluorescent intensities of this dye can be related to a specific capture probe and target, thus enabling multiplexed measurements. After the analytes are allowed to bind, the second fluorescent dye functionalized biomolecule is allowed to bind. This dye is measured by the scanning instrumentation and related to the presence, or concentration, of the target molecule. Figure 1.3 shows the mechanism of detection and sandwich assay formation for proteins and nucleic acids as well as the scanning and detection protocol.

While Luminex makes these measurements in bulk solution, Quanterix has developed a similar platform based on nanowell arrays Here, they use fluorescent magnetic beads to capture specific proteins using a sample dilution where on average there will be at most one analyte

molecule per bead. Following this step, a sandwich assay is formed with an enzyme functionalized antibody after incubation with a sample of interest. The beads are then captured in a nanowell array and an activatable fluorescent substrate is added. If the analyte is present, it is detected via the fluorescent signal of the substrate that is turned over in the presence of the enzyme on the sandwich complex. The scanning instrumentation then determines which analyte is present based on the florescent signal of the bead in the nanowell.[13] Figure 1.4 outlines the detection process as well as shows initial efforts aimed to multiplexed. This is achieved by using a fluorescent-dye functionalized capture bead. The fluorescent signal from the capture bead is this associated with the recognition molecule on the surface and the presence of the activated fluorescent molecule is associated with the target biomolecule.[14]

The last fluorescent platform (commercialized by Nanostring Technologies) also utilizes sandwich assays, but instead of using a concentration gradient like the Luminex platform, conjugates multiple fluorophores together to create a fluorescent barcode specific to each gene (see Figure 1.5).[15] While mainly used for the detection of nucleic acid sequences, this platform has also been adapted for protein expression analysis.[16] While each of the discussed fluorescent assays show respectable figures of merit and facilitate solution phase detection, they either suffer from complex fluorophore conjugation steps, long time to results, poor reproducibility, and inherent limitations in multiplexing capabilities through spectral overlap of fluorescent dyes.

In an effort to avoid the inherent multiplexing challenges of fluorescent moieties, array based technologies have also been engineered to facilitate for multiplexed biomolecular profiling. An example of this type of technology relies on magnetic bead aggregation in the presence on a target biomolecule which induces a shift in the NMR spectrum (commercialized by T2 Biosystems). This assay has been used to quickly determine protein expression in human

tissues[17] as well as determine the phenotype of bacteria in clinical settings,[18] as shown in Figure 1.6. Current generations of this technology match the muliptlexing capabilities of most fluorescent based systems (4-8 targets). Additionally, there are multiple examples of various microarray and modified well plate arrangements that rely on chemiluminescence and electrochemical detection but they will not be discussed here. Most array based technologies suffer from the same drawback that sample volumes need to be aliquoted into different channels or reaction wells for detection because the signal transducer cannot distinguish the differing targets in the same sample volume.

1.3 Introduction to the Theory and Operation of Silicon Photonic Microring Resonators

The Bailey Lab has focused on developing a microresonator-based waveguide sensor platform, part of a larger class of whispering gallery mode sensors,[19,20] for the meso-plex detection of biomolecules, which build upon the shortcomings of previously discussed technologies. First, this planar, array based technology takes advantage of traditional semiconductor fabrication techniques to easily fabricate cost effective sensor arrays with 132 sensors per chip measuring 3 x 4 mm at a scale necessary for eventual clinical placement. Second, with 132 sensors on a sensing chip numerous biomolecules can be studied per sample volume and chips can be run in parallel to easily profile numerous patient samples. Third, this technology detects changes in refractive index to determine solution phase concentration of biomolecules. Refractive index based sensing removes the need to rely on any fluorescent tags or enzymes.

The mechanism of this technology is included in Figure 1.7. To start, a tunable laser is swept through an appropriate spectral window. The laser output is coupled into linear

waveguides via on-chip grating couplers. The light propagates down the waveguides via total internal reflectance. Only specific wavelengths of light couple into the microring structure, as defined by the following equation:

$$m\lambda = 2\pi n_{eff}$$

where m is an integer, λ is the wavelength of light, r is the radius of the ring, and n_{eff} is the effective refractive index of the environment surrounding the sensor. When this resonance condition is not met, all light that is coupled onto the chip then reaches the detector after being coupled off chip via another set of downstream grating couplers. This is reflected by no decrease in the transmission of light as shown in Figure 1.7B. When the resonance condition is met, the specific wavelength is supported by the microring cavity and optical interference occurs between the cavity and the linear waveguide, which prevents the wavelength of light from reaching the detector. This is reflected in a decrease in transmission.

As governed by the equation above, changes in the local refractive index surrounding the microring surface changes the wavelength supported by the microring resonator. This detection platform utilizes this to detect biomolecular binding near the ring surface. When biomolecular binding occurs, the event displaces water which changes n_{eff} and thus the wavelength. The magnitude of biomolecular binding and resulting and shift in resonant wavelength is ultimately related to the solution phase concentration of the biomolecule of interest.

1.4 Introduction RNA Biomarker Detection and Motivation of Thesis Work

The overarching goal of my dissertation work is to develop a multiplexed assay that can detect multiple classes of RNA from clinically relevant samples. While the Bailey Lab has previously developed a universal ultra-sensitive protein detection protocol[21] and is using it in a

host of clinical applications, the same cannot be said for nucleic acids. To date, assays developed in lab have focused on specific RNA types instead of developing an assay for all nucleic acid classes.

The progression of RNA detection over the years has focused on lowering LODs by adding mass tags to the microring surface to amplify the signal response, as summarized in Figure 1.8. In 2010, Qavi et al. were able to detect direct hybridization of four miRNA targets to covalently bound capture probes on the microring resonator surface. This assay took only 15 minutes to complete, but suffered from required total RNA input of 300 μg which precludes its use in the clinic.[22] In 2011, Qavi et al. attempted to increase the sensitivity of the platform by incorporating a way to amplify the signal response after hybridization of the microRNA target.[23] They accomplished this by using an antibody recognizing RNA:DNA heteroduplexes. Upon antibody binding to the miRNA target:DNA capture probe heteroduplex, it significantly increases the mass bound to the sensor surface thus amplifying the original hybridization signal which leads to lower input amounts required. In this case, this signal amplification strategy lowered the input amount from 300 μg to 50 μg, which is still larger than the input required for clinical gold standard techniques where the required input ranges from 1 μg to 1 ng. Similar to the S9.6 strategy, Kindt et al. developed an amplification protocol using streptavidin coated nanoparticles and biotin functionalized chaperone DNA sequences to detect mRNA sequences.[24] This protocol further reduced total RNA requirements to 20 μg, which is still higher than the stated goal of 1 μg or less. Furthermore, these examples provide the proof of concept studies to detect no more than four target sequences per sample.

The overarching goal of my dissertation is three fold (1) to develop a RNA detection assay using input amounts of 1 μg or less, (2) to create an assay that can profile multiple classes

of RNA, and (3) increase multiplexing capabilities of previously established techniques developed in the lab. Progress toward achieving these goals was accomplished by using enzymatic amplification processes, and the following chapters outline the progression. Chapter 2 motivates the need for better technologies to detect microRNAs. Chapters 3 and 4 outline efforts to develop improved microRNA detection protocols. Chapter 5 builds on the work presented in Chapter 4 by utilizing the same detection platform to analyze the expression of long non-coding RNA sequences. Lastly, Chapter 6 outlines avenues of where to take this technology into the future and ultimate placement in the clinic.

1.5 FIGURES

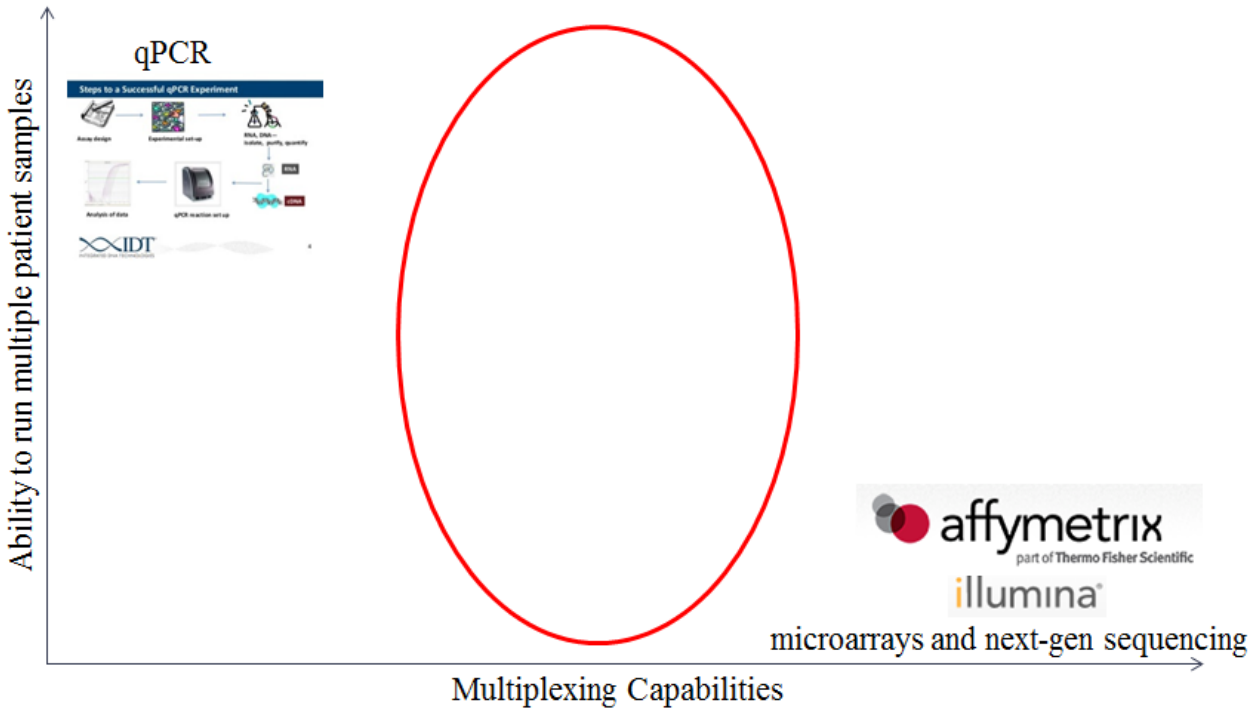

Figure 1.1: Graph showing the void in current technologies. These technologies either focus on analyzing the expression of one biomolecule in multiple samples (qPCR) or on analyzing the expression of all biomolecules present in one sample (microarrays in next-generation sequencing). This void is being filled with novel meso-plex detection methods that are able to detect the expression of multiple biomolecules in multiple samples.

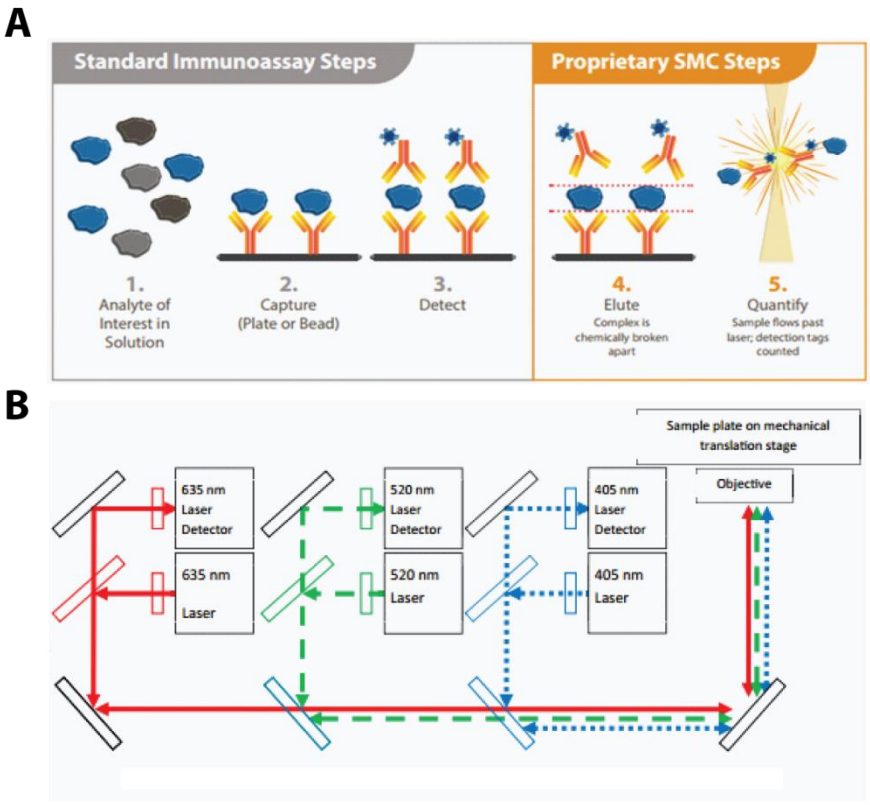

Figure 1.2: Schematic of the Singulex platform.[12] (A) Overview of the detection mechanism, including sandwich assay formation and the solution phase single molecule imaging. Image reproduced from www.singulex.com. (B) Image of the multi-excitation and detection wavelength set up to facilitate multiplexed detection using the Singulex platform. Reproduced from Gilbert, M; Livingston, R.; Felberg, J.; Bishop, J.J. Analytical Biochemistry 2016, 503, 11-20 (ref 12). Copyright 2016 Elsevier.

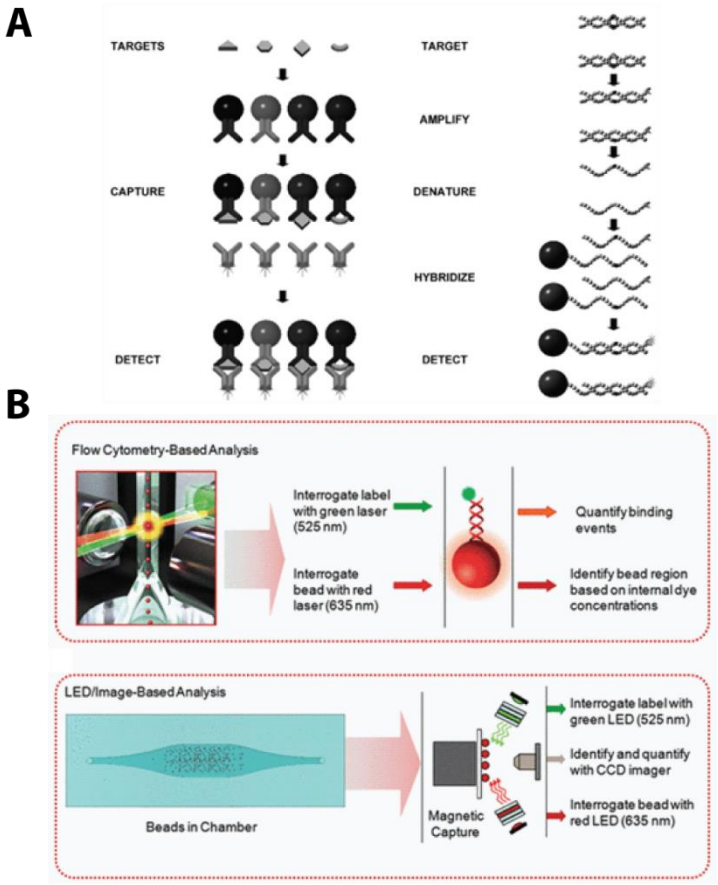

Figure 1.3: Schematic of Luminex platform.[25,26] (A) Mechanism of sandwich assay formation for both protein and nucleic acid targets. The key development of this platform is the use of capture beads with a varying concentration of a fluorophore. Reproduced from Dunbar, S.A.; Vander Zee, C.A.; Oliver, K.G.; Karem, K.L.; Jacobson, J.W. Journal of Microbiological Methods 2003, 53, 245-252 (ref 23). Copyright 2003 Elsevier. (B) Mechanism of target detection. Two fluorophores are imaged, with one related to the specific capture probe used and the other related to the presence or absence of the analyte. Two version of the detection instrumentation are used. Reproduced from Spierings, G. Methods in Molecular Biology 2013, 1015, 115-126 (ref 24). Copyright 2013 Springer.

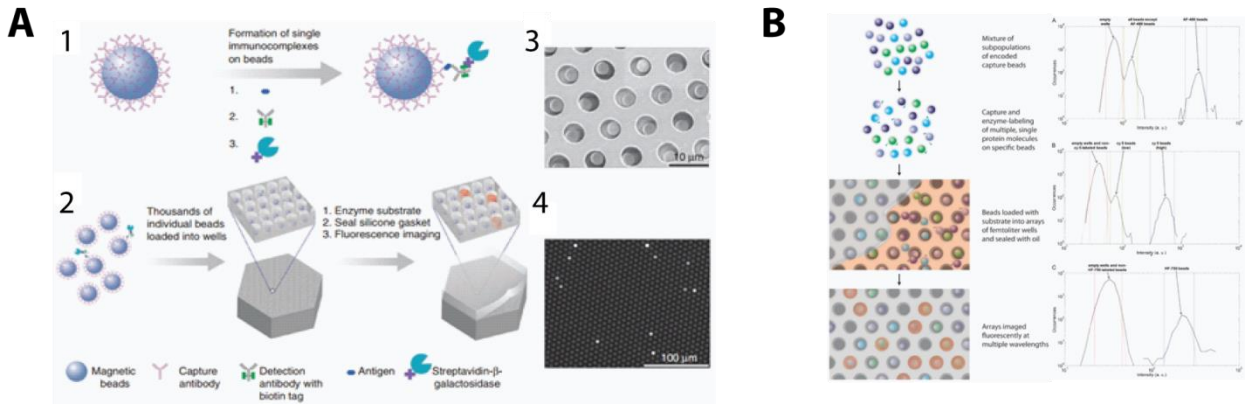

Figure 1.4: Schematic of the Quanterix platform.[13,14] (A) This figure goes through the detection and quantitation of target analytes. Reproduced from Rissin, D.M.; Kan, C.W.; Campbell, T.G.; Howes, S.C.; Fournier, D.R.; Song, L. Nature Biotechnology 2010, 28, 595-599 (ref 13) Copyright 2013 Nature Publishing Group. (B) This image outlines the ability to multiplex by using fluorescent functionalized fluorescent capture beads. Reproduced from Rissin, D.M.; Kan, C.W.; Song, L.; Rivnak, A.J.; Fishburn, M.W.; Shao, Q.; Piech, T.; Ferrell, E.P.; Meyer, R.E.; Campbell, T.G.; Fournier, D.R.; Duffy, D.C. Lab on a Chip 2013, 13, 2902-911 (ref 14). Copyright Royal Society of Chemistry.

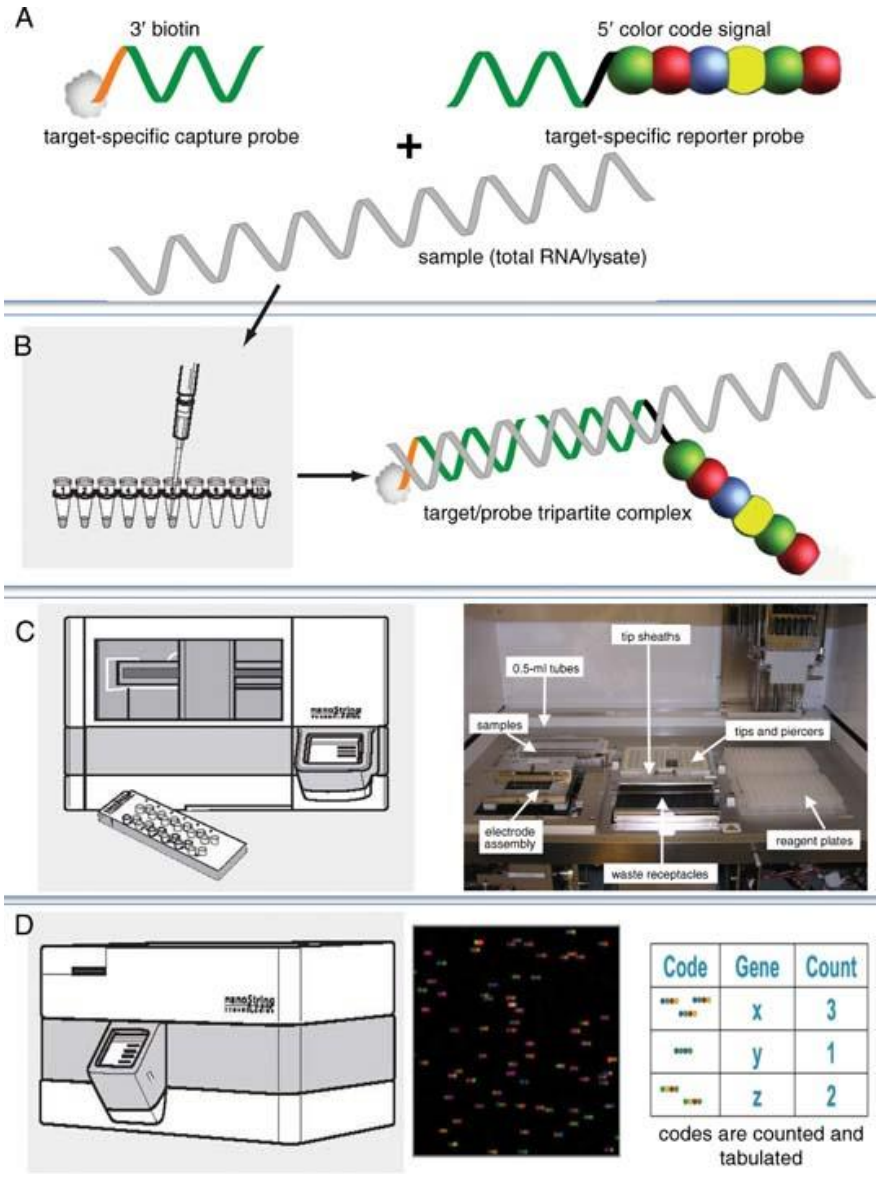

Figure 1.5: Schematic of the Nanostring platform.[15] Key to this schematic is the use of a target-specific fluorescent tag shown in A and B. Reproduced from Kulkarni, M.M. Current Protocols in Molecular Biology, 2011, 94, B.10.1-B.10.25 (ref 15). Copyright 2011 John Wiley & Sons.

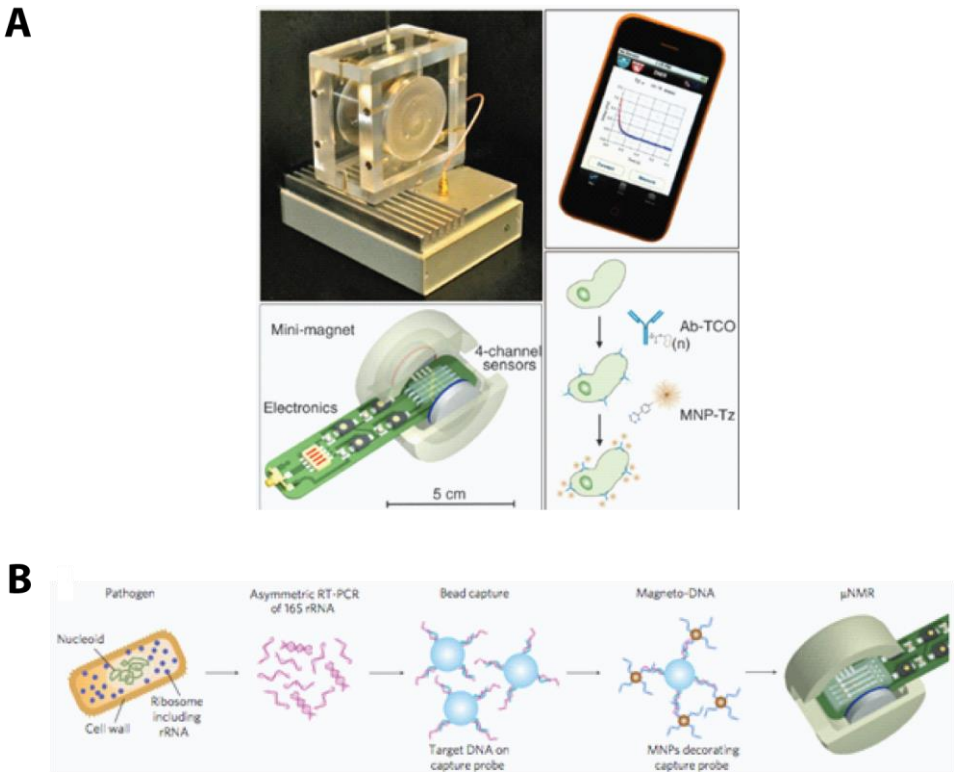

Figure 1.6: Schematic of T2 Biosystems microNMR platform.[17,18] (A) Example of tumor sample analysis using by aggregation of nanoparticles induced by the expression of cell surface proteins. Modest multiplexing capabilities were shown by using four discrete channels within the mini-magnet. Reproduced from Haun, J.B.; Castro, C.M.; Wang, R.; Peterson, V.M.; Marinelli, B.S.; Lee, H.; Weissleder, R. Science Translational Medicine 2011, 3, 1-13 (ref 16). Copyright 2011 American Association for the Advancement of Science. (B) Example of nucleic acid detection based on the aggregation of capture beads and magnetic nanoparticles. Reproduced from Chung, H-J.; Castro, C.M.; Im, H.; Lee, H.; Weissleder, R. Nature Nanotechnology, 2013, 8, 369-375 (ref 17). Copyright 2013 Nature Publishing Group.

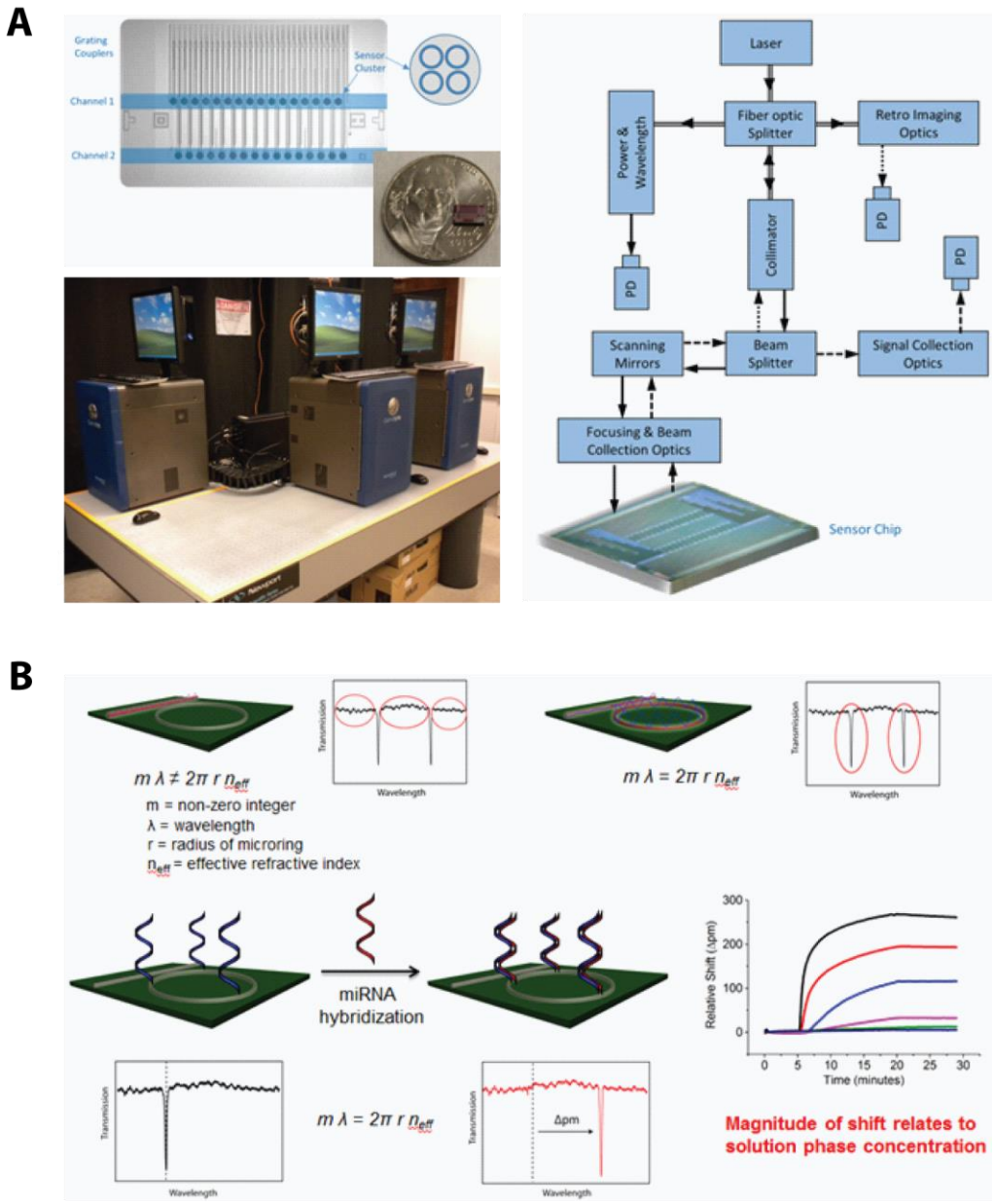

Figure 1.7: Schematic of Genalyte microring resonator detection platform. (A) Renderings of the chip layout, the internal optics of the instrumentation, and the instrumental set up in lab. (B) Outline of the microring resonator detection theory.

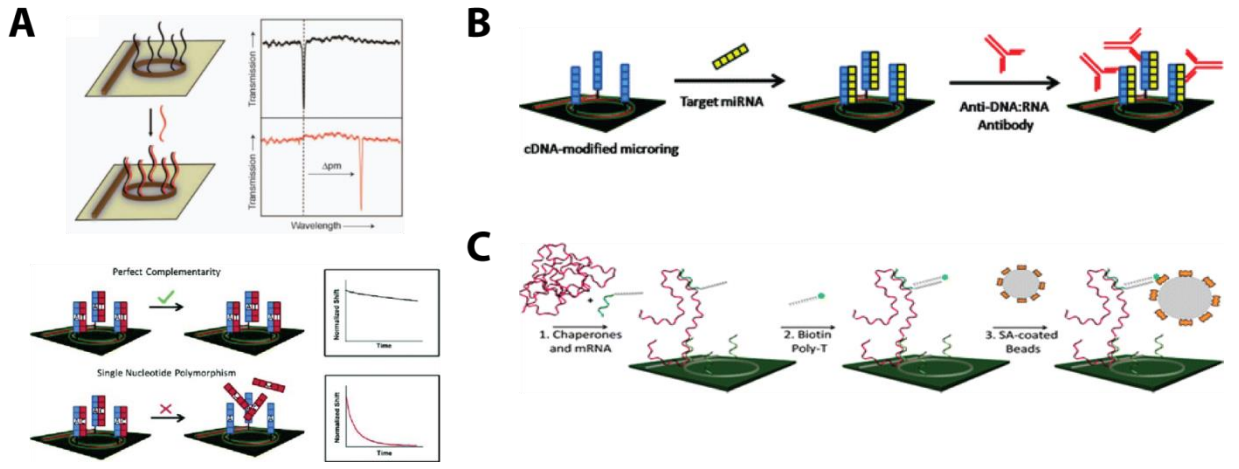

Figure 1.8: Overview of previous RNA detection schemes developed in the Bailey Lab. (A) Label-free, direct detection schemes for DNA and microRNA.[22,27] Reproduced from Qavi, A.J.; Bailey R.C. Angewandte Chemie International Edition 2016, 49, 4608-4611 (ref 20) and Qavi, A.J.; Bailey R.C. Analytical Chemistry 2011, 83, 6827-6833 (ref 25). Copyright 2011 American Chemical Society. (B) Scheme for the detection of microRNA using an antibody as a mass tag to lower limits of detection.[23] Reproduced from Qavi, A.J.; Kindt, J.T.; Bailey R.C. Analytical Chemistry 2011, 83, 5949-5956 (ref 21). Copyright 2011 American Chemical Society. (C) Developed assay for the detection of mRNA using a bead as a mass tag to amplify the microring response and thus lower limits of detection.[24] Reproduced from Kindt, J.T.; Bailey, R.C. Analytical Chemistry 2012, 84, 8067-8074 (ref 22). Copyright 2012 American Chemical Society.

1.6 References

(1) Borrebaeck, C. A. K. *Nat Rev Cancer* **2017**, *advance online publication*.

(2) Scharf, S. J.; Horn, G. T.; Erlich, H. A. *Science* **1986**, *233*, 1076.

(3) Saiki, R. K.; Scharf, S.; Faloona, F.; Mullis, K. B.; Horn, G. T.; Erlich, H. A.; Arnheim, N. *Science* **1985**, *230*, 1350.

(4) Fodor, S. P.; Read, J. L.; Pirrung, M. C.; Stryer, L.; Lu, A. T.; Solas, D. *Science* **1991**, *251*, 767.

(5) Schena, M.; Shalon, D.; Davis, R. W.; Brown, P. O. *Science* **1995**, *270*, 467.

(6) *Nature* **2001**, *409*, 860-921.

(7) Mischel, P. S.; Cloughesy, T. F.; Nelson, S. F. *Nat Rev Neurosci* **2004**, *5*, 782-792.

(8) Domchek, S. M.; Bradbury, A.; Garber, J. E.; Offit, K.; Robson, M. E. *Journal of Clinical Oncology* **2013**, *31*, 1267-1270.

(9) Kris, M. G.; Johnson, B. E.; Berry, L. D.; et al. *JAMA* **2014**, *311*, 1998-2006.

(10) Bhalla, N.; Jolly, P.; Formisano, N.; Estrela, P. *Essays In Biochemistry* **2016**, *60*, 1.

(11) Todd, J.; Freese, B.; Lu, A.; Held, D.; Morey, J.; Livingston, R.; Goix, P. *Clinical Chemistry* **2007**, *53*, 1990.

(12) Gilbert, M.; Livingston, R.; Felberg, J.; Bishop, J. J. *Analytical Biochemistry* **2016**, *503*, 11-20.

(13) Rissin, D. M.; Kan, C. W.; Campbell, T. G.; Howes, S. C.; Fournier, D. R.; Song, L.; Piech, T.; Patel, P. P.; Chang, L.; Rivnak, A. J.; Ferrell, E. P.; Randall, J. D.; Provuncher, G. K.; Walt, D. R.; Duffy, D. C. *Nat Biotech* **2010**, *28*, 595-599.

(14) Rissin, D. M.; Kan, C. W.; Song, L.; Rivnak, A. J.; Fishburn, M. W.; Shao, Q.; Piech, T.; Ferrell, E. P.; Meyer, R. E.; Campbell, T. G.; Fournier, D. R.; Duffy, D. C. *Lab on a Chip* **2013**, *13*, 2902-2911.

(15) Kulkarni, M. M. In *Current Protocols in Molecular Biology*; John Wiley & Sons, Inc., 2001.

(16) Ullal, A. V.; Peterson, V.; Agasti, S. S.; Tuang, S.; Juric, D.; Castro, C. M.; Weissleder, R. *Science Translational Medicine* **2014**, *6*, 219ra219.

(17) Haun, J. B.; Castro, C. M.; Wang, R.; Peterson, V. M.; Marinelli, B. S.; Lee, H.; Weissleder, R. *Science Translational Medicine* **2011**, *3*, 71ra16.

(18) Chung, H. J.; Castro, C. M.; Im, H.; Lee, H.; Weissleder, R. *Nat Nano* **2013**, *8*, 369-375.

(19) Luchansky, M. S.; Bailey, R. C. *Analytical Chemistry* **2012**, *84*, 793-821.

(20) Wade, J. H.; Bailey, R. C. *Annual Review of Analytical Chemistry* **2016**, *9*, 1-25.

(21) Kindt, J. T.; Luchansky, M. S.; Qavi, A. J.; Lee, S.-H.; Bailey, R. C. *Analytical Chemistry* **2013**, *85*, 10653-10657.

(22) Qavi, A. J.; Bailey, R. C. *Angewandte Chemie International Edition* **2010**, *49*, 4608-4611.

(23) Qavi, A. J.; Kindt, J. T.; Gleeson, M. A.; Bailey, R. C. *Analytical Chemistry* **2011**, *83*, 5949-5956.

(24) Kindt, J. T.; Bailey, R. C. *Analytical Chemistry* **2012**, *84*, 8067-8074.

(25) Dunbar, S. A.; Vander Zee, C. A.; Oliver, K. G.; Karem, K. L.; Jacobson, J. W. *Journal of Microbiological Methods* **2003**, *53*, 245-252.

(26) Spierings, G.; Dunbar, S. A. In *Pharmacogenomics: Methods and Protocols*, Innocenti, F.; van Schaik, R. H. N., Eds.; Humana Press: Totowa, NJ, 2013, pp 115-126.

(27) Qavi, A. J.; Mysz, T. M.; Bailey, R. C. *Analytical Chemistry* **2011**, *83*, 6827-6833.

Chapter 2

EMERGING BIOSENSING APPROACHES FOR MICRORNA ANALYSIS

Acknowledgements:

This chapter has been adapted from the review article titled "Emerging Biosensing Approaches for microRNA Analysis" (Graybill, R.M.; Bailey, R.C. *Analytical Chemistry* **2016,** *88*, 431-450), an invited submission as part of the Fundamental and Applied Reviews in Analytical Chemistry 2016 special issue. It has been reproduced here with permission from the American Chemical Society © 2016. Necessary copyrights for all figures in this chapter are noted in the figure captions. In support of this work, I acknowledge financial support from the National Cancer Institute of the Institutes of Health through Grant R33CA1774 and support at UIUC from the NIH National Cancer Institute Alliance for Nanotechnology in Cancer 'Midwest Cancer Nanotechnology Training Center' Grant R25CA154015A.

The original article accessed online at:
http://pubs.acs.org/doi/abs/10.1021/acs.analchem.5b04679

2.1 Introduction

2.1.1 Background and Relevance

Since their discovery more than two decades ago in *C. elegans*,[1] microRNAs (miRNAs) have emerged as an important class of non-protein coding RNA molecules. miRNAs serve as critical gene expression regulators at the transcriptional and post-transcriptional level and are widely conserved across a broad range of animals, plants, and viruses. Landmark studies have associated miRNAs with key biological events like developmental timing in *C. elegans*[2] and zebrafish[3] and cancer development in humans.[4] These studies along with many others that have established miRNA control over numerous biological processes would not have been possible without reliable miRNA detection methods. The impact that these analytical tools have had is reflected in the rapid increase in publications that focus on "miRNA detection", as shown in Figure 2.1. The aim of this review is to outline the current state of the art while also highlighting exciting new biosensing approaches to miRNA detection that might help realize the full potential of miRNA expression profiles in both the contexts of fundamental biology studies and clinical diagnostics.

microRNAs are short, non-coding RNAs that are roughly 22 nucleotides in length. miRNA sequences regulate the expression of mRNA targets with either perfect complementarity, which leads to mRNA degradation, or imperfect complementarity, which often results in repression of translation. While the biogenesis of miRNA has been previously reviewed,[5-7] the basic process of miRNA expression and maturation is outlined in Figure 2.2. The genesis of miRNAs is in the nucleus where primary miRNA transcripts (pri-miRNA) are produced. The pri-miRNA sequence is cleaved by the Drosha-DGCR8 complex to produce a pre-miRNA hairpin.

This precursor hairpin is then transported to the cytoplasm via Exportin-5-Ran-GTP. In the cytoplasm, the Dicer processing complex cleaves the pre-miRNA hairpin to the mature sequence. One strand of the mature miRNA, the guide strand, is loaded into the miRNA-induced silencing complex (RISC), which contains DICER1 and Argonaute proteins, and directs the RISC to target mRNA sequences. This miRNA directed process affects gene expression through mRNA cleavage, translational repression, or deadenylation.[5,6] It is important to note that it is valuable for analytical methodologies to discriminate between pri-, pre-, and mature forms of miRNA sequences.

miRNA regulation ultimately results in altered protein levels and can have profound consequences on cellular homeostasis. In fact, miRNA expression profiling has identified a host of regulated biological processes, including immune response[8], cell differentiation,[9,10] and cell proliferation and death.[11] Furthermore, if the miRNA regulatory machinery that governs these processes is interrupted, it becomes extremely important to identify these disruptions and understand how they evolve as disease drivers. For example, Rosenfeld and co-workers showed how patterns of aberrantly expressed miRNAs could differentiate between tissues of origin across multiple cancer types.[12] Once changes in miRNA expression are better understood in a biological context (i.e. what induces specific upregulation and down regulation patterns), they can then be used as potential therapeutic targets as well as refined into improved diagnostic biomarker panels.[13]

Recent work aimed at understanding how changes in miRNA expression can lead to specific disease states has shown promise. Initial efforts have implicated aberrant miRNA expression with cancer, [14] neurological disorders,[15,16] diabetes,[17] and cardiovascular disease,[18,19] to name just a few. Equally promising is the fact that the detection of these biopanels is not

limited to tissue. A host of studies have shown the ability to detect miRNA biopanels in a variety of biofluids. For example, Weber and co-workers were able to identify meaningful miRNA profiles found in twelve different biofluids, including cerebrospinal fluid, blood, serum, saliva, and urine.[20] As increasing attention is focused on non- or minimally-invasive diagnostic methods, the presence of freely circulating miRNA profiles provides a promising approach to disease monitoring. Other studies have again established disease-correlated miRNA levels in blood;[21,22] however the tools for detection and interpretation of the biological significance of these alterations in expression must still be refined in order to achieve full clinical adoption and translation.

2.1.2 miRNA Profiling Challenges

While the clinical and biological implications of altered miRNA expression are being elucidated, progress remains to be achieved in the development of robust analytical technologies that facilitate routine miRNA analysis. Improved techniques will help realize the impact that miRNA profiling can have on understanding disease onset and progression, and may play a key role in the realization of personalized medicine. In order to provide improved miRNA detection modalities, one must first understand the analytical challenges that miRNA's present and the importance of sample processing and miRNA isolation.

Analytical Challenges

There are many unique characteristics of microRNAs that pose analytical challenges for their accurate detection and quantification. The most important of these characteristics are their small size and thermodynamic considerations, sequence similarity, wide range in abundance, and their ability to regulate multiple targets.[23,24]

The small size of miRNAs presents specific thermodynamic considerations and makes their analysis more difficult than the significantly longer mRNAs. Due to their small length, the GC content variation in miRNA sequences leads to a wide range of melting temperatures (T_m). Since the vast majority of miRNA detection methods rely on some sort of hybridization step, this can introduce sequence-specific bias. Additionally, the small size of miRNAs, roughly the same size a traditional primer, complicates the use of the polymerase chain reaction (PCR).

In addition to thermodynamic constraints, there are additional difficulties that complicate the analysis of miRNAs, as compared to mRNAs, due to the very nature of their seuqence. For example, miRNAs lack the poly(A) tail of mRNAs, which is often used as a universal primer for reverse transcription or selective pre-enrichment. This is especially important as miRNAs make up roughly 0.01% of total RNA extracted from a sample of interest.[25] This means that any bioanalysis platform must be able to differentiate small amounts of miRNA in the presence of a large abundance of total cell RNA. Moreover, the abundance of particular miRNA sequences can vary from single copies to more than 50,000 copies in a single cell,[26] thus requiring exceptional dynamic range. Finally, families of miRNAs are often expressed differing only by single nucleotides and so extremely high sequence selectively is a necessity.

Beyond specificity, selectivity, and large dynamic range, it is also important that analytical methods for miRNA detection allow for multiplexed analysis, whereby levels of more than one miRNA are quantitated simultaneously and from a single sample. This analytical requirement is important on account of the biological mode of action of miRNAs. A single miRNA sequence is capable of regulating up to hundreds of different mRNA sequences and a single mRNA can be targeted by many different miRNAs. Therefore, in order to fully comprehend the biological significance of miRNAs in both health and disease, one must be able

to analyze the ensemble effects of miRNA expression changes and understand the interrelated consequences on multiparametric regulatory networks that extend across all levels of biomolecular information (i.e. DNA, mRNA, miRNA, and proteins). To this end, it is becoming increasingly clear through both experimental results and computational modeling[27,28] that the creation of multiplexed miRNA panels is needed to deconvolute these complex interactions.

Sampling Considerations

It is also worth noting that the reproducibility of experimentally-determined miRNA expression profiles is directly related to the ability to isolate high quality RNA samples. It is possible to isolate miRNAs from cell lines, fresh and formalin fixed paraffin embedded (FFPE) tissue, and various bodily fluids.[20,29] Interestingly, while mRNA often suffer from RNase degradation, particularly in FFPE samples, miRNA have been shown to be more stable.[30,31] Given some of the aforementioned challenges of miRNA analysis compared to mRNAs, the greater stability of miRNAs in a diverse set of sample matrices provides an opportunity to expand their utility through the study of large libraries of archived tissue and blood samples.

Generally, most workflows to isolate RNA from a sample follow the same procedure,[31] using phenol/chloroform purification with chaotrophic salts (i.e. guanidinium thiocynate) to denature RNases and proteins associated with RNAs. After centrifugation, nucleic acids partition into the aqueous and interphase while proteins partition into the organic phase. The RNA from the resulting aqueous phase is then bound to a solid phase silica column and washed. To isolate the small RNA fraction from total RNA, diluted ethanol can be used which will cause large RNAs to dissociate from the silica column and leaves purified small RNAs (<200 nucleotides) in the final elution volume. Finally, the RNA molecules are eluted off the column and analyzed for

purity, using UV-Vis spectroscopy, and integrity, using the band intensity ratio of the 28S to 18S rRNA bands measured using gel or capillary electrophoresis. Low integrity samples containing fragmented RNA suffer from a higher background of small RNA sequences, which then leads to lower quality miRNA profiling data with a higher chance of off-target responses.

2.1.3 Scope

It is clear that miRNAs play incredibly important roles in biology; however, many gains remain in the translation of this fundamental insight into the clinical setting. Key to this achievement will be the development of robust and multiplexed analytical technologies that offer strategic advantages over conventional techniques, such as qRT-PCR, microrarrays, and RNA-sequencing. Motivated by the aforementioned analytical challenges, this review focuses on the recent demonstrations of new microRNA detection platforms, with particular emphases placed on reports published since 2013. At the forefront of promising approaches are advanced biosensor technologies. Beyond a discussion of conventional approaches and emerging techniques, we also provide commentary and perspective regarding the role of bioinformatics in constructing multiplexed miRNA panels, as well as how future advances might impact the clinical adoption of panel-based miRNA diagnostics.

2.2 Conventional Methods

Three major approaches are used at present to determine levels of miRNA expression: (1) reverse transcription-quantitative polymerase chain reaction (qRT-PCR), (2) hybridization-based microarrays and (3) next generation high-throughput sequencing. This section provides details on each as a way of providing context for the development of emerging biosensing technologies.

2.2.1 Quantitative Reverse Transcription-Polymerase Chain Reaction (qRT-PCR)

Quantitative reverse transcription-polymerase chain reaction (qRT-PCR) is the current gold standard for miRNA analysis. It is commonly used to detect levels of single or small, targeted panels of miRNAs and also to validate selected results from more global expression studies (i.e. microarrays and next generation sequencing, as described in subsequent sections). qRT-PCR analysis provides a large dynamic range, inherent sensitivity through the ability of PCR to selectively amplify specific target sequences, lower assay costs compared to next generation sequencing, and the ability to measure multiple miRNAs by running reactions in parallel (normally in 96 or 384 well plates). The major downside to running parallel reactions is higher consumption of the sample of interest, qRT-PCR consumables, and enzymes/master mixes. As mentioned earlier, the short size of miRNAs complicates all PCR-based detection schemes due to similarities between the length of the target and primer. However, two of the more common strategies to achieve this goal are: (1) reverse transcription via stem loop primers and the use of TaqMan PCR, and (2) enzymatic addition of a poly(A) tail to RNAs followed by reverse transcription and SYBR Green based qPCR detection.[30] The overall workflow for both of these qRT-PCR approaches are illustrated in Figure 2.3A.

Stem loop primers are designed to contain a 6-8 nucleotide overhang on the 3' end that is complimentary to a region of the targeted miRNA and can differentiate between closely related sequences as well as different miRNA forms (i.e. pri-, pre-, and mature).[32] Upon hybridization between the stem loop primer and the target miRNA, reverse transcription extends the DNA compliment of the hybridized miRNA from its 3' end. The use of stem loop primers facilitates better specificity by optimizing the melting temperature and effectively lengthens the miRNA target, so that the RT product can then be recognized by a standard PCR primer set. The RT-

extension step is typically performed at temperatures <16°C to preserve the secondary structure of precursor miRNA sequences. PCR amplicons are then generated using a miRNA-specific forward primer that binds to the 3' end of the reverse transcription (RT) product and a universal reverse primer that binds to the conserved stem loop region of all RT products. Additionally, a molecular beacon, or TaqMan, probe is present in the PCR reaction solution and is designed to hybridize in between the forward and reverse primers. As the DNA polymerase proceeds along the template and reaches the TaqMan probe, the probe is hydrolyzed and the fluorescent dye is freed from the quencher, resulting in an emission signal proportional to the total amount of PCR product produced. This signal, measured as a function of cycle number, is then used to determine the overall level of a specific miRNA in a sample.

The poly(A) method involves the 3' polyadenylation of all RNA in a sample normally using either polyadenylate polymerase or T4 ligase. When T4 ligase is used, an additional sequence can be installed following the poly(A) tail that further lengthens the downstream RT product to enable binding of the two PCR primers. After the poly(A) tail addition, binding of a poly(dT) DNA primer, which serves as the reverse transcription primer, initiates the RT reaction and production of cDNA. Conventional PCR primers are then added to initiate amplification, and PCR product formation is measured using a dsDNA-intercalating SYBR green dye.

The main drawback of qRT-PCR is complex primer design requirements and the inability to analyze multiple targets per single sample volume. The design of both RT and PCR primers vary substantially between miRNA targets due to differences in T_m between the resulting primer-target duplexes. However, this problem can be partially alleviated through the use of *Tm*-matched locked nucleic acid primer sequences.[33] It also remains difficult to measure multiple miRNAs from within a single qRT-PCR reaction volume, as qPCR is limited by its reliance on

spectral multiplexing. Run-to-run inconsistencies due to variability in PCR amplification efficiencies is also a complication that requires careful design of internal controls, which often require the use of global mean averaging,[34] referencing common housekeeping genes,[35] the spiking in of non-natural miRNA probes that are added before the RNA extraction step,[36] or some combination of these control methods.[37]

2.2.2 Microarrays

Originally developed in the early 1990s for genomic-scale analysis of DNA, microarrays were redeployed as one of the first methods applied to the global analysis of miRNA expression.[30,38] Typically, miRNAs are first labeled with a fluorescent reporter. This is accomplished by dephosphorylating the 5' end of the miRNA followed by ligation of a fluorescently tagged oligonucleotide or short oligonucleotide strand using T4 ligase. The dephosphorylation of the 5' end is critical to prevent self-circularization of the miRNA and adapter sequences.[39] The functionalized miRNA is then introduced to the array surface where they hybridize to complimentary DNA (cDNA) capture probes immobilized on a glass slide, followed by two channel fluorescent imaging, which can provide expression levels. As a result of being a surface-bound hybridization based assay, microarrays require complimentary base-paring between the cDNA:miRNA. The overall workflow for microarray-based analysis of miRNAs is shown in Figure 2.3B.

Despite the relative ease and historical utility of DNA microarrays, there are some limitations in their application to miRNAs, particularly in light of competing methods.[31] For instance, they are only semi-quantitative due to the absence of a calibration curve from the experimental workflow. As a result, microarrays are best used when comparing miRNA

expression levels between multiple states (i.e. heathy vs. disease). To ensure specificity, microarrays also often require additional validation, which often is achieved via qRT-PCR for select targets of interest. Microarrays also suffer have a smaller dynamic range than both qRT-PCR and next generation sequencing.

Despite these drawbacks, microarrays do offer the advantage of being cheaper than global profiling via next generation sequencing. Additionally, substantial effort has already been invested in the development of T_m-normalized cDNA capture probes that incorporate peptide nucleic acids[40] and locked nucleic acids.[41] The thermal stability of hybridization duplexes across the array can lead to reproducible results and assays with high sensitivity. Other studies have aimed to improve the fluorescent labeling step of the microarray workflow to reduce non-specific background signal. These improvements have focused on the use of labeled binding proteins that only binds to miRNA molecules hybridized at the surface,[42] a hybridization based labeling technique termed stacking-hybridized-universal-tagging (SHUT) that allows for the addition of one universal tag,[43] and a ligase-assisted sandwich hybridization based approach that eliminates the need for miRNA labeling by ligating a signal probe that binds to capture probe:miRNA hybrids at the array surface.[44] The sandwich hybridization based assay improved hybridization efficiency 50,000-fold and allowed quantitation of a synthetic miRNA sequence down to 30 fM. Beyond this limited discussion, other developments in miRNA-detecting microarrays have recently been reviewed.[31,45]

2.2.3 Next-Generation Sequencing

The advent of next generation sequencing (NGS) platforms has enabled a third major approach for miRNA expression profiling, and, with continuing decreases in sequencing cost,

this is quickly becoming a dominant method applied to the analysis of miRNAs. The technologies driving NGS has been reviewed.[46,47] While the procedures vary depending on specific platform, the first step involves the preparation of a small cDNA library from the RNA-containing sample of interest using a reverse transcription process similar to qRT-PCR. Adaptors are ligated to both the 5' and 3' ends of the cDNA products, and the resulting products are attached to either a planar or bead based substrate. This is followed by the massively parallel sequencing of millions of individual cDNA molecules from the library. Bioinformatic analysis of the sequence reads trims the adaptor sequences off of the miRNA sequences. The trimmed sequences are then aligned against a miRNA sequence data base (ex. miRBase) to identify the known miRNAs present in the sample. This sequence data also provides quantification by identifying the number of sequence reads present. Unique to miRNA analysis is the ability for bioinformatic approaches to identify novel miRNA sequences that are not already annotated in miRNA databases by attempting to align to precursor miRNA sequences. This presents a unique set of advantages as well as roadblocks that must be solved to continue to expand the use of next generation sequencing for miRNA profiling. The overall work for the NGS workflow applied to miRNA analysis is outlined in Figure 3.3C.

The major advantage of NGS for miRNA analysis is the ability to obtain a truly global expression profile. In addition to known sequences, which could be detected using a pre-synthesized cDNA microarray, previously unknown short RNA sequences can be discovered *de novo*. Sequencing also obviates the concerns with specificity faced by hybridization-based methods, including qRT-PCR, microarrays, and the majority of the biosensor-based approaches described below. To gain clinical traction, overall sequencing costs, including reagents, still need

to be driven down further. Also, streamlined informatics techniques are needed to simplify and/or automate data analysis for use in clinical settings.

The quality of using NGS for miRNA expression profiling in clinical samples has been analyzed in recent publications that compare the results obtained using RNA-sequencing to both qRT-PCR and microarrays.[48,49] One study found discrepancies between platforms that were attributed to differences in normalization protocols as well as potential sampling biases.[48] The other, though, revealed strong correlation between RNA-seq and qRT-PCR.[49] This report also showed good correlation between expression levels from flash-frozen and FFPE samples, which is important for analysis of current and archived clinical samples. Additional studies validating RNA-seq and other conventional analysis methods are important and needed to help put into perspective the vast literature reporting miRNA expression results obtained by different platforms and, ideally, may result in the identification of clinically-useful miRNA based tests.

Given the breadth of expression data provided by NGS-based miRNA analysis it is reasonable to consider that most of the resulting information will not be informative in the context of human health and disease. Moreover, an infomatically-robust panel of miRNAs might be extracted from global data sets and correlated with different diagnostic or prognostic outcomes.[50,51] Therefore, the workflow by which RNA-seq can be used to identify and translate multiplexed miRNA panels to cost effective biosensing technologies remains an important goal. Once promising panels of miRNAs are proposed, cheaper and less time consuming technologies might be a better fit for high throughput analyses, as well as eventual use in the clinical setting. Going forward, NGS will, if it has not already, become the preferred technique for global miRNA expression profiling and novel sequence identification that establishes correlations with

disease. Subpanels may then be informatically-selected and then validated and translated to the clinic using the emerging technologies described in the following section.

2.2.4 Summary of Conventional miRNA Analysis Methods

qRT-PCR, microarrays, and next generation sequencing have all played key roles in advancing our knowledge as to how miRNAs play key roles in regulating gene expression and in beginning to translate this fundamental insight to application in clinical diagnostics. A high level comparison of the attributes of each of these general classes of techniques is presented in Table 2.1. However, these technologies face critical hurdles to achieve widespread clinical adoption that justify the development of emerging biosensing technologies. qRT-PCR methods are incredibly sensitive, relatively rapid, and cost effective; however they can only measure levels of one miRNA per assay, thus requiring multiple sample aliquots to profile a panel of targets, which is prohibitive for sample-limited specimens. Microarrays are exceptionally well-suited to multiplexed analyses, but are typically slow, less sensitive, and minimally-quantitative. Next generation sequencing technologies are also well-suited to give a global analysis of all miRNAs present in a sample, but require complex processing steps, an even longer time-to-result, and can present challenges with back end informatics. Therefore, there exists a pressing need for the development of multiplex diagnostic capabilities whereby focused panels of 10s of miRNAs can be simultaneously interrogated using rapid, cost effective, and highly scalable technologies. Such technologies would have broad-reaching utility in both basic and clinical research and be applicable to both tissue and biofluid-based diagnostic applications.

2.3 Biosensor Methods

miRNAs have been a focus of biosensor development over the past decade, with many micro- and nanoscale sensing technologies being applied to this class of analytes. Benefits of many of these schemes lie in their potential for diagnostics at the point of care. However, it is important to point out that for many diagnostic needs, analyses performed in a central laboratory over the multi-hour-to-day timeframe are completely acceptable for many applications, such as in the diagnostic or longitudinal monitoring of relatively slowly progressing diseases, such as cancer. Coupled with these devices have been a number of novel signal transducers, incorporation of modified nucleic acid capture sequences, and the development of new signal amplification strategies. The past few years have shown a movement away from proof-of-principle technology demonstrations and an increasing emphasis on obtaining the sensitivity and sequence selectivity required for clinical applications. A number of reports have also explored low levels of multiplexing; however, most of these studies only analyze 2-3 sequences at a time. Here, we focus broadly on some of the most recent reports considering promising optical, electrochemical/electrical, and magnetoresistive technologies for miRNA detection, emphasizing improvements to analytical sensitivity and selectivity and highlighting some of the more promising demonstrations of multiplexing.

2.3.1 Optical Detection

A wide range of optical detection methods have been applied to miRNA detection. Fluorescent dyes and quantum dots directly conjugated to nucleic acids detection probes have been widely explored in FRET-based analyses and also coupled with enzymatic methods for enhanced performance. In these examples, multiplexing must typically be achieved spectrally,

which places some constraints on the number of sequences that can be simultaneously assayed. Electrochemiluminescent assays have also been developed that offer promising enzyme- and nucleic acid-based signal enhancement strategies. Surface-tethered optical methods based on plasmons or waveguide properties promise higher levels of multiplexing through the creation of spatially-resolved sensor arrays, but th ese measurements are constrained to binding on sensor surfaces.

FRET and related approaches

To improve upon microarrays, which most commonly require labeling of the miRNA before detection, fluorescent assays today aim to use fluorescent reporters that bind to the miRNA target via a detection probe. To provide the appropriate specificity, strategies have been designed to ensure that the fluorescent signal is "off" with no miRNA signal is present and "on" when the target is present. Forster resonance energy transfer (FRET) is a common approach to facilitate "on/off" detection schemes. An overview of different FRET-based miRNA detection methods is provided in Figure 3.4.

A simple, but effective, FRET approach used a DNA strand-displacement scheme, where fluorescently tagged DNA capture probes were initially hybridized with a quencher functionalized compliment. When present, the target miRNA displaced the quenching strand and turned "on" the fluorescent signal. This approach was used to detect the presence of 3 miRNA sequences across multiple cell lines with an LOD of 1 fM and a dynamic range of 4 orders of magnitude.[52] Despite its simplicity, the main drawback of this approach is the false positive rate, whereby closely related species might displace the quenching strand giving an erroneous result.

Molecular beacons aim to improve specificity by incorporating a fluorescent tag on one end of the sequence and a fluorescent quencher on the other, thus creating a FRET pair on a single capture sequence. With no miRNA present, the strand adopts a thermodynamically stable hairpin geometry with the fluorophore in close proximity to the quenching molecule. Upon hybridization of a target miRNA, the beacon linearizes, causing separation of the fluorophore and quencher and turning "on" the fluorescence.[53] The opposite scheme has also been developed where a molecular beacon was created that was initially held "open" via an interaction with a reporter sequence that featured multiple base pair mismatches. In this case, the fluorophore and quencher started off spatially separate, and the presence of the miRNA of interest displaced, allowing the beacon to fold on itself turning "off" the fluorescent signal.[54] This simplified assay took only could be run in as little as 10 minutes and achieved better specificity by using locked nucleic acid detection strands. However, the limit of detection (LOD) was limited to 10 nM. Greater multiplexing capabilities of this molecular beacon-FRET approach were achieved with quantum dots, due to their increased brightness and inherent color tunability. Here, three miRNAs were detected in diluted serum without the need for any washing steps, and a LOD of 1 nM was reported.[55]

While the aforementioned molecular beacon approaches achieved nanomolar LODs, different FRET pairs have shown improved assay performance. Graphene oxide was used as a quencher, where fluorescently tagged miRNA compliments were absorbed onto the surface.[56] In the presence of the miRNA target, the capture probe was released and hybridized with the target, generating a fluorescent signal. Further improvements to specificity were made by incorporating peptide nucleic acids into the molecular beacon sequence absorbed onto the graphene oxide surface.[57] Improved performance was also achieved by using DNA probes that were

approximately three times larger than the miRNA target, thus offering a higher affinity for adsorption onto the substrate and effectively eliminating non-specific desorption of the fluorescent nucleic acid sequence.[58] The target binds a region of the capture probe and an exonuclease cleaves the DNA:miRNA hybrid from the quenching substrate turning "on" the fluorescent signal. LODs as low as 3 fM were reported; however, multiplexing capabilities were not investigated.

While the simplicity of FRET based assays provide many advantages for *in vitro* diagnostics, they also can facilitate the quantitative profiling of miRNA expression in vivo. For example, a duplex DNA FRET probe was used to detect the intracellular presence of miRNA-294, a marker for neuronal cell differentiation,[59] and a molecular beacon approach allowed for imaging of miRNA-126 as a general marker for ischemia.[53] Another interesting development involved a single stranded FRET probe that was delivered into cells, where it bound to the complimentary miRNA, and was loaded into the RISC complex. The FRET probe was then hydrolyzed and liberated the fluorescent reporter, allowing the detection of miR-10b, a metastatic marker associated with breast cancer.[60] Ryoo, et.al. described an approach with graphene oxide as the quenching substrate used to simultaneously detect the presence of 3 miRNA in living cells.[61] A similar approach employed carbon nitride nanosheets as a quencher.[62] While these devices are able to identify the presence of miRNA targets in living cells, these workflows ultimately suffer from poor sensitivity and a limited dynamic range.

The aforementioned FRET-based strategies were stoichiometric, that is a single miRNA molecule led to a single fluorophore being turned "on" or "off". In order to achieve better signal gain, several target recycling strategies have been reported by which a single miRNA can lead to

the generation of fluorophore signals per sequence. Several promising target recycling strategies are highlighted schematically in Figure 3.5.

Duplex-specific nuclease (DSN), and enzyme that recognizes and selectively cleaves the DNA strand from a DNA:miRNA duplex was employed to detect miRNA, resulting in the release of either a fluorophore or a DNA strand to induce a detectable signal. After cleavage of the DNA, the miRNA is free to bind to another DNA capture sequence and the DSN process is repeated. In this way, a single miRNA strand can interact with thousands of reporter sequences giving high levels of signal gain. This general strategy has been broadly incorporated into a wide variety of optical detection assays, including a fluorescently-tagged molecular beacons,[63] DNAzyme capture probes,[64] graphene oxide quenching assays,[65] WS_2 quenching assays,[66] magnetic beads,[67] gold nanoparticle quenching assays,[68] and gold nanoparticle aggregation assays.[69] A great example showing the potential of the DSN assay was shown by Yin and co-workers, who designed a simple FRET-based strategy that allowed three miRNA sequences to be simultaneously detected down to 1 fM across a dynamic range close to 5 orders of magnitude.[70]

Other target regeneration strategies utilized toehold-mediated recycling and nickase based recycling. In both of these approaches, after target recycling the capture probes are introduced to the sample of interest and when the miRNA is present it either linearizes upon hybridization[71] or dissociates from a quenching substrate.[72] These techniques eliminate the need for fluorescent dye conjugated directly capture probes by staining the hybrid product with an intercalating fluorescent dye. This strategy achieved picomolar detection limits and a dynamic range of 3-4 orders of magnitude. The nickase based strategy immobilized the target miRNA on a graphene oxide substrate to protect from RNases. A stem loop primer was then introduced and hybridized with the miRNA target, which caused desorption of the miRNA from the graphene

oxide. Exponential amplification was then achieved in the presence of a DNA polymerase through target recycling using a nicking enzyme. The resulting dsDNA products were stained with an intercalating fluorescent dye. The intercalating dye approach has the advantage of having multiple fluorescent dyes per target rather than only a single fluorophore conjugated to a single capture probe, giving a LOD of 11 fM and 3 order of magnitude dynamic range.[73] Of course the limitation of the intercalating dye approach is that the dye will stain any nucleic acid duplex without the sequence specificity that can be engineered using covalently attached fluorophores conjugated to specific strands. Another nickase based recycling approach relied on the formation of a three way junction consisting of the target miRNA sequence, an assistant DNA probe, and an Hg^{2+} intercalated molecular beacon. Upon complex formation, the intercalated Hg^{2+} was liberated and able to quench the fluorescent signal from the linearized molecular beacon.[74] This approach gave a detection limit of detection of 0.16 nM and a dynamic range of 3 orders of magnitude.

Electrochemiluminescence

Like fluorescence, electorchemiluminescence (ECL) can be used to produce a detectable optical signal that is proportional to the miRNA concentration in a sample. ECL is an alternative approach to lamp or laser based excitation, where an electrochemical excitation can create a luminescent response in the presence of an ECL reporter molecule. This flexible excitation approach, which generally turns "on" response, does not require the use of specific wavelength lasers to selectively excite a fluorescent dye. Additionally, these approaches often show exquisite sensitivity due to the elimination of background fluorescent interfering species in solution. As an example of an ECL-based approach to detect miRNAs, a sandwich hybridization approach was successfully used to profile a single miRNA in three cell lines.[75] Without any sample recycling

or signal amplification, this strategy produced an LOD of 100 pM and a dynamic range of approximately 3 orders of magnitude. While these numbers are respectable, signal amplification strategies can be invoked to further increase limits of detection, improve specificity, and extend dynamic range.

Variations of the hybridization chain reaction and enzymatic amplification can both be utilized for eletrochemiluminescent signal amplification. The hybridization chain reaction allows for a dramatic increase in dsDNA length that is catalyzed in the presence of a target miRNA. This allows for various ECL co-reactants, such as $[Ru(phen)_3]^{2+}$ [76] and hemin-conjugated DNAzymes,[77] to intercalate into the resulting duplex. The LODs for these techniques were 1 and 1.7 fM, respectively, with linear dynamic range of 4 orders of magnitude.

Enzymatic amplification strategies have been deployed using rolling circle amplification to form DNAzymes,[78] cyclic exponential amplification recycling,[79] doxorubicin conjugated quantum dots,[80] T7 exonuclease recycling and downstream silver deposition,[81] ECL quenching via Phi29 DNA polymerase mediated strand displacement,[82] and a dual target amplification strategy with combined ECL and fluorescence detection.[83] With one exception, all of these strategies report LODs ranging between 10 fM and 100s of aM with dyamic ranges varying 2-5 orders of magnitude. The stand displacement system reported a remarkable detection limit of 3.3 aM and a dynamic range of 5 order of magnitude.[82] Importantly, none of these examples demonstrated multiplexing capacity, likely in part due to the fact that ECL reporter molecules are not specific to an individual miRNA sequence, similar to that described above for the intercalating dye systems.

Plasmonic and Photonic Approaches

While fluorescence based detection has the benefit of enabling detection in free-solution, it is ultimately limited by the fact that a label is required for detection. Likewise, there are a fixed number of labels (i.e. fluorescent dyes or FRET pairs) that are easily detected with unique, non-overlapping signatures, which limits multiplexing capabilities. Additionally, it is often difficult remove excess fluorescent reporter sequences from solution if a FRET pair is not used, creating a large amount of background signal. In the case of electrochemiluminescence, multiplexing capabilities are difficult due to the need for multi-electrode arrays that can require unique potentiostatic control, and the fact that many ECL reporter molecules are not specific to an individual miRNA sequence. As alternatives that capture the spatial multiplexing features of traditional microarrays, methods that detect surface-hybridization through changes in optical properties, such as refractive index in the case of surface plasmon resonance (SPR) and other approaches, have grown in popularity. These techniques can often be operated in label-free sensing modes or combined with different enhancement strategies to further improve analytical performance metrics.

In addition to established label free detection modalities, such as conventional Kretschmann geometry surface plasmon resonance[84], other sensing mechanisms have been explored for applications in miRNA analysis, including nano-particle scattering on flexible silicon substrates,[85] surface enhanced Raman spectroscopy,[86] functionalized gold nanoprisims attached to silanized glass,[87] Mach-Zehender interferometers,[88] and total internal fluorescence microscopy.[89] An impressive gold nanowire plasmonic based detection mechanism was developed as a microfluidic lateral flow assay. A detection limit of 100 aM was achieved for a bi-temperature sandwich based hybridization scheme. The cDNA-modified gold nanowire was incubated at a low temperature to ensure specific base pairing with a target miRNA in solution,

followed by an elevated temperature exposure to a LNA functionalized presenting a Cy5 moiety that was detected via its surface-enhanced Raman scattering signal.[90] This strategy showed the multiplexing capacity to detect 4 miRNAs simultaneously over a dynamic range of six orders of magnitude. A schematic representation of this detection method is shown in in Figure 2.6A.

Additional label free miRNA sensors aimed to improve upon previously outlined weaknesses. For instance, to avoid diffusion limitations experienced by surface based measurement modalities, a solution-based stem loop primer-functionalized plasmonic nanoparticle aggregation assay was developed. Upon hybridization of the target, the plasmon resonance shifts due to a change in distance between nanoparticles in the aggregate. The magnitude of this shift can then be related to the solution phase concentration.[91] The LOD of this assay is 10s of fM; however, the dynamic range was limited to a single order of magnitude.

In an effort to achieve point-of-care miRNA detection, Gao and co-authors developed a lateral flow nanoparticle aggregation assay. Hybridization of a miRNA to cDNA-modified particles produced a visual colorimetric change on account of nanoparticle aggregation in less than 20 minutes.[92] To increase sensitivity, a next generation sensor was developed that used nanoparticles conjugated to horseradish peroxidase that, in a subsequent step, catalyzed the oxidation of TMB to produce a blue product. This amplification step improved the limit of detection from 60 pM to 7.5 pM.[93] A potential drawback is the lack of multiplexing capabilities as different targets would require parallel detection using separate devices or channels.

Techniques like traditional Kretschmann geometry SPR and SPR imaging have previously been applied to the detection of miRNAs; however, when operated in label-free assays, limits of detection are only modest, as the small size of a captured miRNA does not cause

a large change in refractive index at the sensor surface. To improve upon these detection limits, several label-included signal amplification strategies have been developed. Many of these approaches involve a high mass recognition element that can recognize and bind directly to the cDNA:miRNA duplex at the sensor surface. A simple example is that of Vaisocherova and coworkers, where a DNA functionalized nanoparticle recognized half of a miRNA sequence where the other half will be bound to an SPR sensor, forming a conventional sandwich complex. Using this approach, illustrated in Figure 2.6B, they demonstrated a 4-plex assay for miRNA detection in cell lysate with a LOD of 0.5 pM.[94] Another approach used biotin-streptavidin interactions to engender a 24-fold increase in detection sensitivity.[95] Lastly, an alternative method used DSN and monitored the decrease in signal over time as the cDNA strand was displaced from the surface. Importantly, the miRNA released from the SPR chip surface can rebind to other cDNAs thereby effectively recycling the target. This assay gave a detection limit of 3 fM and could differentiate miR-21 concentrations in total RNA solutions extracted from the blood of a variety of cancer patients.[96]

Two notable non-plasmonic, photonic detection technologies have also recently shown promise for miRNA analysis. Cunningham and co-workers have pioneered the development photonic crystals for biosensing applications and have demonstrated their applicability to the detection of miRNAs. Photonic crystals were engineered to enhance the fluorescence signal of tagged miRNA sequences hybridized to a cDNA capture probes on the sensor surface.[97] Due to the localization of the electric field the fluorophores experience during excitation and enhanced signal extraction of the fluorophore emission through coupling to modes of the photonic crystal, signal gains of more than 8,000 were reported. This sensor was used to quantitate the expression of miRNA-21 and achieved a 0.1 pM LOD. It is also interesting that the ability to quantitate

both miRNA and proteins using the same sensing modality. In attempts to cut down the volume needed to complete analysis, the fluorescence enhanced photonic crystal approach was adapted to a submicron fluid channel.[98] This hybridization based assay was dependent on miRNAs binding with molecular beacons functionalized at the photonic crystal surface. Using the narrower channel geometry, only 20 nL of sample was needed to complete analysis.

Silicon photonic microring resonators have also been demonstrated for the detection of miRNAs, [99] [100] as well as full length mRNAs.[101] A simple detection scheme was developed by monitoring direct hybridization of miRNA targets to DNA capture probes on the photonic ring resonator surface.[99] The binding event caused a change in refractive index, which, in turn, created a detectable change in resonant wavelength that can be related to the concentration of the target of interest. Using this approach, it took ten minutes to simultaneously profile four miRNAs, and an LOD of 2 nM was reached. To improve the sensing attributes of the platform, a RNA:DNA heteroduplex specific antibody, S9.6, was used.[100] After miRNA:DNA capture probe hybridization, the antibody was introduce to the sensor surface and allowed to bind. The added mass of the antibody at the sensor surface caused a larger shift in the resonance wavelength due to a larger change in the refractive index close to the sensor surface. This resulted in improvements to the LOD of over 2 orders of magnitude (10 pM) and a dynamic range over 4 orders of magnitude. Impressively, this assay was able to quantitate four miRNA simultaneously from total RNA isolated from mouse brain tissue.

2.3.2 Electrochemical Detection

Electrochemical sensors are well-established for a number of classes of target analytes, and obvious successes, such as the portable glucose meter, have established their capabilities for

simple, rapid, and low cost bioanalysis. Not surprisingly, there has been considerable growth in the area of electrochemical biosensors for miRNA. Given the requirement for making measurements at a solid electrode, electrochemical miRNA biosensors are typically based on hybridization at the electrode surface, and similar to plasmonic and photonic optical sensors, can be operated in label free and label-enhanced assay formats. As discussed below, detection is commonly achieved through the measurement of a redox signal or a change in capacitance or impedance.

Label-free approaches to electrochemical detection

Label free detection assays are the simpliest electrochemical measurement schemes, relying only upon target hybridization to a surface-bound capture probe. An example of this strategy involved a novel carbon nanofiber functionalized screen printed electrode functionalized with a capture probe having electrochemically-inactive inosine in place of guanine. Hybridization of the miRNA target then generated a detectable guanine oxidation peak that was measured using differential pulse voltammetry with a detection limit of 1.5 μM.[102] However, in comparison with other techniques, the sensitivity of this assay can be greatly improved.

Alternative electrode materials have resulted in significantly improved sensitivity. For instance, a RNA duplex specific binding protein, p19, was immobilized on an electrode surface and only when an RNA duplex was present was a signal due to tryptophan oxidation detected. The LOD of this assay was reported at 160 nM.[103] Carbon nanotube functionalized glassy carbon electrodes were used to increase guanine oxidation current density by a factor of ~3 over conventional glassy carbon electrodes, achieving a LOD of 1 pM.[104] Another method involved using a quinone based conducting polymer as a redox transducer on a functionalized electrode

surface. Differential currents were detected based on the orientation of the DNA capture probe—collapsed on the surface in the absence of the target, yet linear and lifted off the electrode when hybridized to the target miRNA, allowing for more efficient diffusion of counter-ions to the surface. Here, the electrode material had a large influence on the sensitivity, where an LOD of 650 fM was obtained using a glassy carbon electrode[105] and 8 fM for a carbon nanotube functionalized electrode.[106] Using a similar diffusion based mechanism, a Pd-nanoparticle functionalized electrode was used and changes in the ability of H_2O_2 to diffuse to the electrode surface was measured. When the miRNA was present, it effectively prohibited diffusion in a concentration dependent manner. A detection limit of 1.7 pM can be achieved using this method.[107] Additionally, these techniques show an extended dynamic ranging from 3-5 orders of magnitude.

Labeling with electroactive tags

Another approach to detect hybridization events is to label the miRNA:capture probe duplex with an electroactive species to yield a detectable signal. This was achieved by introducing copper ions to the hybrid which electrostatically interact with the negative nucleic acid backbone and catalyze the turnover of ascorbate.[108] Similar approaches used methylene blue as a label.[109] Methylene blue has a higher affinity for ssDNA versus miRNA hybrids. miRNA binding therefore decreased the electrochemical for methylene blue, as detected via voltammetry. The limits of detection for these approaches were reported as 8.2 fM and 0.5 fM, respectively.

A further improvement is to directly label the miRNA:capture probe duplexes with either electroactive or catalytic labels. For example, aptamer based capture probes have been designed to bind HRP only when the miRNA is present. This approach offered picomolar LODs, but

suffered from the poor specificity of the aptamer sequence.[110] Specificity was improved by using a miRNA:DNA specific antibody, S9.6, which, as illustrated in Figure 2.7A, could then be bound by an ALP-modified IgG antibody and used to achieve a LOD of 0.4 fM.[111] Another approach involved ferrocene-boronic acid modified gold nanoparticles, where the boronic acid could form a covalent bond with the ribose sugar of the miRNA bound at the electrode surface. The electrochemical signal from the ferrocene group was then detected using differential pulse voltammetry to give a miRNA detection limit of 1 nM.[112]

Sandwich hybridization based assays have also been shown to facilitate the addition of electroactive species, where a functionalized reporter DNA sequence hybridizes to a DNA capture probe only in the presence of the miRNA target. This approach had the benefit of facilitating the use of a wide variety of reporter tags and electroactive labels. Methylene blue (MB) labeled reporter sequences were designed to bind with the capture probe as well as additional helper sequences to allow the binding of 4 MB molecules per miRNA sequence. An LOD of 100 fM was reported using this assay, coined Sens^{Q}, and multiplexing capabilities were demonstrated by the simultaneous quantitation of 3 miRNAs.[113] The mechanism of this promising detection platform is shown in Figure 2.7B.

Another approach utilized amino-functionalized reporter detection probes covalently bound to apoferritin-encapsulated copper nanoparticles. Hybridization of the target miRNA led to a pH shift at the electrode, resulting in the release of copper ions from the nanoparticles, which were detected with a LOD of 3.5 fM and a linear range spanning from 0.01 to 10 pM.[114] This assay was further modified using streptavidin functionalized reporter sequences to effectively bind multiple apoferritin nanoparticles per reporter strand due to the fact that streptavidin molecules can bind multiple biotins. Trypsase was used to digest the nanoparticles

and induce Cu release, and the multivalent streptavidin linkage improved the detection limit by a factor of 10—down to 0.35 fM, with a corresponding improvement in dynamic range.[115]

Biotinylated reporter probes were also used to bind with ALP functionalized streptavidin to provide 0.4 pM LODs and a linear range from 1 pM to 100 nM.[116] A similar approach using digoxin functionalized reporter sequences to bind with a HRP-functionalized anti-digoxin antibody claimed a LOD of 0.79 fM with a seven order of magnitude dynamic range. The key innovation of the digoxin based assay that leads to large improvement in sensitivity was the use of a Au and Ag modified dendrimer-chitosan-graphene composite electrode.[117] The largest sensitivity enhancements were seen using biotinylated reporter sequences to bind with streptavidin functionalized titanium phosphate nanospheres that have incorporated Cd^{2+} ions. After binding of the nanospheres to the miRNA:capture probe duplex, $[Ru(NH_3)_6]^{3+}$ electrostatically interacted with the nucleic acid backbone and served as an electron carrier between the electrode surface and the nanosphere. The electrochemical response of Cd^{2+} was then used to quantify the presence of miRNA sequences. Impressively, this workflow reaches an LOD of 0.76 aM with linear range spanning seven orders.[118] This impressive detection strategy is shown in Figure 2.7C.

Redox cycling reactions have also been developed in an attempt to provide high sensitivity miRNA detection. These labeling approaches seek to eliminate diffusion limitations in solution using mercaptophenylboronic acid,[119] APBA[120] and DNAzyme[121] functionalized gold nanoparticles. Despite promise, these early efforts did not show performance metric improvements over the previously discussed electroactive tagging approaches.

Signal amplification via conjugation of multiple electroactive reporters

The small size of miRNA typically means that the sequence can only be covalently tagged with a single label. Similar to that described above for optical methods, target recycling methods can be employed to generate larger per-target electrochemical signals through either the hybridization chain reactions or enzymatic lengthening processing. Particularly effective strategies in this vein are highlighted in Figure 2.8.

Enzyme free miRNA recycling techniques, such as mismatch catalytic hairpin assemblies that convert one miRNA molecule into a DNA duplex[122] and toehold mediated strand displacement reactions[123] have been interfaced with electrochemical detection to reach limits of detection of 0.6 pM and 1.4 fM, respectively. Sensitivities of the catalyzed hairpin assembly were improved 3-fold using TiO_2 nanoparticles and redox cycling.[124] Enzymatic recycling can also be achieved using double-stranded nuclease[125] and T7 exonuclease,[126] where LODs were 1 fM and 0.17 fM, respectively. Significant improvements in sensitivity were when LNA G-quaduplex-hemin DNAzymes were located in close proximity to the electrode surface. As the target miRNA target bound, it was degraded by double stranded nuclease making the DNAzyme more accessible to hemin binding and signal amplification. This gave an impressive detection limit of 8 aM; however, the linear range reported was prohibitively narrow.[127]

Hybridization chain reactions are another amplification technique that do not require enzymatic processing yet can provide signal gain by improving accessibility for signal reporter molecules to intercalate between base pairs. Studies have used this workflow with $[Ru(NH_3)_6]^{3+}$ as an intercalating agent to achieve a six order of magnitude dynamic range and an LOD of 100 aM.[128] Li and co-workers were able to combine multiple p19 proteins on a magnetic bead and use a hybridization chain reaction mechanism using novel DSA molecules as signal reporters reporting a detection limit of 6 aM.[129] Unfortunately, this assay is only linear over one order of

magnitude. Target recycling via RNaseA was also combined with the hybridization chain reaction using GC rich sequences that allow for enhanced DNAzyme activity resulting in a LOD of 100 fM with a dynamic range of over 5 orders of magnitude.[130]

Other methodologies have combined DNA lengthening and target recycling amplification techniques. For example, catalyzed hairpin assembly and hybridization chain reaction were combined with a methylene blue-based read-out,[131] and a nicking enzyme and DNA polymerase were utilized to amplify the miRNA target before a hybridization cascade using stem loop primers, which facilitated silver nanocluster association.[132] Unfortunately, the limit of detection in both cases was higher than other electrochemical detection based systems, most likely due to the off target response of closely related miRNA species.[131] Both assays reported dynamic ranges of 5 orders of magnitude.

Additional enzymatic amplification approaches have also been investigated using a variety of DNA polymerase processing approaches. A simple approach used DNA polymerase to add biotinylated nucleotides as the miRNA strand was elongated to facilitate downstream streptavidin conjugated gold nanoparticle association and signal amplification. This provided a LOD of 99.2 fM and a dynamic range of four orders of magnitude. [133] An alternative approach used strand displacement amplification, enabled by a nicking enzyme and DNA polymerase, followed by sandwich hybridization of the capture probe, the amplification product, and then a biotinylated reporter sequence to bind to streptavidin-HRP conjugates. Using this approach an LOD of 40 pM is achieved with a dynamic range of 2 orders of magnitude.[134] A third strategy relied on rolling circle amplification to lengthen a DNA sequence through the production of thousands of repeated sequences. This added sequence was used to conjugate redox probes[135] or to prevent diffusion of electroactive species from the electrode surface,[136] resulting in LODs of

100 fM and 1.2 fM and dynamic ranges of 4 and 2 order of magnitudes, respectively. Isothermal exponential amplification reaction (EXPAR) has also been explored via sandwich hybridization of the EXPAR product and a biotinylated reporter for ALP amplification[137] or DNAzyme formation.[138]

Lastly, an emerging method, shown in Figure 9A, used design rules from DNA nanotechnology to improve the orientation of capture probes at the surface, thereby mitigating the negative consequences of poor sterics of the electroactive labeling species and reducing and non-specific binding to the electrode surface. This general approach method was utilized in several different assay formats, including a sandwich hybridization assay,[139] a target recycling process using a silver nanoparticle functionalized signal probe,[140] a rolling circle amplification process,[141] and with a hybridization chain reaction scheme.[142] The LODs for these respective assays were 1 fM, 0.4 fM, 50 aM, and 10 aM respectively. Additionally, dynamic ranges spanned between 4-6 orders of magnitude. These results underscore how rational surface functionalization can have a profound effect on the ultimate performance of the sensor.

Electrochemical impedance

Electrochemical impedance is another electrochemical property that can be measured in a way to reflect the presence of a targeted miRNA sequence. Strategies to induce a change in charge transfer include the enzymatic turnover of an insulating polymer via DNAzymes,[143] hemin conjugated carboxylic graphene[144] and DNAzyme functionalized gold nanoparticles.[145] These assays reported detection limits ranging from 100s of aM to 10 of fM LODs with dynamic ranges of 1.5, 3.5, and 4.5 orders, respectively. The assay that shows the largest gain to sensitivity and specificity of any label addition method is based on a three part impedance

system and developed by Labib and coworkers.[146] Here, the first step of the assay was to measure the hybridization event of the target miRNA and RNA capture probe. If the signal could not be detected, the p19 RNA binding protein, which is specific to small 21-23 bp RNA duplex via electrostatic and hydrogen bonding interactions between the β-sheet formed by the p19 homodimer and the sugar-phosphate backbone of the dsRNA, was used to amplify the impedance signal. Lastly, a DNA compliment could be added to induce the disassociation of the p19 protein from the electrode signal to further amplify the signal. All three steps form a "three-mode" electrochemical sensor, and each "mode" had a different linear range that together allowed quantitative detection between 10 aM and 1 μM. This multi-step assay is highlighted in Figure 2.9B. Because of the non-specific nature of the p19 protein, multiplexing must be achieved by splitting the sample into separate volumes; however, the team reported a 3 plex assay in total RNA and validated the results with qPCR.

Magnetic bead-enhanced electrochemical detection

Mass transfer limits are significant hurdles to ultrasensitive target detection. An appealing general approach to circumvent these Langmurian limitations is to use magnetic beads that can diffuse quickly through solution to capture targets of interest, but then be localized onto the surface of a detection element using an external magnetic field. This approach has been widely exploited as a method of sample pre-concentration for a range of analyte classes in both label and label free measurement strategies. Below are several examples where magnetic beads were combined with electrochemical-based read out schemes.

Using a similar inosine-substituted capture probe as described above, arrays of screen printed electrodes were used in combination with magnetic beads to enable multiplexed

measurement of miRNAs with increased sensitivity. After pre-concentration with magnetic beads, an alkaline treatment released the duplexes from the beads where they are then absorbed on graphite screen printed electrodes and guanine oxidation is measured. Multiplexing capabilities were shown by running three reactions in parallel with a limit of detection of 143 nM.[147] A different iteration of this workflow incubated miRNA solutions with Os(VI)bipy, which electrostatically associates to the miRNA. Magnetic beads with complimentary DNA capture probes were then used to capture target miRNA. The labeled target miRNA were thermally released and quantitated using the peak current detected from the Os label using a mercury drop electrode.[148] The main drawback of this strategy this the limited dynamic range that covers approximately 1 order of magnitude. Additionally, redox cycling can improve specificity and extend dynamic range. Workflows have been presented that are dependent on the ligation of a magnetic bead functionalized capture probe and a biotinylated reporter sequence. Conjugation of SA-ALP to the complex catalyzes the production of an electroactive species, 1-naphthol. The supernatant of this process is collected and introduced to a separate electrode, where the concentration of 1-napthol is measured through redox cycling. The LOD was reported to be 3.55 fM and a dynamic range of 4 orders of magnitude.[149]

Magnetic moieties and electrodes have also been employed in tandem. For example, magnetic beads were used to detect biotinylated duplex specific nuclease products. In the presence of the target miRNA, the biotinylated probe was fully digested; however, in the absence of target, it was left intact. These products were absorbed onto a streptavidin coated magnetic bead and pulled down to a magnetic electrode, where an impedance measurement was made. The fully digested probes give lower impedance values compared to the intact capture probes that have a high charge density. This workflow resulted in an LOD of 60 aM and a dynamic range of

2 orders of magnitude.[150] An alternative approach uses branching magnetic beads that hybridize to multiple miRNA targets through the formation of Y junctions. As a result of this branching, multiple HRP moieties could bind to the y junctions, and when pulled down to the electrode surface, could give a LOD of 0.22 aM and a four order of magnitude dynamic range.[151]

An additional approach immobilizes the RNA duplex specific protein, p19, on magnetic beads and uses it as a capture probe for biotinylated RNA capture probe:miRNA hybrids following streptavidin-HRP conjugation. This complex was then pulled down to the electrode where a detectable catalytic current was measured giving a 40 pM LOD.[152] However, the approximately 1 order of magnitude is limiting for many applications. The ultimate limit of this p19-based detection approach results from the nanomolar affinity of the RNA duplex:p19 interaction, as a higher affinity would yield lower limits of detection. Lastly, a DNA ligase-dependent sandwich hybridization/redox amplification strategy was reported having a gold nanocluster-ALP complex functionalized to a sequence-specific reporter. After ligation to the MB in the presence of the miRNA, the gold nanocluster-ALP complex catalyzed the production of silver nanoclusters which absorbed onto the bound DNA strand. The resulting product was then brought to the surface via a magnetic electrode and the silver content quantitated. The limit of detection using this approach is 21.5 aM with a dynamic range of 3 orders of magnitude.[153]

2.3.3 Field Effect Transistors

Field effect transistors (FETs) are an attractive class of sensors from the perspective of potentially low-cost devices that have high sensitivity to binding-induced changes in charge near the sensor surface. FETs have the added advantage of being easy to fabricate arrays of sensors, which enables facile multiplexing capabilities. The sensing mechanism of FETs is illustrated in

Figure 2.9C. Recent efforts have aimed at demonstrating the versatility of this transducer through the use of CMOS-compatible silicon nanowire transistors,[154] gold nanoparticle functionalized graphene FETs,[155] and p19 functionalized FETs,[156] with LODs of 0.13 fM, 10 fM, and 1 aM, respectively. The main drawback of this assay is the shallow sensing depth in solution, which is limited by the Debye length. This precludes the use of many labeling or strand extension techniques as they will occur outside the sensing window.

2.4 Perspectives

Since their discovery in the 1990s, our understanding of miRNAs has unraveled a new layer of regulatory control over gene expression in organisms. As the importance of miRNAs has become clearer, the number of platforms available to analyze these molecules has grown. Initially efforts focused on applying and modifying traditional techniques from molecular biology to allow for the analysis of miRNAs. For example, the creation of stem loop primers and new enzymatic methods that facilitated qRT-PCR and microarrays to be applied to this class of small RNAs. These techniques were essential to early breakthroughs; however, they are now being replaced with new workflows that offer greater coverage of global expression changes, as evidenced by the rapid gains in next generation sequencing.

While RNA sequencing will continue to be a valuable tool for discovery and fundamental studies, emerging biosensor technologies are posed to play a role in translating basic biomolecular insights into the clinic. The last few years have seen tremendous growth in this area. Optical and electrochemical biosensors have been prominent for decades, but recent improvements in sensitivity, dynamic range, time to result, and surface functionalization have rendered them amenable to miRNA analysis. Novel materials and reagents, such as metallic

nanoparticles, semiconductor quantum dots, and intercalating small molecule fluorescent dyes, as well as advantageous electrical and optical properties of innovative micro- and nanostructures continue to open up new opportunities, resulting in detection limits down to aM levels and dynamic ranges spanning seven orders of magnitude. Additionally, these measurements have been made in a wide array of biofluids with minimal, if any, sample pre-treatment, greatly simplifying the analytical workflows compared to existing gold standard techniques from molecular biology. Armed with these and other new detection methodologies, the analytical community is now poised to shift attention from sensor development to deployment where the ultimate successes will be judged by the ability to make meaningful impacts in the clinical space.

2.4.1 Future Improvements

While emerging techniques have shown tremendous improvements in sensitivity, specificity, and dynamic range, advances are needed on several fronts in order for the ultimate potential of these technologies to be realized. More attention needs to be given to make these assays capable of making multiplexed measurements. Moreover, the development of disease-relevant diagnostics will only be achieved through coupling with bioinformaticians to parse global expression profiles into clinically-actionable biomarker panels

Challenges with multiplexing

In recent years, it is becoming increasingly clear that miRNA panels can be used in clinical applications, as numerous reports describe the use of miRNA biomarkers for a range of human diseases.[157,158] Additionally, systems level studies are revealing the interconnectivity between miRNAs and targets within regulatory networks. To this end, predictive bioinformatic

approaches are still needed to both predict miRNA targets and help deconvolve complex miRNA-mRNA regulatory interactions.

Quite possibly due to a paucity of robust technologies able to perform multiplexed analysis on statistically-relevant patient populations, there are a limited number of reports that demonstrate the utility of multiplexed panels. As the push towards multiplexing continues, considerable challenges must be overcome in terms of differentiating between sequences having high levels of similarity, which is difficult to achieve because of subtle thermodynamic differences in hybridization-based assays. A further complication with multiplexing is dynamic range, as miRNAs expression levels can vary by more than 5 orders of magnitude, which would be difficult to span is sequences having highly disparate concentrations were included in a single panel.

Optical detection methods have led the way in terms of the analytical capacity to perform multiplexed detection. Studies featuring both fluorescence and plasmonic sensors were used to demonstrate three-[52,55,61,70] and four-plex[90,94] assays with a relatively short time to result. However, increased clinical utility will likely be gained beyond proof-of-principle studies as the multiplexing is increased into the 10s of targets. Electrochemical sensors have also been shown to be promising for miRNA detection, with reported demonstrations of up to three-plex assays using a variety of different specific detection mechanisms.[113,146,147,151] However, the instrumentation required to facilitate multiplexed detection requires either parallel analysis, which then requires multiple sample aliquots, or more complex instrumentation that involves multi-electrode configurations and multiple potentiostats.

Challenges in informatics and the identification of disease-relevant miRNA panels

While the engineering of multiplexed detection approaches is promising from the perspective of technology alone, a significant challenge remains in the informatics behind panel construction. Next generations sequencing approaches can provide an almost overwhelming amount of expression information that must be informatically-reduced in the appropriate disease and population statistical context. As multiplexed detection approaches continue to mature, progress in informatics will ideally ripen at an equivalent rate.

One difficulty in correlating miRNA expression with their functional effects on disrupting mRNA translation stems from how miRNAs are bioinformatically identified. As opposed to siRNA, miRNAs do not require a perfect antisense match against a potential mRNA target. These so-called "noncanonical" miRNA-mRNA interactions are not confined to translational repression through binding to the 3' untranslated region (UTR) of the mRNA, as originally suspected, but play multiple complex and not completely understood roles in mRNA regulation.[159] To this end, recent studies have aimed to build bioinformatics approaches that broadly consider both canonical and noncanonical miRNA-mRNA targets,[160,161] and other promising computational tools applied to miRNAs have recently been reviewed.[162]

In addition to challenges associated with target prediction, another layer of computational complexity lies in the fact that multiple miRNAs often act on single mRNA targets, and therefore it is difficult to conclude what effect a single miRNA has on a biological state. Despite this multi-factorial regulation, a number of single miRNA knockout studies exist in the literature although their relevance to a broad understanding of miRNAs in disease is not clear. Therefore, incredible opportunities exist for sensor scientists to work together with bioinformaticians to develop multiplexed panels that can together assemble technologies and relevant panels to help elucidate deep and meaningful correlations between multi-node regulatory networks.

Challenges in matching technologies to appropriate clinical needs

In order to achieve widespread use outside academic labs, miRNA assays must be cost-effective and easy to use. This is an important consideration when engineering signal amplification steps that require complicated liquid handling protocols. Additionally, researchers must consider the tradeoff between time to result and assay sensitivity. Depending on the application, label free assays that can be completed in 10 minutes might suffice; whereas, signal amplification techniques that provide sensitivity improvements that take 2 hours or more to complete might be required for other applications. Lastly, the pre-analytical requirements for different technologies and applications must be considered. That is, a label free assay might suffice for applications where miRNA has been extracted for a sample of interest, whereas one may have to leverage signal amplification and pre-concentration strategies to make high fidelity measurements directly from highly complex matrices.

In order to optimize assays and determine the appropriate balance between time to result, sensitivity, and multiplexing capabilities, interdisciplinary collaborations between analytical chemists, clinical chemists, clinical practitioners, and statisticians/bioinformaticians will be essential. Appropriate large sample set studies will not only validate emerging sensor technologies, but more importantly also establish the broad utility of panel-based diagnostics that will then have impact beyond any one specific technology platform.

2.4.2 Brief Conclusions

Though many of the challenges outlined above are significant, the miRNA sensing field is poised for a bright future. Keeping in mind the great strides that have been made to overall

assay attributes (i.e. sensitivity and dynamic range), miRNA detection using emerging biosensing technologies is far beyond the proof-of-principle stage. The next few years will hopefully show a shift away from fundamental sensor development towards the identification and validation of multiplexed panels, and then onto clinical translation. Strategic collaborations should enhance this process as bioinformatic approaches evolve alongside detection technology maturation. These collaborations will help catalyze this shift in focus from further pushing LODs and performing proof-of-concept sensing studies to placing instrumentation in clinical settings to revolutionize diagnostic capabilities by supporting or replacing current gold standard techniques. Although there are sure to be challenges along the way, the ultimate goal of sensitive, multiplexed, and easy to use miRNA detection devices is on the horizon, and will hopefully help miRNAs fill a key role in the realization of informative diagnostics guiding individualized medicine.

2.5 FIGURES AND TABLES

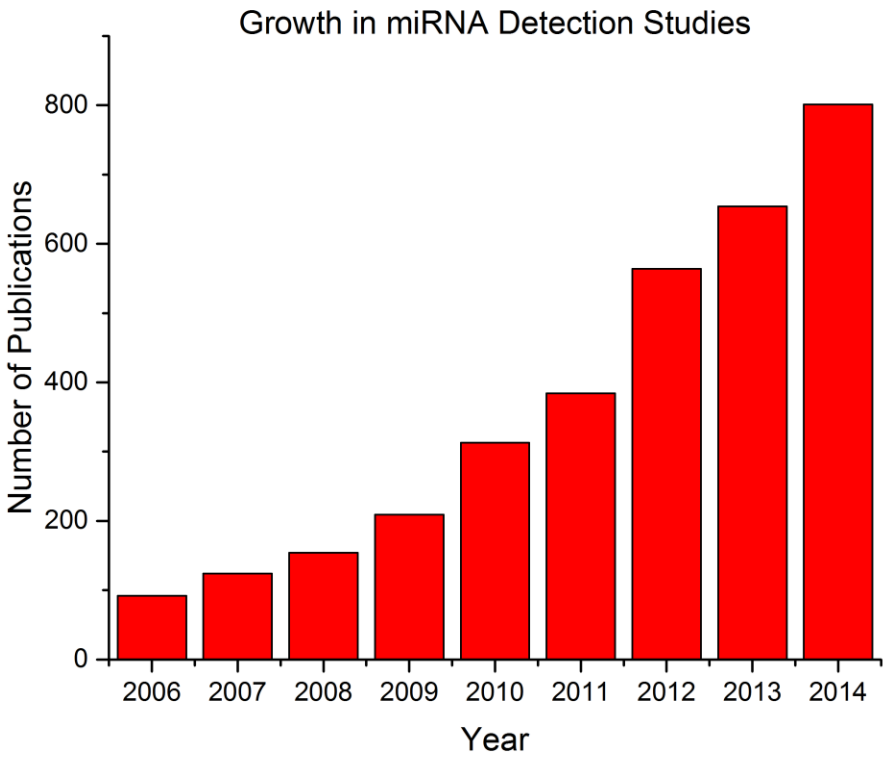

Figure 2.1: Growth in publications in microRNA profiling since 2006. These results were obtained from a SciFinder search using the key words "microRNA detection".

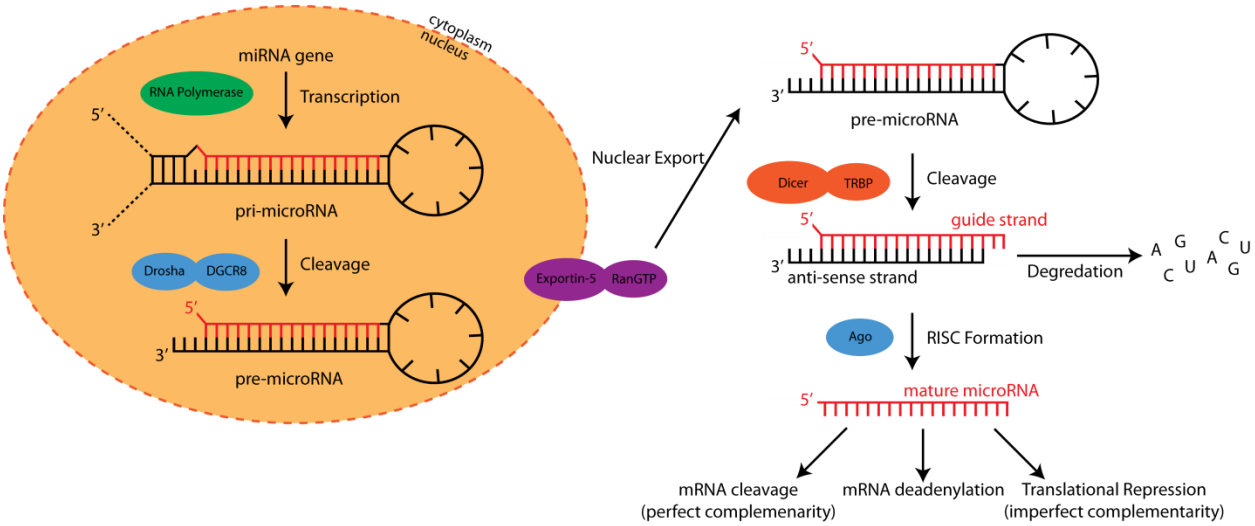

Figure 2.2: Biogenesis of miRNA that starts with transcription in the nucleus and ends with affecting gene translation in the cytoplasm.

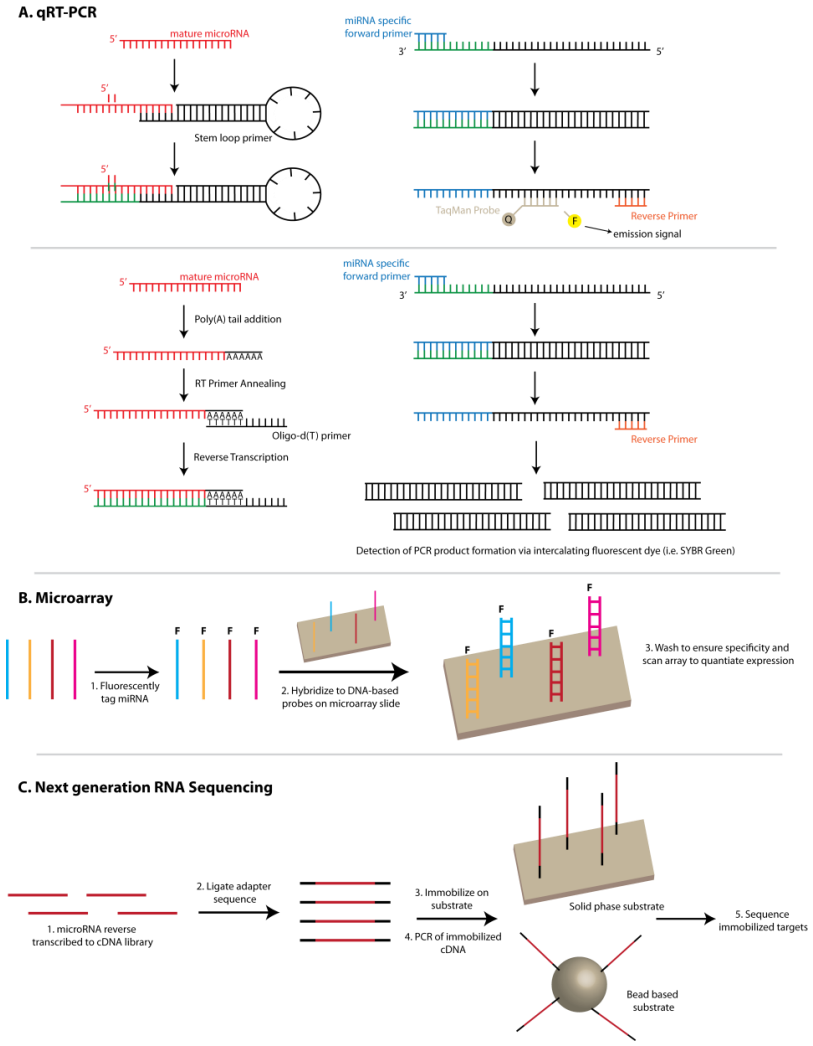

Figure 2.3: Overview of conventional techniques: (a) qRT-PCR, (b) microarrays and (c) next generation RNA sequencing. (A) When using TaqMan qRT-PCR, the reverse transcription process utilizes stem-loop primers specific to the miRNA target of interest. During PCR amplification, the DNA polymerase proceeds along the template strands produces by miRNA specific forward and reverse primers and hydrolyses the TaqMan probe bound to the template. This liberates the fluorescent dye from the quencher and results in light emission. In SYBR green-based approaches, miRNAs are typically polyadenylated at the 3' end and d(T) oligos are used as the reverse transcription primer. PCR amplification is carried out using miRNA specific forward primer and reverse primer. SYBR Green, an intercalating dsDNA dye, is then used to monitor PCR product formation. (B) DNA-based capture probes immobilized on the microarray are used to capture fluorescently tagged miRNAs. The fluorescent signal is then quantitated and the intensity is related to the relative miRNA expression. (C) Most RNA-sequencing workflows begin by reverse transcribing miRNA into a cDNA library. This is followed by adaptor ligation that allows for immobilization on a substrate that are used to obtain sequencing data.

	qRT-PCR	Microarrays	Next Gen. Sequencing
Time to result	Hours	Days	Weeks
Cost	$$	$	$$$
Biochemical processing	Ligation with T4 (SYBR Green) Annealing of primers	No ligation steps	Ligate barcode
Input	Low (ng)	Large (ng-µg)	Large (ng-µg)
Drawbacks	Results need validation Long time to result	Single plex	Don't always need global view

Table 2.1: Comparison of conventional miRNA detection platforms

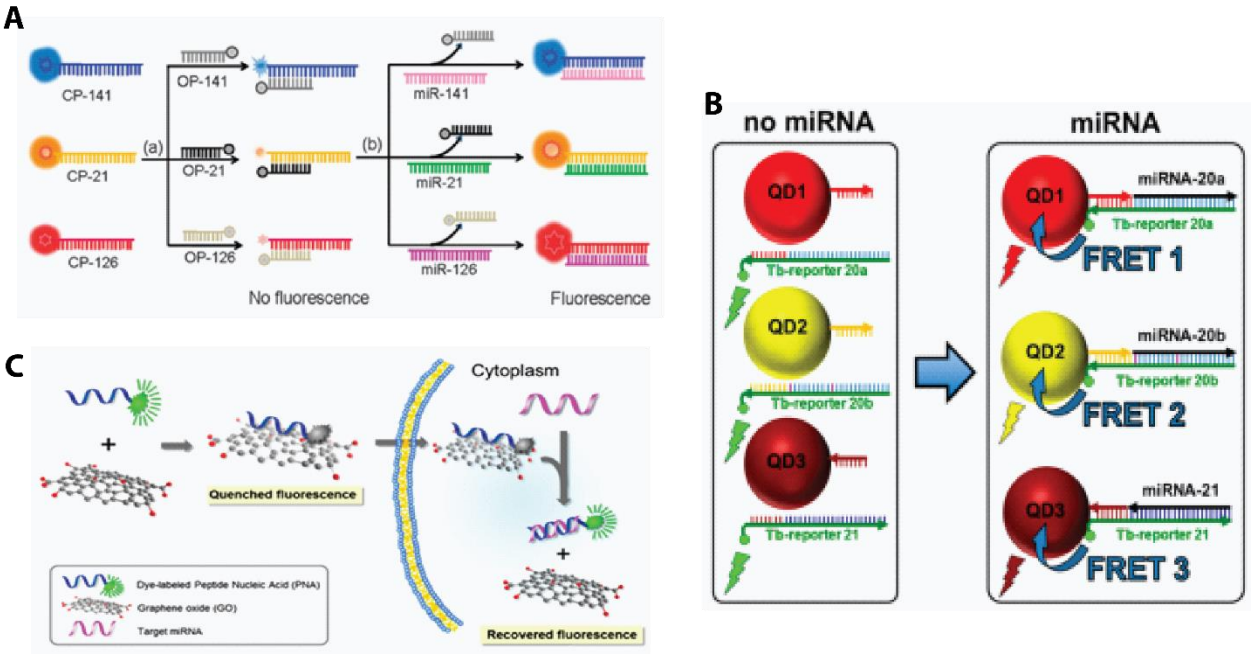

Figure 2.4: Promising multiplexed detection schemes. (A) Fluorescent FRET pairs were used to probe miRNAs-141, 21, and 126 in multiple cancer cell lines. Reproduced from Wu, P.; Tu, Y.; Qian, Y.; Zhang, H.; Cai, C. Chemical Communications 2014, 50, 1012-1014 (ref 52), with permission of The Royal Society of Chemistry. (B) Quantum dot FRET pairs were also used to profile three miRNAs from diluted serum. Reproduced from Qiu, X.; Hildebrandt, N. ACS Nano 2015, 9, 8449-8457 (ref 55). Copyright 2015 American Chemical Society. (C) FRET-based detection was achieved using a fluorescent peptide nucleic acid detection probe adsorbed onto a graphene oxide nanosheet as a quencher. miRNA-21, 125b, and 96 were quantitated in living cells and the relative expression levels were shown to correlate well with Northern blotting. Reproduced from Ryoo, S.-R.; Lee, J.; Yeo, J.; Na, H.-K.; Kim, Y.-K.; Jang, H.; Lee, J. H.; Han, S. W.; Lee, Y.; Kim, V. N.; Min, D.-H. ACS Nano 2013, 7, 5882-5891 (ref 61). Copyright 2013 American Chemical Society.

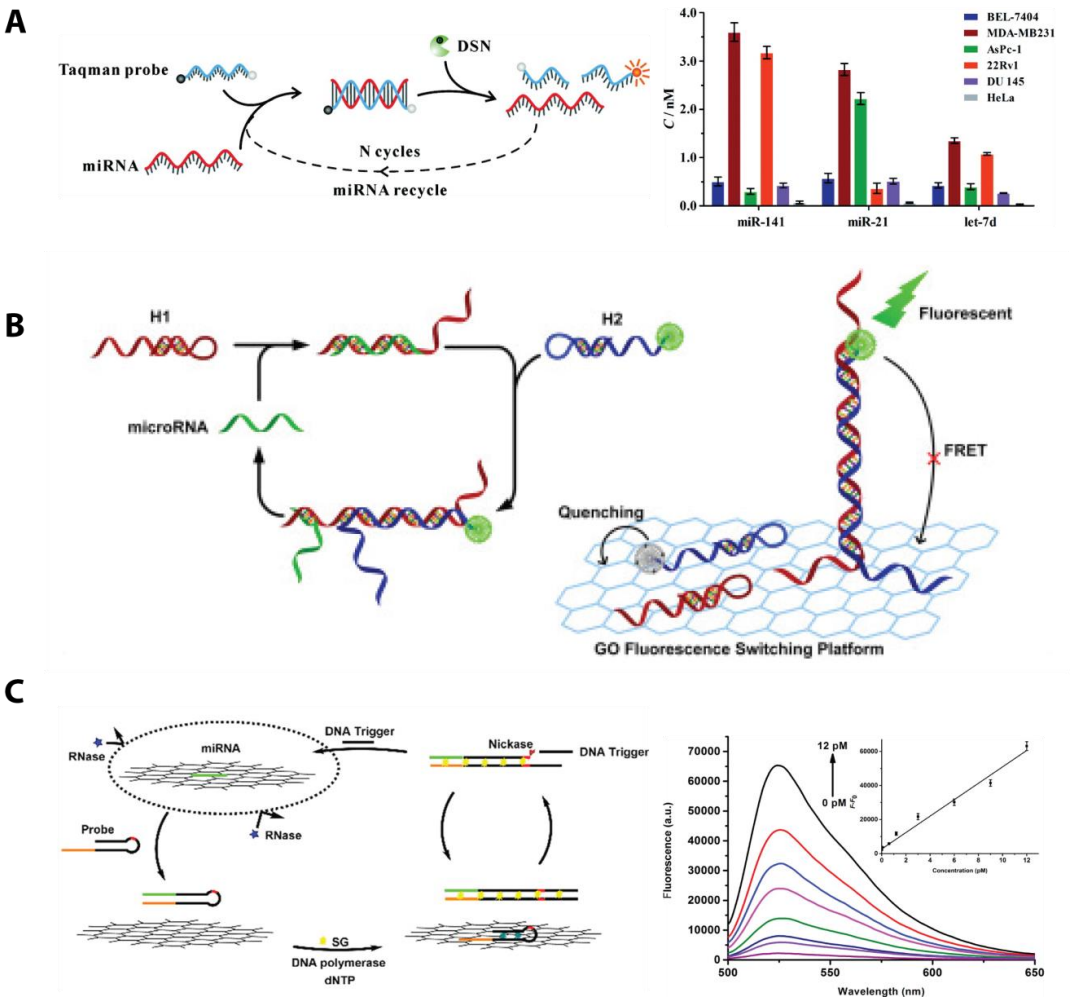

Figure 2.5: Target recycling approaches. (A) Duplex specific nuclease recycling was used to study the differential expression of three miRNAs in six cancer cell lines. Reproduced from Yin, B.-C.; Liu, Y.-Q.; Ye, B.-C. Journal of the American Chemical Society 2012, 134, 5064-5067 (ref 70). Copyright 2012 American Chemical Society. (B) Toehold-mediated amplification facilitated effective target recycling and detection of miRNA-21 in four cell lines. However, improvements to this assay could focus on quantitating multiple targets per sample. Reprinted from Analytica Chemica Acta, Vol. 888, Huang, R.; Liao, Y.; Zhou, X.; Xing, D. Toehold-mediated nonenzymatic amplification circuit on graphene oxide fluorescence switching platform for sensitive and homogeneous microRNA detection, pp. 162-172 (ref 71). Copyright 2015, with permission from Elsevier. (C) A nickase based recycling strategy combined with the use of a DNA polymerase exponentially amplified nucleic acid sequences related to the target of interest. These dsDNA produces were stained with an intercalating fluorescent dye, and the signal intensity was proportional to the initialtarget concentration. Reproduced from Liu, H.; Li, L.; Wang, Q.; Duan, L.; Tang, B. Analytical Chemistry 2014, 86, 5487-5493 (ref 73). Copyright 2014 American Chemical Society.

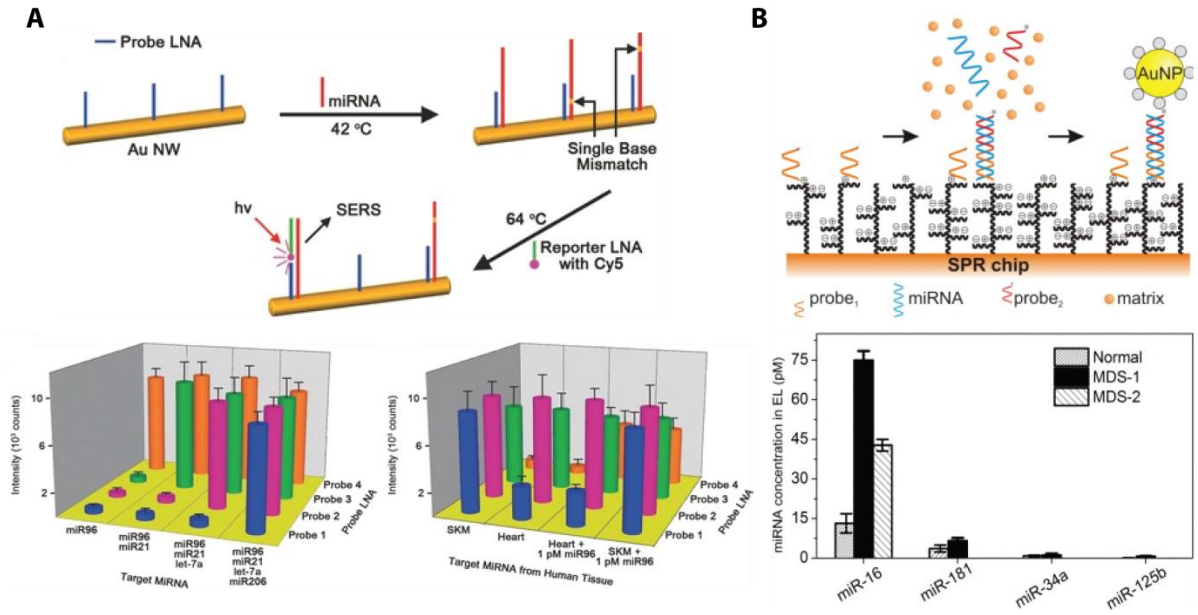

Figure 2.6: Successful multiplexing strategies using plasmonic based biosensors. (A) Plasmonic nanowires detected the presence of four miRNA targets using locked nucleic acid capture probes and Cy5 functionalized reporter locked nucleic acid sequences. These optimized nanosensors were used to profile the expression of four miRNAs from RNA isolated from two tissue types. Reproduced from Ultra-Specific Zeptmole microRNA Detection by Plasmonic Nanowire Interstice Sensor with Bi-Temperature Hybridization, Kang, T.; Kim, H.; Lee, J. M.; Lee, H.; Choi, Y.-S.; Kang, G.; Seo, M.-K.; Chung, B. H.; Jung, Y.; Kim, B. Small, Vol. 10, Issue 20 (ref 91). Copyright 2014 Wiley. (B) A novel ultra-low fouling surface plasmon resonance imaging biosensor detected four miRNAs from erythrocyte lysate. A gold nanoparticle signal enhancement strategy was used to improve limits of detection. Clinical utility was shown by analyzing chances in expression profiles of miR-16, 181, 34a, and 125b in 'normal' clinical samples and ones with myelodysplastic syndrome. Reprinted from Biosensors and Bioelectronics, Vol. 70, Vaisocherová, H.; Šípová, H.; Víšová, I.; Bocková, M.; Špringer, T.; Laura Ermini, M.; Song, X.; Krejčík, Z.; Chrastinová, L.; Pastva, O.; Pimková, K.; Dostálová Merkerová, M.; Dyr, J. E.; Homola, J., Rapid and sensitive detection of multiple microRNAs in cell lysate by low-fouling surface plasmon resonance biosensor, pp. 226-231 (ref 95). Copyright 2015, with permission from Elsevier.

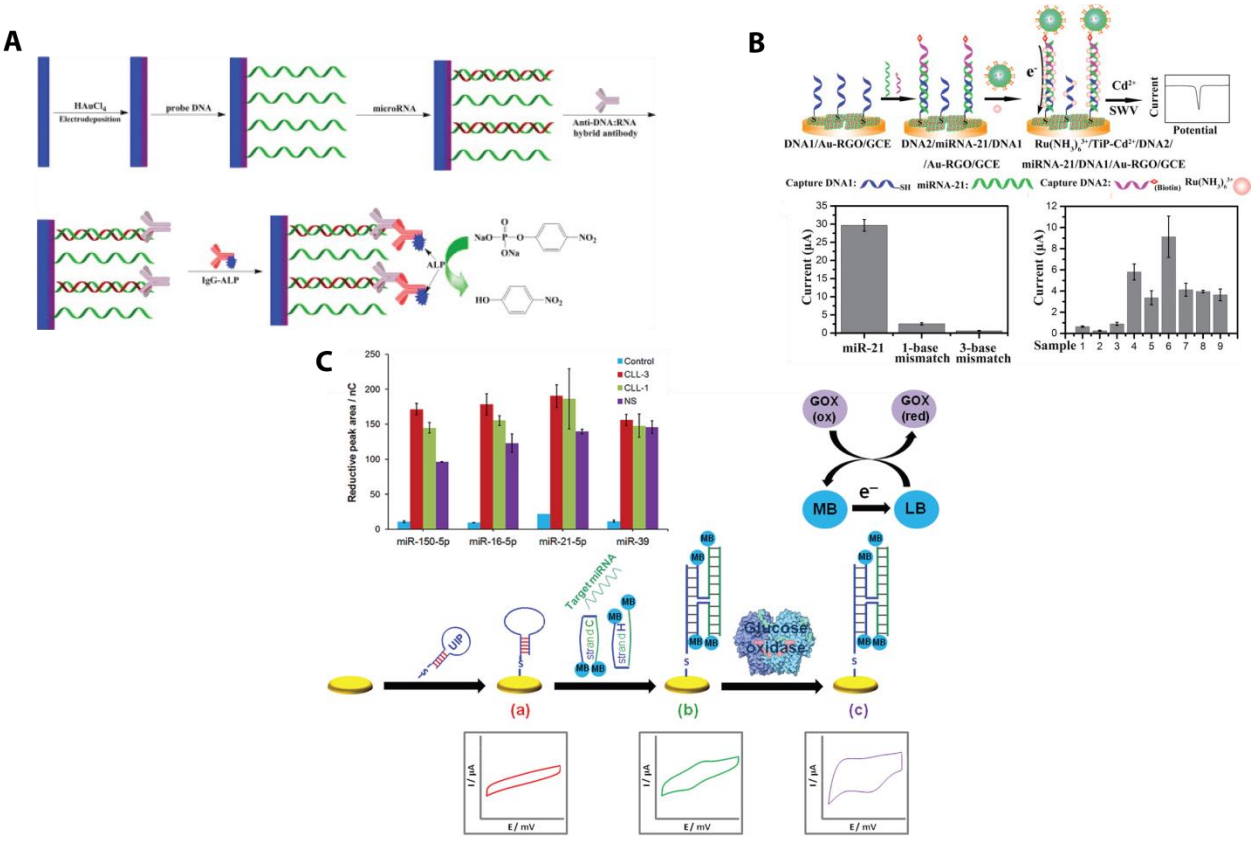

Figure 2.7: Promising electrochemical signal enhancement approaches by adding an electroactive label to miRNA:DNA hybrids. (A) Labeling was achieved using the S9.6 antibody that binds specifically to RNA:DNA heteroduplexes. After antibody binding, ALP was then conjugated to the surface and provided an electrochemical signal. Reprinted from Electrochemica Acta, Vol. 165, Wang, M.; Li, B.; Zhou, Q.; Yin, H.; Zhou, Y.; Ai, S. Label-free, Ultrasensitive and Electrochemical Immunosensing Platform for microRNA Detection Using Anti-DNA:RNA Hybrid Antibody and Enzymatic Signal Amplification, pp. 130-135 (ref 111). Copyright 2015, with permission from Elsevier. (B) Nanoparticle labeling was achieved using biotin-streptavidin attachement chemistry. This approach was used to identify changes in miRNA-21 expression in serum between healthy patients and patients with various cancer types. Reproduced from Cheng, F.-F.; He, T.-T.; Miao, H.-T.; Shi, J.-J.; Jiang, L.-P.; Zhu, J.-J. ACS Applied Materials & Interfaces 2015, 7, 2979-2985 (ref 118). Copyright 2015 American Chemical Society. (C) A sandwich hybridization based labeling approach was developed using methylene blue conjugated reporter probes that bound to the surface only when the miRNA was present. This strategy effectively placed four methylene blue molecules near the electrode for every one target miRNA, allowing for effective signal amplification. The power of this strategy was sown by detecting three miRNAs in parallel. Reproduced from Labib, M.; Khan, N.; Berezovski, M. V. Analytical Chemistry 2015, 87, 1395-1403 (ref 113). Copyright 2015 American Chemical Society.

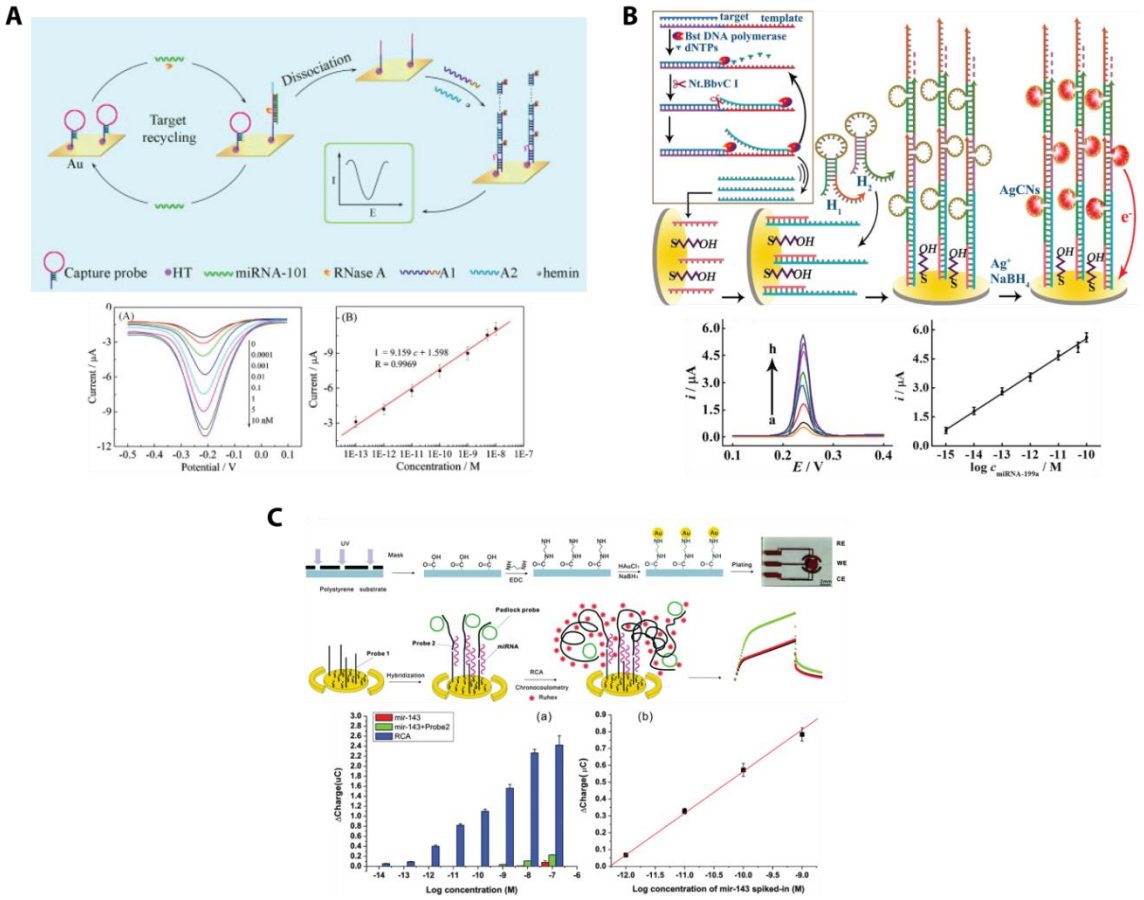

Figure 2.8: Electrochemical signal amplification using enzymatic approaches to modify the miRNA:capture probe structure at the sensor surface. (A) Target recycling via RNase A was initially used to increase the number of targets that bound to the surface. The detectable electrochemical signal was then amplified via hybridization chain reaction which formed multiple hemin associated G-quadruplexes and thus an electrochemical signal. Reprinted from Sensors and Actuators B, Vol. 195, Xiang, G.; Jiang, D.; Luo, F.; Liu, F.; Liu, L.; Pu, X. Sensitive detection of microRNAs using hemin/G-quadruplex concatamers as trace labels and RNA endonuclease-aided target recycling for amplification, pp. 515-519 (ref 130). Copyright 2014, with psermission from Elsevier. (B) A nicking enzyme based recycling strategy that relies on DNA polymerase amplification was used to create multiple detection sequences that are proportional to the miRNA target concentration. This is followed by hybridization chain reaction where the primers are designed to associate with silver nanoclusters. Reproduced from Yang, C.; Shi, K.; Dou, B.; Xiang, Y.; Chai, Y.; Yuan, R. ACS Applied Materials & Interfaces 2015, 7, 1188-1193 (ref 132). Copyright 2015 American Chemical Society. (C) Rolling circle amplification was also shown to be an effective way to facilitate binding of multiple electroactive species, in this case Ruhex, per miRNA target. Reproduced from Yao, B.; Liu, Y.; Tabata, M.; Zhu, H.; Miyahara, Y. Chemical Communications 2014, 50, 9704-9706 (ref 135), with permission of The Royal Society of Chemistry.

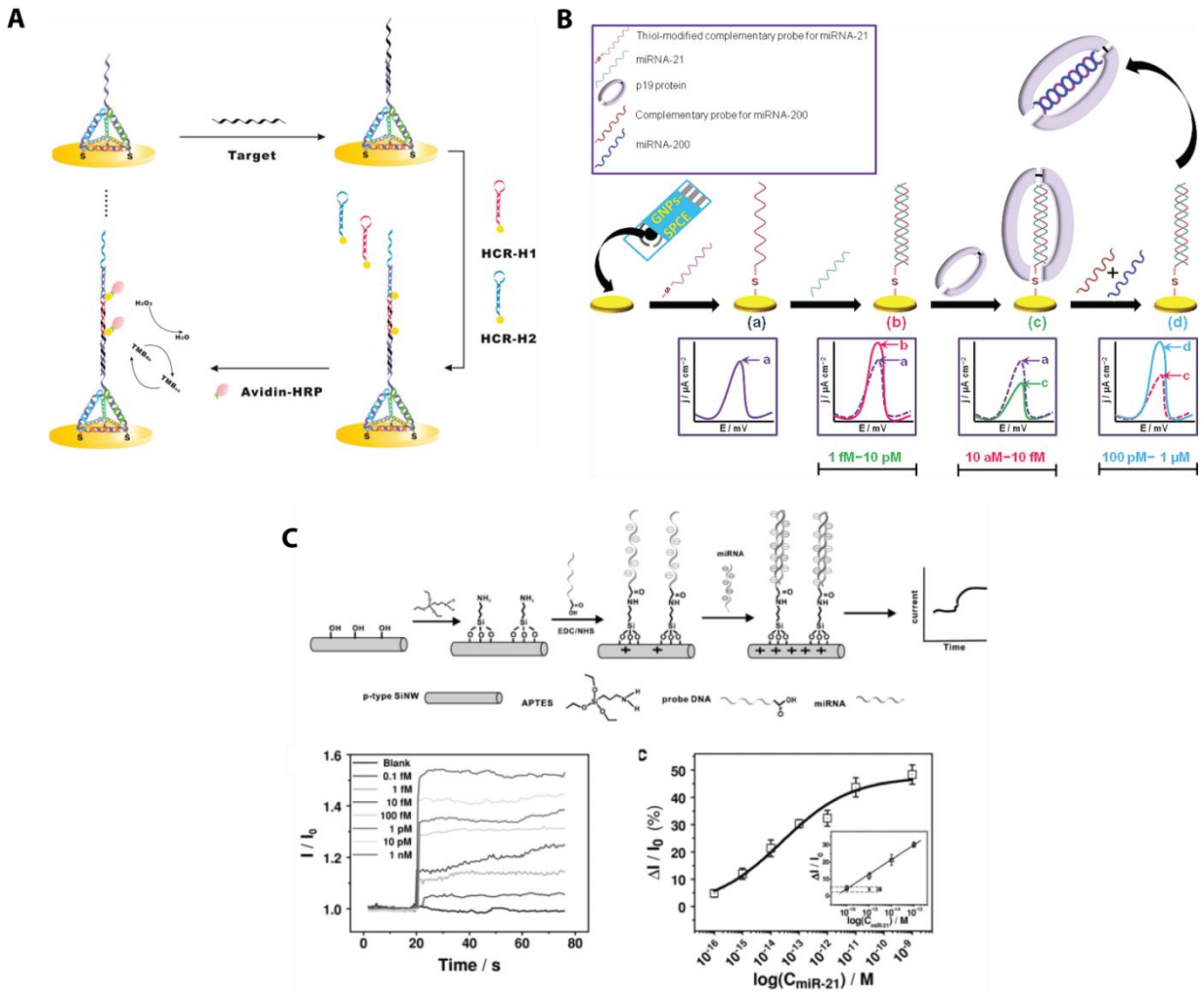

Figure 2.9: General electrochemical sensing improvements and additional strategies for generating a detectable signal. (A) DNA nanotechnology has been used to improve surface functionalization by ensuring reproducible capture probe orientation at the electrode surface. Reproduced from Ge, Z.; Lin, M.; Wang, P.; Pei, H.; Yan, J.; Shi, J.; Huang, Q.; He, D.; Fan, C.; Zuo, X. Analytical Chemistry 2014, 86, 2124-2130 (ref 142). Copyright 2014 American Chemical Society. (B) Impedance can be used to detect the presence of miRNAs. Here, three different detection regimes (label free detection, protein binding based signal amplification, and protein dissociation based signal amplification) were identified to extend the dynamic range over 10 orders of magnitude. Reproduced from Labib, M.; Khan, N.; Ghobadloo, S. M.; Cheng, J.; Pezacki, J. P.; Berezovski, M. V. Journal of the American Chemical Society 2013, 135, 3027-3038 (ref 146). Copyright 2013 American Chemical Society. (C) Based on impedance, field effect transistors are a simple way to achieve multiplexing capabilities with very low limits of detection. Reproduced from CMOS-Compatible Silicon Nanowire Field-Effect Transistors for Ultrasensitive and Label-Free microRNAs sensing, Lu, N.; Gao, A.; Dai, P.; Song, S.; Fan, C.; Wang, Y.; Li, T. Small, Vol. 10, Issue 10, (ref 154). Copyright 2014, Wiley.

2.6 References

(1) Wightman, B.; Ha, I.; Ruvkun, G. *Cell* **1993**, *75*, 855-862.

(2) Reinhart, B. J.; Slack, F. J.; Basson, M.; Pasquinelli, A. E.; Bettinger, J. C.; Rougvie, A. E.; Horvitz, H. R.; Ruvkun, G. *Nature* **2000**, *403*, 901-906.

(3) Wienholds, E.; Kloosterman, W. P.; Miska, E.; Alvarez-Saavedra, E.; Berezikov, E.; Bruijn, E. d.; Horvitz, H. R.; Kauppinen, S.; Plasterk, R. H. A. *Science* **2005**, *309*, 310-311.

(4) Lu, J.; Getz, G.; Miska, E. A.; Alvarez-Saavedra, E.; Lamb, J.; Peck, D.; Sweet-Cordero, A.; Ebert, B. L.; Mak, R. H.; Ferrando, A. A.; Downing, J. R.; Jacks, T.; Horvitz, H. R.; Golub, T. R. *Nature* **2005**, *435*, 4653-4662.

(5) Winter, J.; Jung, S.; Keller, S.; Gregory, R. I.; Diederichs, S. *Nature Cell Biology* **2009**, *11*, 228-234.

(6) Lin, S.; Gregory, R. I. *Nat Rev Cancer* **2015**, *15*, 321-333.

(7) Ha, M.; Kim, V. N. *Nat Rev Mol Cell Biol* **2014**, *15*, 509-524.

(8) O'Connell, R. M.; Rao, D. S.; Baltimore, D. *Annual Review of Immunology* **2012**, *30*, 295-312.

(9) Johnston, R. J.; Hobert, O. *Nature* **2003**, *426*, 845-849.

(10) Shenoy, A.; Blelloch, R. H. *Nat Rev Mol Cell Biol* **2014**, *15*, 565-576.

(11) Hwang, H. W.; Mendell, J. T. *Br J Cancer* **2006**, *94*, 776-780.

(12) Rosenfeld, N.; Aharonov, R.; Meiri, E.; Rosenwald, S.; Spector, Y.; Zepeniuk, M.; Benjamin, H.; Shabes, N.; Tabak, S.; Levy, A.; Lebanony, D.; Goren, Y.; Silberschein, E.; Targan, N.; Ben-Ari, A.; Gilad, S.; Sion-Vardy, N.; Tobar, A.; Feinmesser, M.; Kharenko, O.; Nativ, O.; Nass, D.; Perelman, M.; Yosepovich, A.; Shalmon, B.; Polak-Charcon, S.; Fridman,

E.; Avniel, A.; Bentwich, I.; Bentwich, Z.; Cohen, D.; Chajut, A.; Barshack, I. *Nat Biotech* **2008**, *26*, 462-469.

(13) Keshavarz, M.; Behpour, M.; Rafiee-pour, H.-A. *RSC Advances* **2015**, *5*, 35651-35660.

(14) Xie, B.; Ding, Q.; Han, H.; Wu, D. *Bioinformatics* **2013**, *29*, 638-644.

(15) Kumar, P.; Dezso, Z.; MacKenzie, C.; Oestreicher, J.; Agoulnik, S.; Byrne, M.; Bernier, F.; Yanagimachi, M.; Aoshima, K.; Oda, Y. *PLoS ONE* **2013**, *8*, e69807.

(16) Shafi, G.; Aliya, N.; Munshi, A. *Canadian Journal of Neurological Sciences / Journal Canadien des Sciences Neurologiques* **2010**, *37*, 177-185.

(17) Guay, C.; Regazzi, R. *Nature Reviews Endocrinology* **2013**, *9*, 513-521.

(18) Thum, T.; Mayr, M. *Cardiovascular Research* **2012**, *93*, 543-544.

(19) Olson, E. N. *Science Translational Medicine* **2014**, *6*, 239ps233-239ps233.

(20) Weber, J. A.; Baxter, D. H.; Zhang, S.; Huang, D. Y.; How Huang, K.; Jen Lee, M.; Galas, D. J.; Wang, K. *Clinical Chemistry* **2010**, *56*, 1733-1741.

(21) Mitchell, P. S.; Parkin, R. K.; Kroh, E. M.; Fritz, B. R.; Wyman, S. K.; Pogosova-Agadjanyan, E. L.; Peterson, A.; Noteboom, J.; O'Briant, K. C.; Allen, A.; Lin, D. W.; Urban, N.; Drescher, C. W.; Knudsen, B. S.; Stirewalt, D. L.; Gentleman, R.; Vessella, R. L.; Nelson, P. S.; Martin, D. B.; Tewari, M. *Proceedings of the National Academy of Sciences* **2008**, *105*, 10513-10518.

(22) Schwarzenbach, H.; Hoon, D. S. B.; Pantel, K. *Nat Rev Cancer* **2011**, *11*, 426-437.

(23) Cissell, K. A.; Shrestha, S.; Deo, S. K. *Analytical Chemistry* **2007**, *79*, 4754-4761.

(24) Qavi, A.; Kindt, J.; Bailey, R. *Anal Bioanal Chem* **2010**, *398*, 2535-2549.

(25) Dong, H.; Lei, J.; Ding, L.; Wen, Y.; Ju, H.; Zhang, X. *Chemical Reviews* **2013**, *113*, 6207-6233.

(26) Bartel, D. P. *Cell* **2004**, *116*, 281-297.

(27) Rajewsky, N. *Nat Genet* **2006,** *38*, S8-S13.

(28) Muniategui, A.; Nogales-Cadenas, R.; Vázquez, M.; L. Aranguren, X.; Agirre, X.; Luttun, A.; Prosper, F.; Pascual-Montano, A.; Rubio, A. *PLoS ONE* **2012**, *7*, e30766.

(29) Meng, W.; McElroy, J. P.; Volinia, S.; Palatini, J.; Warner, S.; Ayers, L. W.; Palanichamy, K.; Chakravarti, A.; Lautenschlaeger, T. *PLoS ONE* **2013**, *8*, e64393.

(30) Pritchard, C. C.; Cheng, H. H.; Tewari, M. *Nature Reviews Genetics* **2012**, *13*, 358-369.

(31) Hunt, E. A.; Broyles, D.; Head, T.; Deo, S. K. *Annual Reviews in Analytical Chemistry* **2015**, *8*, 217-237.

(32) Chen, C.; Ridzon, D. A.; Broomer, A. J.; Zhou, Z.; Lee, D. H.; Nguyen, J. T.; Barbisin, M.; Xu, N. L.; Mahuvakar, V. R.; Andersen, M. R.; Lao, K. Q.; Livak, K. J.; Guegler, K. J. *Nucleic Acids Research* **2005**, *33*, e179-e179.

(33) Ballantyne, K. N.; van Oorschot, R. A. H.; Mitchell, R. J. *Genomics* **2008**, *91*, 301-305.

(34) D'haene, B.; Mestdagh, P.; Hellemans, J.; Vandesompele, J. In *Next-Generation MicroRNA Expression Profiling Technology*, Fan, J.-B., Ed.; Humana Press, 2012, pp 261-272.

(35) Peltier, H. J.; Latham, G. J. *RNA* **2008**, *14*, 844-852.

(36) Sarkar, D.; Parkin, R.; Wyman, S.; Bendoraite, A.; Sather, C.; Delrow, J.; Godwin, A. K.; Drescher, C.; Huber, W.; Gentleman, R.; Tewari, M. *Nucleic Acids Research* **2009**, *37*, e17-e17.

(37) Roberts, T. C.; Coenen-Stass, A. M. L.; Wood, M. J. A. *PLoS ONE* **2014**, *9*, e89237.

(38) Thomson, J. M.; Parker, J.; Perou, C. M.; Hammond, S. M. *Nat Meth* **2004**, *1*, 47-53.

(39) Berezikov, E.; Cuppen, E.; Plasterk, R. H. A. *Nat Genet* **2006**.

(40) Weiler, J.; Gausepohl, H.; Hauser, N.; Jensen, O. N.; Hoheisel, J. D. *Nucleic Acids Research* **1997**, *25*, 2792-2799.

(41) Castoldi, M.; Schmidt, S.; Benes, V.; Noerholm, M.; Kulozik, A. E.; Hentze, M. W.; Muckenthaler, M. U. *RNA* **2006**, *12*, 913-920.

(42) Lee, J. M.; Cho, H.; Jung, Y. *Angewandte Chemie International Edition* **2010**, *49*, 8662-8665.

(43) Duan, D.; Zheng, K.-X.; Shen, Y.; Cao, R.; Jiang, L.; Lu, Z.; Yan, X.; Li, J. *Nucleic Acids Research* **2011,** *39*, e154.

(44) Ueno, T.; Funatsu, T. *PLoS ONE* **2014**, *9*, e90920.

(45) Li, W.; Ruan, K. *Anal Bioanal Chem* **2009**, *394*, 1117-1124.

(46) Metzker, M. L. *Nat Rev Genet* **2010**, *11*, 31-46.

(47) Mardis, E. R. *Annual Review of Analytical Chemistry* **2013**, *6*, 287-303.

(48) Git, A.; Dvinge, H.; Salmon-Divon, M.; Osborne, M.; Kutter, C.; Hadfield, J.; Bertone, P.; Caldas, C. *RNA* **2010**, *16*, 991-1006.

(49) Tam, S.; de Borja, R.; Tsao, M.-S.; McPherson, J. D. *Lab Invest* **2014**, *94*, 350-358.

(50) Calin, G. A.; Ferracin, M.; Cimmino, A.; Di Leva, G.; Shimizu, M.; Wojcik, S. E.; Iorio, M. V.; Visone, R.; Sever, N. I.; Fabbri, M.; Iuliano, R.; Palumbo, T.; Pichiorri, F.; Roldo, C.; Garzon, R.; Sevignani, C.; Rassenti, L.; Alder, H.; Volinia, S.; Liu, C.-g.; Kipps, T. J.; Negrini, M.; Croce, C. M. *New England Journal of Medicine* **2005**, *353*, 1793-1801.

(51) Schultz, N. A.; Dehlendorff, C.; Jensen, B. V.; et al. *JAMA* **2014**, *311*, 392-404.

(52) Wu, P.; Tu, Y.; Qian, Y.; Zhang, H.; Cai, C. *Chemical Communications* **2014**, *50*, 1012-1014.

(53) Lee, C. H.; Chae, J. i.; Ko, H. Y.; Kim, S. *Journal of Molecular Imaging & Dynamics* **2013**, *2*.

(54) Larkey, N. E.; Almlie, C. K.; Tran, V.; Egan, M.; Burrows, S. M. *Analytical Chemistry* **2014**, *86*, 1853-1863.

(55) Qiu, X.; Hildebrandt, N. *ACS Nano* **2015**, *9*, 8449-8457.

(56) Zhang, H.; Wang, Y.; Zhao, D.; Zeng, D.; Xia, J.; Aldalbahi, A.; Wang, C.; San, L.; Fan, C.; Zuo, X.; Mi, X. *ACS Applied Materials & Interfaces* **2015**, *7*, 16152-16156.

(57) Lee, J.; Park, G.; Min, D.-H. *Chemical Communications* **2015**, *51*, 14597-14600.

(58) Tu, Y.; Li, W.; Wu, P.; Zhang, H.; Cai, C. *Analytical Chemistry* **2013**, *85*, 2536-2542.

(59) Ko, H. Y.; Lee, J.; Lee, Y. S.; Gu, H.-N.; Ali, B. A.; Al-Khedhairy, A. A.; Heo, H.; Cho, S.; Kim, S. *Chemical Communications* **2015**, *51*, 2159-2161.

(60) Yoo, B.; Kavishwar, A.; Ghosh, S. K.; Barteneva, N.; Yigit, M. V.; More, A.; Medarova, Z. *Chemistry & Biology* **2014**, *21*, 199-204.

(61) Ryoo, S.-R.; Lee, J.; Yeo, J.; Na, H.-K.; Kim, Y.-K.; Jang, H.; Lee, J. H.; Han, S. W.; Lee, Y.; Kim, V. N.; Min, D.-H. *ACS Nano* **2013**, *7*, 5882-5891.

(62) Liao, X.; Wang, Q.; Ju, H. *Analyst* **2015**, *140*, 4245-4252.

(63) Lin, X.; Zhang, C.; Huang, Y.; Zhu, Z.; Chen, X.; Yang, C. J. *Chemical Communications* **2013**, *65*, 7243-7245.

(64) Yan, L.; Yan, Y.; Pei, L.; Wei, W.; Zhao, J. *Scientific Reports* **2014**, *4*, 7400.

(65) Guo, S.; Yang, F.; Zhang, Y.; Ning, Y.; Yao, Q.; Zhang, G.-J. *Analytical Methods* **2014**, *6*, 3598-3603.

(66) Xi, Q.; Zhou, D.-M.; Kan, Y.-Y.; Ge, J.; Wu, Z.-K.; Yu, R.-Q.; Jiang, J.-H. *Analytical Chemistry* **2014**, *86*, 1361-1365.

(67) Shen, W.; Yeo, K. H.; Gao, Z. *Analyst* **2015**, *140*, 1932-1938.

(68) Degliangeli, F.; Kshirsagar, P.; Brunetti, V.; Pompa, P. P.; Fiammengo, R. *Journal of the American Chemical Society* **2014**, *136*, 2264-2267.

(69) Wang, Q.; Li, R.-D.; Yin, B.-C.; Ye, B.-C. *Analyst* **2015**, *140*, 6306-6312.

(70) Yin, B.-C.; Liu, Y.-Q.; Ye, B.-C. *Journal of the American Chemical Society* **2012**, *134*, 5064-5067.

(71) Huang, R.; Liao, Y.; Zhou, X.; Xing, D. *Analytica Chimica Acta* **2015**, *888*, 162-172.

(72) Zhu, D.; Zhang, L.; Ma, W.; Lu, S.; Xing, X. *Biosensors and Bioelectronics* **2015**, *65*, 152-158.

(73) Liu, H.; Li, L.; Wang, Q.; Duan, L.; Tang, B. *Analytical Chemistry* **2014**, *86*, 5487-5493.

(74) Dong, H.; Hao, K.; Tian, Y.; Jin, S.; Lu, H.; Zhou, S.-F.; Zhang, X. *Biosensors and Bioelectronics* **2014**, *53*, 377-383.

(75) Liu, W.; Zhou, X.; Xing, D. *Biosensors and Bioelectronics* **2014**, *58*, 388-394.

(76) Liu, T.; Chen, X.; Hong, C.-Y.; Xu, X.-P.; Yang, H.-H. *Microchim Acta* **2014**, *181*, 731-736.

(77) Zhang, P.; Wu, X.; Chai, Y.; Yuan, R. *Analyst* **2014**, *139*, 2748-2753.

(78) Zhang, P.; Wu, X.; Yuan, R.; Chai, Y. *Analytical Chemistry* **2015**, *87*, 3202-3207.

(79) Hao, N.; Li, X.-L.; Zhang, H.-R.; Xu, J.-J.; Chen, H.-Y. *Chemical Communications* **2014**, *50*, 14828-14830.

(80) Chen, Y.; Xiang, Y.; Yuan, R.; Chai, Y. *Analytica Chimica Acta* **2015**, *891*, 130-135.

(81) Zhang, P.; Zhuo, Y.; Chang, Y.; Yuan, R.; Chai, Y. *Analytical Chemistry* **2015**.

(82) Chen, A.; Gui, G.-F.; Zhuo, Y.; Chai, Y.-Q.; Xiang, Y.; Yuan, R. *Analytical Chemistry* **2015**, *87*, 6328-6334.

(83) Hao, N.; Dai, P.-P.; Yu, T.; Xu, J.-J.; Chen, H.-Y. *Chemical Communications* **2015**, *51*, 13504-13507.

(84) Fang, S.; Lee, H. J.; Wark, A. W.; Corn, R. M. *Journal of the American Chemical Society* **2006**, *128*, 14044-14046.

(85) Lee, J.; Park, J.; Lee, J.-Y.; Yeo, J.-S. *Advanced Science* **2015**, *2*, n/a-n/a.

(86) Guven, B.; Dudak, F. C.; Boyaci, I. H.; Tamer, U.; Ozsoz, M. *Analyst* **2014**, *139*, 1141-1147.

(87) Joshi, G. K.; Deitz-McElyea, S.; Johnson, M.; Mali, S.; Korc, M.; Sardar, R. *Nano Letters* **2014**, *14*, 6955-6963.

(88) Liu, Q.; Shin, Y.; Kee, J. S.; Kim, K. W.; Rafei, S. R. M.; Perera, A. P.; Tu, X.; Lo, G.-Q.; Ricci, E.; Colombel, M.; Chiong, E.; Thiery, J. P.; Park, M. K. *Biosensors and Bioelectronics* **2015**, *71*, 365-372.

(89) Ho, S.-L.; Chan, H.-M.; Wong, R. N.-S.; Li, H.-W. *Analytica Chimica Acta* **2014**, *823*, 61-68.

(90) Kang, T.; Kim, H.; Lee, J. M.; Lee, H.; Choi, Y.-S.; Kang, G.; Seo, M.-K.; Chung, B. H.; Jung, Y.; Kim, B. *Small* **2014**, *10*, 4200-4206.

(91) Wang, Y.; MacLachlan, E.; Nguyen, B. K.; Fu, G.; Peng, C.; Chen, J. I. L. *Analyst* **2015**, *140*, 1140-1148.

(92) Gao, X.; Xu, H.; Baloda, M.; Gurung, A. S.; Xu, L.-P.; Wang, T.; Zhang, X.; Liu, G. *Biosensors and Bioelectronics* **2014**, *54*, 578-584.

(93) Gao, X.; Xu, L.-P.; Wu, T.; Wen, Y.; Ma, X.; Zhang, X. *Talanta* **2016,** *146*, 648-654.

(94) Vaisocherová, H.; Šípová, H.; Víšová, I.; Bocková, M.; Špringer, T.; Laura Ermini, M.; Song, X.; Krejčík, Z.; Chrastinová, L.; Pastva, O.; Pimková, K.; Dostálová Merkerová, M.; Dyr, J. E.; Homola, J. *Biosensors and Bioelectronics* **2015**, *70*, 226-231.

(95) Zhang, D.; Yan, Y.; Cheng, W.; Zhang, W.; Li, Y.; Ju, H.; Ding, S. *Microchim Acta* **2013**, *180*, 397-403.

(96) Qiu, X.; Liu, X.; Zhang, W.; Zhang, H.; Jiang, T.; Fan, D.; Luo, Y. *Analytical Chemistry* **2015**, *87*, 6303-6310.

(97) George, S.; Chaudhery, V.; Lu, M.; Takagi, M.; Amro, N.; Pokhriyal, A.; Tan, Y.; Ferreira, P.; Cunningham, B. T. *Lab on a Chip* **2013**, *13*, 4053-4064.

(98) Tan, Y.; Sutanto, E.; Alleyne, A. G.; Cunningham, B. T. *Journal of Biophotonics* **2014**, *7*, 266-275.

(99) Qavi, A. J.; Bailey, R. C. *Angewandte Chemie International Edition* **2010**, *49*, 4608-4611.

(100) Qavi, A. J.; Kindt, J. T.; Gleeson, M. A.; Bailey, R. C. *Analytical Chemistry* **2011**, *83*, 5949-5956.

(101) Kindt, J. T.; Bailey, R. C. *Analytical Chemistry* **2012**, *84*, 8067-8074.

(102) Erdem, A.; Eksin, E.; Congur, G. *Journal of Electroanalytical Chemistry* **2015**, *755*, 167-173.

(103) Kilic, T.; Nur Topkaya, S.; Ozsoz, M. *Biosensors and Bioelectronics* **2013**, *48*, 165-171.

(104) Li, F.; Peng, J.; Wang, J.; Tang, H.; Tan, L.; Xie, Q.; Yao, S. *Biosensors and Bioelectronics* **2014**, *54*, 158-164.

(105) Tran, H. V.; Piro, B.; Reisberg, S.; Anquetin, G.; Duc, H. T.; Pham, M. C. *Anal Bioanal Chem* **2014**, *406*, 1241-1244.

(106) Tran, H. V.; Piro, B.; Reisberg, S.; Tran, L. D.; Duc, H. T.; Pham, M. C. *Biosensors and Bioelectronics* **2013**, *49*, 164-169.

(107) Wu, X.; Chai, Y.; Yuan, R.; Su, H.; Han, J. *Analyst* **2013**, *138*, 1060-1066.

(108) Wang, Z.; Si, L.; Bao, J.; Dai, Z. *Chemical Communications* **2015**, *51*, 6305-6307.

(109) Li, F.; Peng, J.; Zheng, Q.; Guo, X.; Tang, H.; Yao, S. *Analytical Chemistry* **2015**, *87*, 4806-4813.

(110) Cai, Z.; Song, Y.; Wu, Y.; Zhu, Z.; James Yang, C.; Chen, X. *Biosensors and Bioelectronics* **2013**, *41*, 783-788.

(111) Wang, M.; Li, B.; Zhou, Q.; Yin, H.; Zhou, Y.; Ai, S. *Electrochimica Acta* **2015**, *165*, 130-135.

(112) Xia, N.; Wang, X.; Deng, D.; Wang, G.; Zhai, H.; Li, S.-J. *International journal of Electrochemical Science* **2013**, *8*, 9714-9722.

(113) Labib, M.; Khan, N.; Berezovski, M. V. *Analytical Chemistry* **2015**, *87*, 1395-1403.

(114) Wang, M.; Yin, H.; Fu, Z.; Guo, Y.; Wang, X.; Zhou, Y.; Ai, S. *J Solid State Electrochem* **2014**, *18*, 2829-2835.

(115) Yin, H.; Wang, M.; Zhou, Y.; Zhang, X.; Sun, B.; Wang, G.; Ai, S. *Biosensors and Bioelectronics* **2014**, *53*, 175-181.

(116) Wu, S.; Chen, H.; Zuo, Z.; Wang, M.; Luo, R.; Xu, H. *International journal of Electrochemical Science* **2015**, *10*, 3848-3858.

(117) Liu, L.; Jiang, S.; Wang, L.; Zhang, Z.; Xie, G. *Microchim Acta* **2015**, *182*, 77-84.

(118) Cheng, F.-F.; He, T.-T.; Miao, H.-T.; Shi, J.-J.; Jiang, L.-P.; Zhu, J.-J. *ACS Applied Materials & Interfaces* **2015**, *7*, 2979-2985.

(119) Xia, N.; Zhang, L.; Wang, G.; Feng, Q.; Liu, L. *Biosensors and Bioelectronics* **2013**, *47*, 461-466.

(120) Liu, L.; Xia, N.; Liu, H.; Kang, X.; Liu, X.; Xue, C.; He, X. *Biosensors and Bioelectronics* **2014**, *53*, 399-405.

(121) Xia, N.; Zhang, Y.; Wei, X.; Huang, Y.; Liu, L. *Analytica Chimica Acta* **2015**, *878*, 95-101.

(122) Zhang, Y.; Yan, Y.; Chen, W.; Cheng, W.; Li, S.; Ding, X.; Li, D.; Wang, H.; Ju, H.; Ding, S. *Biosensors and Bioelectronics* **2015**, *68*, 343-349.

(123) Shi, K.; Dou, B.; Yang, C.; Chai, Y.; Yuan, R.; Xiang, Y. *Analytical Chemistry* **2015**, *87*, 8578-8583.

(124) Wu, X.; Chai, Y.; Zhang, P.; Yuan, R. *ACS Applied Materials & Interfaces* **2015**, *7*, 713-720.

(125) Ren, Y.; Deng, H.; Shen, W.; Gao, Z. *Analytical Chemistry* **2013**, *85*, 4784-4789.

(126) Wang, M.; Fu, Z.; Li, B.; Zhou, Y.; Yin, H.; Ai, S. *Analytical Chemistry* **2014**, *86*, 5606-5610.

(127) Zhang, X.; Wu, D.; Liu, Z.; Cai, S.; Zhao, Y.; Chen, M.; Xia, Y.; Li, C.; Zhang, J.; Chen, J. *Chemical Communications* **2014**, *50*, 12375-12377.

(128) Hong, C.-Y.; Chen, X.; Liu, T.; Li, J.; Yang, H.-H.; Chen, J.-H.; Chen, G.-N. *Biosensors and Bioelectronics* **2013**, *50*, 132-136.

(129) Li, C.; Liu, Z.; Cai, S.; Wen, F.; Wu, D.; Liu, Y.; Wu, F.; Lan, J.; Han, Z.; Chen, J. *Electrochemistry Communications* **2015**, *60*, 185-189.

(130) Xiang, G.; Jiang, D.; Luo, F.; Liu, F.; Liu, L.; Pu, X. *Sensors and Actuators B: Chemical* **2014**, *195*, 515-519.

(131) Wu, X.; Chai, Y.; Yuan, R.; Zhuo, Y.; Chen, Y. *Sensors and Actuators B: Chemical* **2014**, *203*, 296-302.

(132) Yang, C.; Shi, K.; Dou, B.; Xiang, Y.; Chai, Y.; Yuan, R. *ACS Applied Materials & Interfaces* **2015**, *7*, 1188-1193.

(133) Peng, Y.; Jiang, J.; Yu, R. *Analytical Methods* **2014**, *6*, 2889-2893.

(134) Wang, M.; Shen, B.; Yuan, R.; Cheng, W.; Xu, H.; Ding, S. *Journal of Electroanalytical Chemistry* **2015**, *756*, 147-152.

(135) Yao, B.; Liu, Y.; Tabata, M.; Zhu, H.; Miyahara, Y. *Chemical Communications* **2014**, *50*, 9704-9706.

(136) Tian, Q.; Wang, Y.; Deng, R.; Lin, L.; Liu, Y.; Li, J. *Nanoscale* **2015**, *7*, 987-993.

(137) Yan, Y.; Zhao, D.; Yuan, T.; Hu, J.; Zhang, D.; Cheng, W.; Zhang, W.; Ding, S. *Electroanalysis* **2013**, *25*, 2354-2359.

(138) Yu, Y.; Chen, Z.; Shi, L.; Yang, F.; Pan, J.; Zhang, B.; Sun, D. *Analytical Chemistry* **2014**, *86*, 8200-8205.

(139) Lin, M.; Wen, Y.; Li, L.; Pei, H.; Liu, G.; Song, H.; Zuo, X.; Fan, C.; Huang, Q. *Analytical Chemistry* **2014**, *86*, 2285-2288.

(140) Miao, P.; Wang, B.; Chen, X.; Li, X.; Tang, Y. *ACS Applied Materials & Interfaces* **2015**, *7*, 6238-6243.

(141) Miao, P.; Wang, B.; Meng, F.; Yin, J.; Tang, Y. *Bioconjugate Chemistry* **2015**, *26*, 602-607.

(142) Ge, Z.; Lin, M.; Wang, P.; Pei, H.; Yan, J.; Shi, J.; Huang, Q.; He, D.; Fan, C.; Zuo, X. *Analytical Chemistry* **2014**, *86*, 2124-2130.

(143) Wan, J.; Liu, X.; Zhang, Y.; Gao, Q.; Qi, H.; Zhang, C. *Sensors and Actuators B: Chemical* **2015**, *213*, 409-416.

(144) Zhou, Y.; Wang, M.; Xu, Z.; Ni, C.; Yin, H.; Ai, S. *Biosensors and Bioelectronics* **2014**, *54*, 244-250.

(145) Meng, X.; Zhou, Y.; Liang, Q.; Qu, X.; Yang, Q.; Yin, H.; Ai, S. *Analyst* **2013**, *138*, 3409-3415.

(146) Labib, M.; Khan, N.; Ghobadloo, S. M.; Cheng, J.; Pezacki, J. P.; Berezovski, M. V. *Journal of the American Chemical Society* **2013**, *135*, 3027-3038.

(147) Erdem, A.; Congur, G. *Talanta* **2014**, *118*, 7-13.

(148) Bartosik, M.; Hrstka, R.; Palecek, E.; Vojtesek, B. *Analytica Chimica Acta* **2014**, *813*, 35-40.

(149) Cheng, F.-F.; Zhang, J.-J.; He, T.-T.; Shi, J.-J.; Abdel-Halim, E. S.; Zhu, J.-J. *Analyst* **2014**, *139*, 3860-3865.

(150) Zhang, J.; Wu, D.-Z.; Cai, S.-X.; Chen, M.; Xia, Y.-K.; Wu, F.; Chen, J.-H. *Biosensors and Bioelectronics* **2016**, *75*, 452-457.

(151) Wang, Z.; Zhang, J.; Guo, Y.; Wu, X.; Yang, W.; Xu, L.; Chen, J.; Fu, F. *Biosensors and Bioelectronics* **2013**, *45*, 108-113.

(152) Campuzano, S.; Torrente-Rodríguez, R. M.; López-Hernández, E.; Conzuelo, F.; Granados, R.; Sánchez-Puelles, J. M.; Pingarrón, J. M. *Angewandte Chemie International Edition* **2014**, *53*, 6168-6171.

(153) Si, Y.; Sun, Z.; Zhang, N.; Qi, W.; Li, S.; Chen, L.; Wang, H. *Analytical Chemistry* **2014**, *86*, 10406-10414.

(154) Lu, N.; Gao, A.; Dai, P.; Song, S.; Fan, C.; Wang, Y.; Li, T. *Small* **2014**, *10*, 2022-2028.

(155) Cai, B.; Huang, L.; Zhang, H.; Sun, Z.; Zhang, Z.; Zhang, G.-J. *Biosensors and Bioelectronics* **2015**, *74*, 329-334.

(156) Ramnani, P.; Gao, Y.; Ozsoz, M.; Mulchandani, A. *Analytical Chemistry* **2013**, *85*, 8061-8064.

(157) Lujambio, A.; Lowe, S. W. *Nature* **2012**, *482*, 347-355.

(158) Li, Y.; Qiu, C.; Tu, J.; Geng, B.; Yang, J.; Jiang, T.; Cui, Q. *Nucleic Acids Research* **2014**, *42*, D1070-D1074.

(159) Agarwal, V.; Bell, G. W.; Nam, J.-W.; Bartel, D. P. *eLife* **2015**, *4*.

(160) Khorshid, M.; Hausser, J.; Zavolan, M.; van Nimwegen, E. *Nat Meth* **2013**, *10*, 253-255.

(161) Marín, R. M.; Šulc, M.; Vaníček, J. *RNA* **2013**, *19*, 467-474.

(162) Peterson, S. M.; Thompson, J. A.; Ufkin, M. L.; Sathyanarayana, P.; Liaw, L.; Congdon, C. B. *Frontiers in Genetics* **2014**, *5*.

Chapter 3

PCR-FREE, MULTIPLEXED EXPRESSION PROFILING OF MICRORNAS USING SILICON PHOTONIC MICRORING RESONATORS

Acknowledgments:

This chapter has been adapted from the article "PCR-Free, Multiplexed Expression Profiling of microRNAs using Silicon Photonic Microring Resonators" (Graybill, R.M.; Para, C.S.; Bailey, R.C. *Analytical Chemistry* **2016,** *88*, 10347-10351. It has been reproduced here with permission from the American Chemical Society © 2016.

The authors gratefully acknowledge financial support from the National Cancer Institute of the Institutes of Health through Grant R33CA1774 and the National Science Foundation through Grant CHE 12-14081. RMG acknowledges support from the National Cancer Institute Alliance for Nanotechnology in Cancer 'Midwest Cancer Nanotechnology Training Center' Grant R25 CA154015A. We also appreciate the support provided through UIUC's Institute for Genomic Biology.

The original article accessed online at:
http://pubs.acs.org/doi/abs/10.1021/acs.analchem.6b03350

3.1 Introduction

MicroRNAs (miRNAs) constitute an important class of non-coding RNAs that regulate gene expression at the transcriptional and post-transcriptional level. As potent gene regulators, miRNAs have been linked to important developmental processes that establish and maintain tissue differentiation.[1,2] Not surprisingly, miRNA expression in tissue and blood samples is associated with disease and has substantial diagnostic utility.[3,4] However, the short sequence lengths, large variability in per-cell copy number, and high sequence similarity within families of expressed miRNAs conspire to make them challenging analytical targets. Furthermore, miRNAs often function in complex regulatory networks whereby many miRNAs work cooperatively to regulate the expression of a single mRNA transcript. However, each miRNA may be involved in many different transcript-targeting regulatory networks. Therefore, the multiplexed detection of many miRNAs simultaneously is an important consideration for both fundamental and translational application of miRNA analysis technologies. For clinical applications, these complications are further exacerbated by technical and practical requirements, including small sample sizes, low cost, and relative ease of use. Therefore, candidate miRNA detection technologies need to offer: high sensitivity; wide dynamic range; high sequence specificity; multiplexing capability; and minimal sample processing and handling.[5]

Current miRNA detection techniques are lacking in one, or more, of these attributes. Specifically, reverse transcription-quantitative polymerase chain reaction (RT-qPCR) methods are incredibly sensitive, relatively rapid, and cost effective; however, they typically measure levels of only a single miRNA sequence per assay. Conversely, microarrays are well-suited to multiplexed analyses but are typically slow, less sensitive, more expensive, and require PCR amplification, which can introduce sequence biases. Next-generation sequencing technologies

give a comprehensive picture of miRNA expression levels; however, this global approach, which requires complex library construction and onerous informatics, is both time- and cost-prohibitive for many diagnostic applications. Moreover, advances in database informatics have found that reduced subsets of miRNAs can be identified that offer robust and actionable diagnostic utility.[6] Therefore, technologies that can robustly determine expression levels of targeted panels of miRNAs from a single, clinically-relevant sample could be important in the widespread realization of translational miRNA-based diagnostics.

Silicon photonic microring resonators, which belong to a larger class of whispering gallery biosensors,[7] are an intrinsically multiplexable, array-based technology that has been applied to a range of biomolecular detection applications.[8-13] The operational theory and measurement instrumentation behind the technology has been previously discussed in detail.[14-15] Briefly, a tunable wavelength laser centered around 1550 nm is coupled into linear waveguides via on chip grating couplers. The laser is swept through the appropriate spectral window to determine wavelengths of optical resonance. Changes in the local refractive index near the sensor surface induced by biomolecular binding cause a shift in the resonance, with shifts directly proportional to the amount of surface bound biomolecules, which in turn reflects the solution phase analyte concentration. A more detailed description of this technology is presented in the Supporting Information.

Our group previously demonstrated the detection of miRNAs using microring resonators in both a label-free[16] and capture-agent-enhanced[17] assay format, the latter using a DNA:RNA heteroduplex-specific antibody. Here we report a sandwich-based detection protocol that uses reverse transcription to create cDNA products of targeted miRNAs that are subsequently detected using an enzymatic chemical signal enhancement strategy. Compared to prior work

from our group,[17] we report improved limits of detection, increased levels of multiplexing, but most dramatically, an ~85% reduction in analysis time (from 12-15 hours to 2.5 hours). To our knowledge, this is the first report that directly detects cDNA products resulting from miRNA reverse transcription using specific stem loop primers (SLP), rather than being integrated with the standard RT-qPCR framework, which has intrinsic limits in terms of multiplexing capacity. We demonstrate the broad applicability of this approach by profiling the expression levels of 7 miRNAs, and an off target control sequence, to differentiate between different tissue types, showing good correlation with previous RT-qPCR analyses.

3.2 Experimental Details

3.2.1 Materials

UltraPure DEPC-treated water (Life Technologies) was used for all experiments. A 10X PBS buffer (pH 7.4) was diluted to 1X and used to reconstitute all nucleic acid samples. A high stringency hybridization buffer consisting of 30% formamide, 0.2% sodium dodecyl sulfate, 4× saline−sodium phosphate−ethylenediaminetetraacetic acid (EDTA) buffer (SSPE, USB Corp.), and 3× Denhardt's solution (Invitrogen) was used for all nucleic acid hybridization steps. A PBS running buffer (pH 7.4) was reconstituted with 0.05% Tween20 and was used to dilute all protein containing steps. The silane (3-aminopropyl)triethoxysilane (APTES) was purchased from Fisher. All custom synthesized nucleic acid sequences were obtained from Integrated DNA Technologies (IDT; Coralville, Iowa). Nucleic acid sequences are included in Table 3.1. miRNA RT-PCR kits used for RT-qPCR profiling were purchased from Life Technologies, and target specific assay IDs are listed in Table 3.2. Drycoat Assay Stabilizer solution was purchased from Virusys Corporation and used as received. Streptavidin-conjugated horseradish peroxidase (SA-

HRP), one-step 4-chloro-1-napthol solution, and all other reagents were purchased from ThermoFisher and used as received.

3.2.2 Instrumentation

Sensor chips and read-out instrumentation were obtained from Genalyte, Inc. (San Diego, CA). Sensor chips were fabricated at a silicon foundry on 8 in. silicon-on-insulator wafers using deep UV photolithography and dry etch methods, spin-coated with a fluoropolymer cladding layer, and diced into individual 4 × 6 mm chips, each having an array of 132 individually addressable microrings. The fluoropolymer cladding is selectively removed from 128 of the rings, leaving these exposed to the solution and responsive to binding events. The four occluded rings serve as control elements for subtracting thermal drift. Chips were fitted with a laser etched Mylar gasket, which defines flow chambers when sandwiched with a Teflon lid, and loaded into the readout instrumentation. All experiments were performed with automated fluidic handling using the recipes summarized in Table 3.3.

Resonant wavelengths for each microring were determined by coupling a tunable laser source (centered at 1560 nm) into an adjacent linear waveguide via on-chip grating couplers. The laser output was then swept through an appropriate spectral window and the light intensity at the distal end of the linear waveguide was used to determine the resonance wavelength. This process was then serially repeated for each ring in the array, and the resultant shifts in resonance as a function of time were recorded.

The resonance condition that is supported by the microring resonators is governed by the following equation:

$$m\lambda = 2\pi r n_{eff}$$

where m equals a nonzero integer, λ is the wavelength of propagating light, r is the microring radius, and n_{eff} is the effective refractive index of the local microring environment. Boundary conditions of light propagating in linear waveguides via total internal reflectance result in an evanescent field extending into a region very close to the ring surface. Interactions between the evanescent field and the local environment cause a change in the resonant wavelength, which is then monitored by the optical scanning instrumentation. Therefore, the binding of higher refractive index biomolecules and accompanying displacement of water results in a resonance shift to longer wavelengths: a positive shift that is listed in units of Δ picometers (Δpm).

3.2.3 Sensor Surface Functionalization with Capture Probes

Prior to covalent modification of capture probes, sensor chips were cleaned in a piranha solution (3:1 H_2SO_4/30% H_2O_2) for 35 seconds. (Caution: Piranha solutions are extremely dangerous and react explosively with organics.) Following a 2 min rinse in acetone, chips were incubated in APTES (5% in acetone) for 4 minutes. After rinsing sensor chips in acetone (2 min) followed by IPA (2 min), a bis(sulfosuccinimidyl)suberate solution (25 μL, 2.85 mg/mL in acetic acid), an amino-to-amine crosslinker, was pipetted onto the sensor surface and left to incubate for 3 minutes. Chips were dried with N_2, and then small aliquots (300 nL) of an aminated DNA capture probe specific to an individual miRNA target were deposited onto the microring surface so that the solution covers a specific set of microrings. The chips were left in a humidity chamber (1 hour). Then, they were rinsed in Drycoat Assay Stabilizer solution and stored at 4°C until use.

3.2.4 Preparation and Addition of miRNA Target to Sensor Surface

Target miRNA solutions were first reverse transcribed according to the manufacturer's protocol (TaqMan microRNA Reverse Transcription Kit, Life Technologies) using the following

thermal profile: 16°C (30 min), 42°C for (30 min), and 85°C (5 min). Following reverse transcription, the solution was incubated in equal volume alkaline hydrolysis buffer (50 mM Na_2CO_3, 1 mM EDTA, pH 8.5) at 95°C for 30 min. An aliquot of this solution was then diluted 100 fold in hybridization buffer (4 μL sample aliquot in 396 μL hyb) and to that a biotinylated DNA probe (0.4 μL, 200 μM) that is complimentary to the "stem" region of the stem loop primer is added. This solution is incubated at 72°C for 10 min. After incubation, the solution is allowed to cool back to room temperature and loaded into a 96 well plate for subsequent analysis on chip.

For on chip analysis, the diluted miRNA target sequences were flowed at 15 μL/min for 14 min. For total RNA analysis, the solution was allowed to hybridize for 25 minutes. A sensor baseline was established before and after hybridization by flowing hybridization buffer (30 μL/min) for 3 min and 1 min respectively.

3.2.5 Horseradish Peroxidase Enzymatic Amplification

Following miRNA hybridization, a PBST (0.05% Tween20) solution is flowed across the surface (30 μL/min) for 5 minutes to establish a new baseline resulting from the running buffer change. Afterwards, a solution of SA-HRP (4 μg/mL) is introduced (30 μL/min, 3 min) and binds to the biotinylated compliment that is bound on the sensor surface. This is followed by another PBST rinse (30 μL/min, 2 min) to prepare the surface for 4-CN precipitation. 4-CN is then introduced to the sensor (30 μL/min) for 9 min, and a final buffer rinse (30 μL/min) is conducted for 3 min to establish the net sensor response before and after 4-CN amplification. It is important to note that the surface can be regenerated on the microring sensor chips without a decrease in performance.

*Complete outline of automated fluidic handling shown in Table 3.3.

3.2.6 Total RNA Samples

Both brain (Lot No. 1307018) and lung (Lot No. 1410019) total RNA samples isolated from patient tissue were obtained commercially (Life Technologies) and stored at -80°C until further use. Samples were thawed on ice for approximately 2 hours prior to use, and a 1 µg and 100 ng input amount was used for microring and RT-qPCR analysis respectively.

3.2.7 Data Analysis

Data analysis was performed using Origin Pro 9.0. All data was corrected for temperature drift, bulk refractive index shifts and differential sensor response by subtracting the response of control rings functionalized with a non-complementary capture probe from the active rings. To calculate the initial slope of DNA binding, we used a modified 1:1 Langmuir Binding Isotherm, as described by:

$$S(t) = A(1 - e^{-B(t-t_0)})$$

To determine the initial slope of the binding response, the first derivative of the previous equation was evaluated at $t = t_0$, yielding:

$$\frac{dS}{dt} = AB$$

The average of the initial slopes was taken over a number of sensors for each concentration. As a general rule, the first 5 minutes of collected data was used to obtain the fit. For low concentrations where the modified Langmuir Binding Isotherm could not effectively fit the sensor trace, a linear fit was used to approximate the initial slope.

3.2.8 RT-qPCR

For RT-PCR experiments, total RNA (100 ng) was used. Reverse transcription was performed using TaqMan microRNA Reverse Transcription Kit (Life Technologies) and miRNA-specific stem loop primers provided in the kit (see Table S2 for miRNA specific Assay IDs). Reverse Transcription was carried out on a BioRad T100 Thermal cycler at 16°C (30 min), 42°C for (30 min), and 85°C (5 min). RT products were then subjected to quantitative PCR in triplicate using PCR primers from the same miRNA Assay Kit. The reaction was performed at 95°C (10 min), followed by 40 two-step cycles of (1) 95°C for 15 s and (2) 60°C for 1 min. All quantitative PCR work was done using an Applied Biosystems 7900HT Fast Real-Time PCR System. All procedures and reactions were carried out according to the protocols provided by the manufacturer. Levels of miRNAs were normalized to miR-26a, and fold change was calculated using the 2^(-ΔΔCt) method.

3.3 Results and Discussion

A schematic of the reverse transcription-horseradish peroxidase (RT-HRP) assay is shown in Figure 3.1. SLPs are designed with a universal stem loop sequence and a 7-8 nucleotide overhang sequence specific for particular miRNA targets. Hybridization of the miRNA target to the SLP followed by extension via reverse transcription yields the DNA complement to the miRNA sequence. The miRNA is then degraded via base hydrolysis (Figure 3.2) leaving the RT product accessible to bind to the capture probe attached to the sensor surface. Without degradation, the hybridized miRNA can block the capture probe recognition site on the RT product (Figure 3.3).

After extension and RNA degradation (RT SLP), a biotinylated tag sequence of DNA complementary to the conserved stem loop region common to all of SLPs was added to the

solution containing RT products. This solution is incubated at 72°C, which allows for the stem loop sequence to linearize and hybridize to the tag. SLPs were designed with a one base pair mismatch in the stem region so that tag-RT SLP complexes are thermodynamically preferred over the secondary structure of the SLPs themselves (T_m of tag-RT SLP > T_m SLP secondary structure). In this way, the complex remains linear and able to hybridize to surface-bound capture probes on the microring sensors, leading to a 20-fold increase in sensitivity when compared to results obtained using conventional stem loop primers with the RT-HRP assay (Figure 3.3). Importantly, this strategy is capable of targeting multiple miRNAs in a single sample volume by adding multiple SLP sequences to the initial RT reaction and presents a streamlined sample preparation process that consists of only 3 incubation steps over the course of ~1.75 hours.

The HRP-enhanced sensing strategy of the target sequences is shown in Figure 3.1B. While we have previously utilized HRP signal amplification for protein detection,[11] this is the first report to use HRP for the detection of miRNAs. The solution containing tag-RT SLPs is diluted in a high stringency hybridization buffer to ensure complementary binding and then flowed across an array of microring sensors uniquely-functionalized with target-specific DNA capture sequences. Additionally, capture probes were designed to avoid hybridization with non-extended SLPs. After hybridization of tag-RT SLPs to the ssDNA capture probes and a streptavidin-HRP conjugate was flowed across the sensor surface. A solution of 4-chloro-1-napthol (4-CN) was then introduced and enzymatically converted into insoluble 4-chloro-1-napthon (4-CNP) by bound HRP. The deposition of the 4-CNP precipitate causes a dramatic shift in the resonance wavelengths of the microrings (measured in Δpicometers; Δpm) that is directly related to the number of surface bound HRP moieties and thus the concentration of target miRNAs in the original sample matrix.

To demonstrate the quantitative ability of the developed scheme, we exposed the microring sensors functionalized with a target specific capture probe to 7 cDNA product solutions of the miRNA target ranging in initial concentrations from 2 μM to 2 nM, as well as a blank (no input RNA). Calibration curves were generated by diluting synthetic miRNA sequences to the different concentrations, subjecting these solutions to the RT-HRP protocol, and quantitating the initial slope of the HRP amplification response. Figure 3.4A shows representative binding curves that were used to compile the calibration curves in Figure 3.4B. Clear concentration-dependent responses were seen across a 4 order of magnitude dynamic range, as shown in Figure 3.4B, which also lists the determined limits of detection for each target sequence.

Next, we show the applicability of this approach for multiplexed measurements of seven different miRNA targets. Notably, the use of the conserved region on the biotinylated stem loop primers as a universal recognition element reduces assay complexity by eliminating the need for multiple tagging sequences. Microring resonators were spatially arrayed via functionalization with eight unique capture probes (7 specific to miRNA targets and one negative control). Seven chips were identically functionalized and each exposed to solutions containing the RT-product of individual miRNAs at a constant input of 10 picomoles. This process was repeated for each of the seven miRNA targets, and the compiled results are shown in Figure 3.5. Each column in the figure represents a different sensor array incubated with the RT product of the target on the column heading. As can be seen, this detection approach had high sequence specificity for the targeted miRNAs and minimal cross-reactive response.

To demonstrate that this approach is able to probe more complex samples, and also to benchmark the assay against gold standard techniques (i.e. RT-qPCR), we simultaneously

profiled the expression of seven miRNAs from brain and lung total RNA samples (Figure 3.6). The detected concentrations are shown in Figure 3.7A. Likewise, we used RT-qPCR to compile expression profiles from the same sample (see Table 3.4 for C(t) values). After normalizing both data sets by dividing by the concentration measured for miR-26a, which corrects for sampling differences,[17] the fold change of brain:lung miRNA expression was determined and plotted in Figure 3.7B, together with ratios calculated based upon a previous study.[18]

The relatively large fold-change deviations for miR-219 might be explained by the fact that the low overall expression levels cause the analysis to approach the C(t) cutoff threshold for reliable detection using RT-qPCR, and also increase the microring measurements susceptibility to any analytical errors. That said, both platforms are in agreement with the literature that miRNA-219 is more abundant in brain tissue.[19] Similarly, the detection of miR-21 could also be unreliable since it is an oncogene that is upregulated during cancer progression,[20] whereas the samples analyzed were not from cancer patients. Interestingly though, if the expression is assumed to be one order of magnitude lower than our limit of detection, the brain:lung fold change correlates well with literature precedent,[18] as well as our in-house RT-qPCR measurements.

3.4 Conclusions

In conclusion, we have developed a new approach for the sensitive and multiplexed analysis of miRNAs using a reverse-transcription-enabled enzymatic signal enhancement strategy coupled with detection using silicon photonic microring resonators. While only shown for seven targets here, this technology is capable of delivering significantly higher levels of multiplexing, which exceed that of many other emerging miRNA detection strategies.[5] Moreover, this type of platform offers the capacity to analyze for panels of miRNAs not easily

accessible via RT-qPCR while avoiding the cost and informatics required for RNA sequencing, and therefore may be well-positioned to fit an important niche in helping translate miRNA-based diagnostics to the clinic. Future efforts to further improve the analytical performance metrics of the methods will be required in addition to more clinically- relevant demonstrations more closely-targeted to specific disease diagnoses and from expanded patient cohorts.

3.5 FIGURES AND TABLES

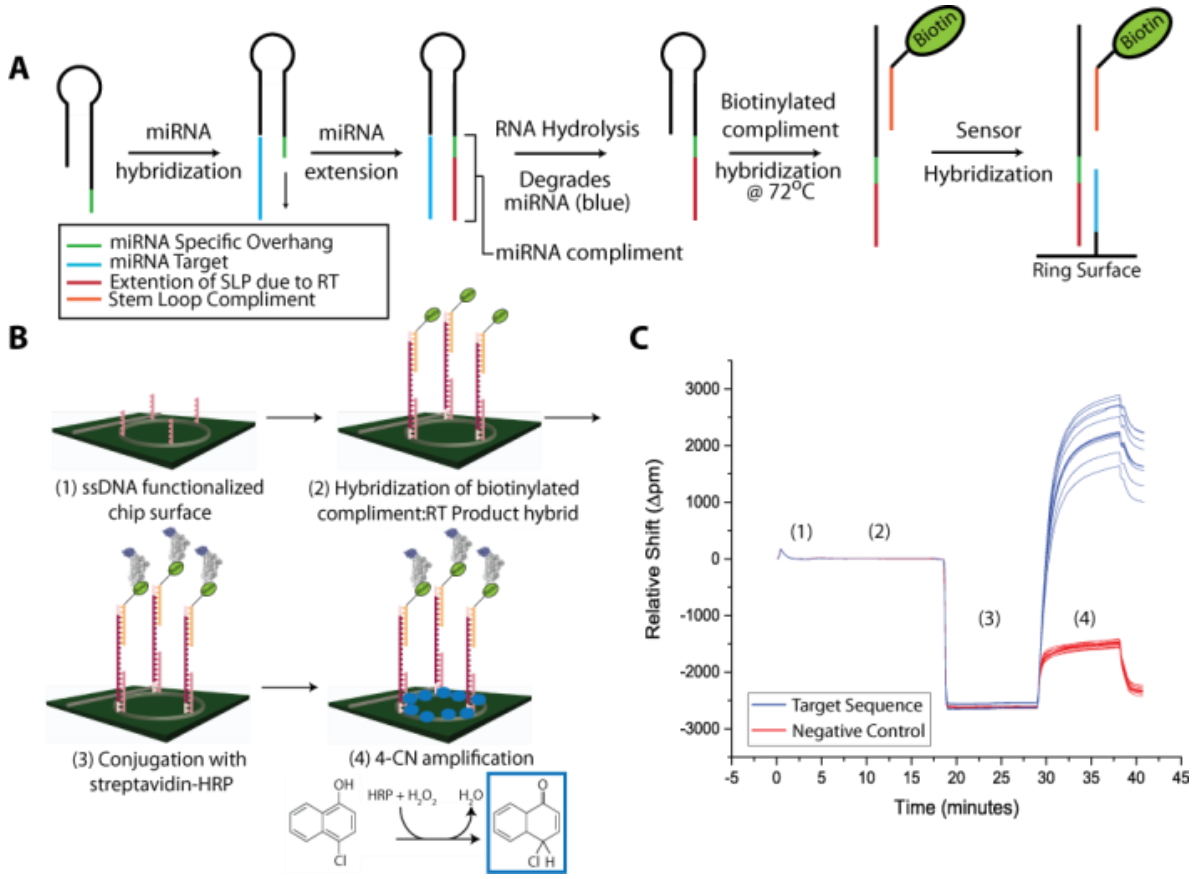

Figure 3.1: A) Schematic diagram of miRNA processing to prepare for on chip detection. **B)** Illustration of RT product detection and HRP signal amplification. **C)** The representative binding curve shows data corresponding to the detection of a 10 picomole miRNA-26a sample subjected to the workflow in A and B. The large signal gain at 30 minutes is obtained from the 4-chloro-1-napthon deposition.

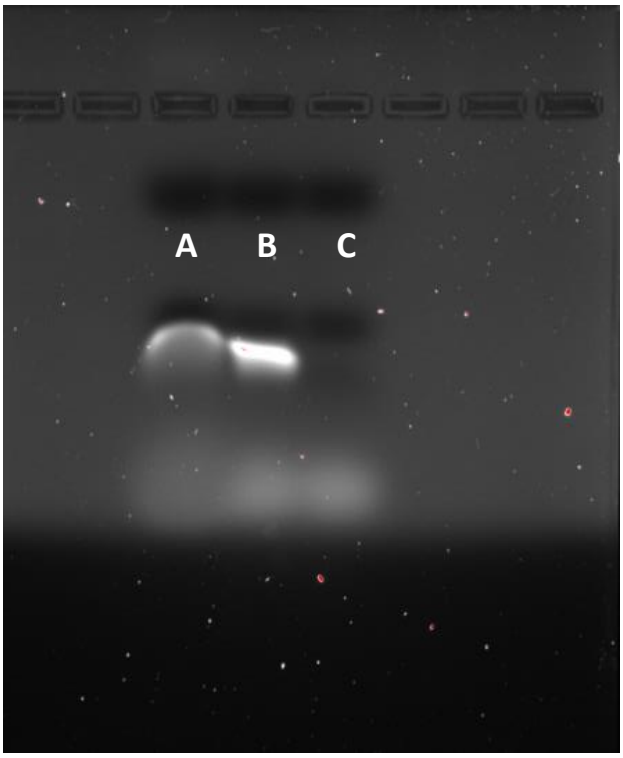

Figure 3.2: Agarose gel analysis hydrolysis buffer efficiency. Three samples were analyzed on an ethidium bromide stained 2% agarose gel (0.5x TBE running buffer) to assess the efficiency of the alkaline hydrolysis buffer. Lanes A and B show samples that have been reverse transcribed (30 picomole input of miR-26a) and incubated with either alkaline hydrolysis buffer (lane A) or water (lane B). This result confirms that the alkaline hydrolysis buffer successfully hydrolyzes the RNA. The band intensity analysis (ImageJ) shows that the hydrolyzed sample is approximately 50% less intense than the control group.

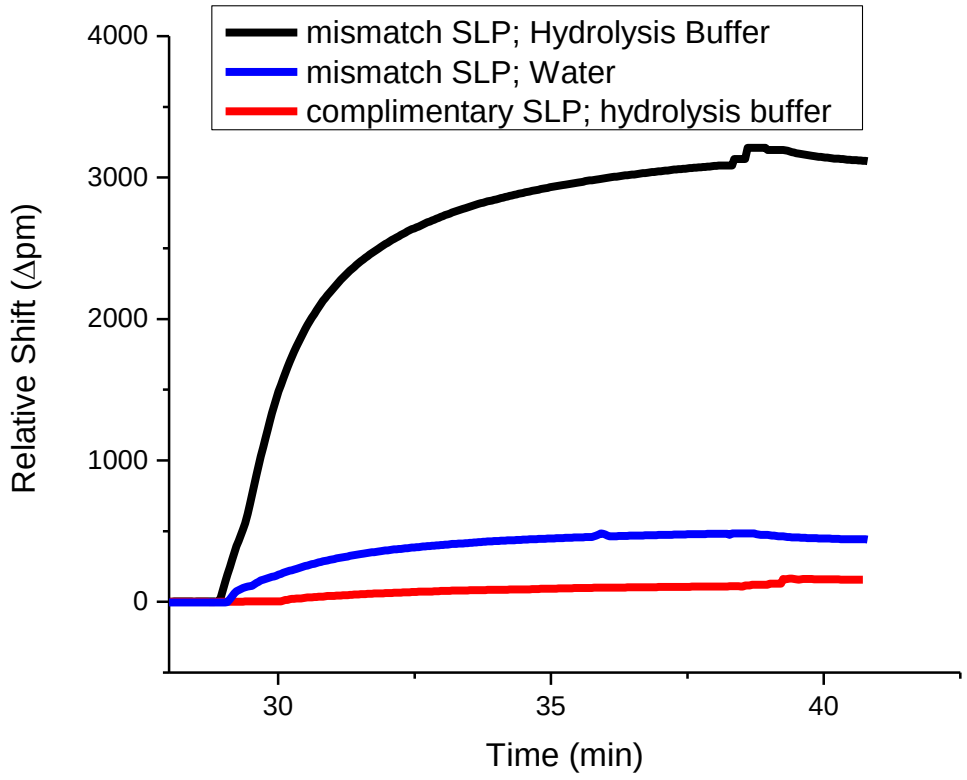

Figure 3.3: Effect of alkaline hydrolysis buffer and stem loop primer construction on sensor response. A 10 picomole input of miRNA-26a was used and subjected to the RT-HRP assay under three different conditions. The response for experiments that had a perfectly complimentary SLP (T_m = 79.6°C) showed no binding response as the probe was not linearized and able to bind to the sensor surface. Responses were observed when a single nucleotide mismatch was introduced into the SLP design (T_m = 61.8°C); however, the signal was dramatically increased when the miRNA was degraded using hydrolysis buffer. These results show that the stem loop primer choice and miRNA degradation via alkaline hydrolysis are essential steps in the assay design.

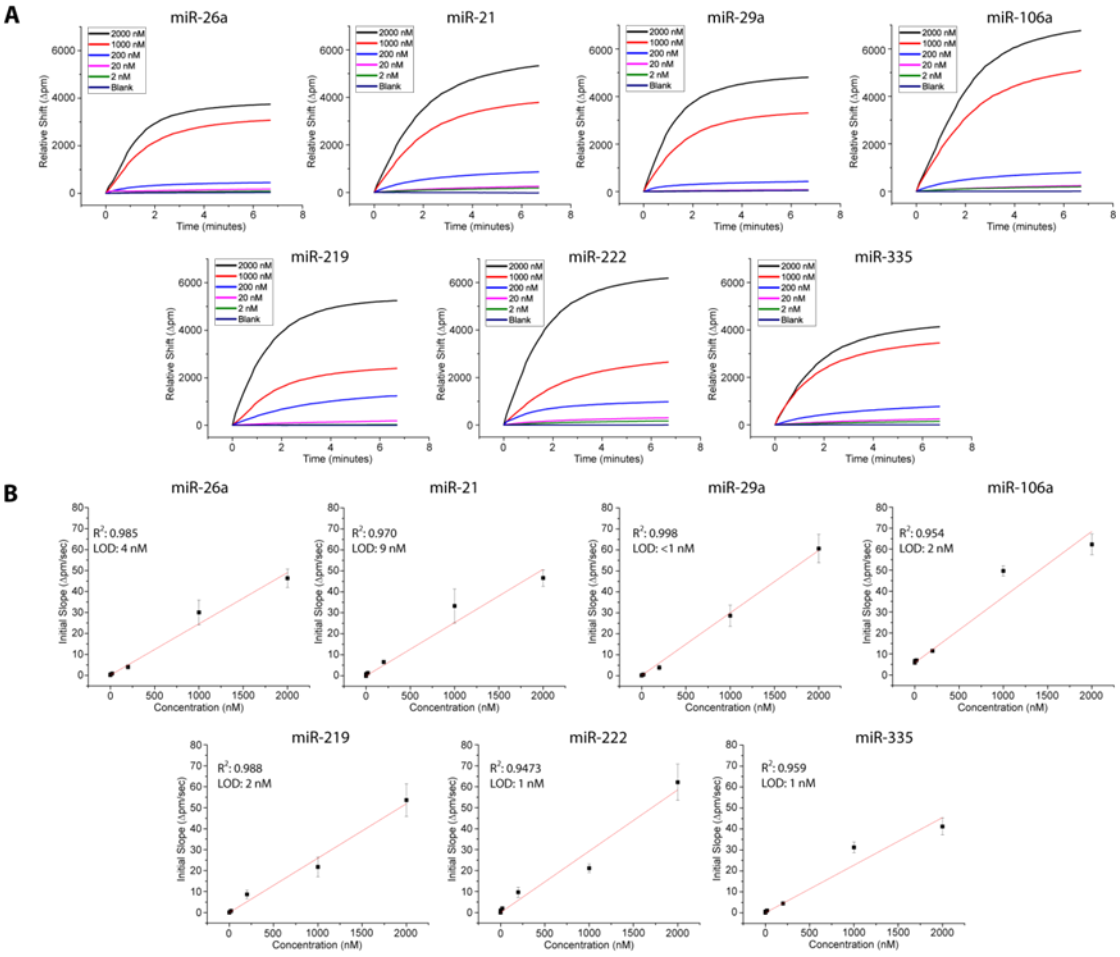

Figure 3.4: A) Overlay of the signal responses achieved for each concentration dilution of target miRNA cDNA product. Initial concentrations utilized were: 2 μM (black), 1 μM (red), 200 nM (blue), 20 nM (pink), 2 nM (green), and a blank (purple). **B)** Calibration curves for the HRP response of each miRNA target. The red curves represent linear fits of the initial slope of the HRP amplification step. Error bars represent the standard deviation of between 8 and 20 technical replicates at each concentration.

Figure 3.5: Detection of specific miRNA target products with minimal off target response from non-complementary capture probes. Each column represents a sensor chip arrayed with different capture probes and exposed to the miRNA RT product listed as the column heading. Each row represents the response at the target-specific microring exposed to the different RT-products in different experiments. Importantly, sensors only show responses at the when exposed to the specifically-targeted miRNA RT product, demonstrating the potential for multiplexed miRNA measurements.

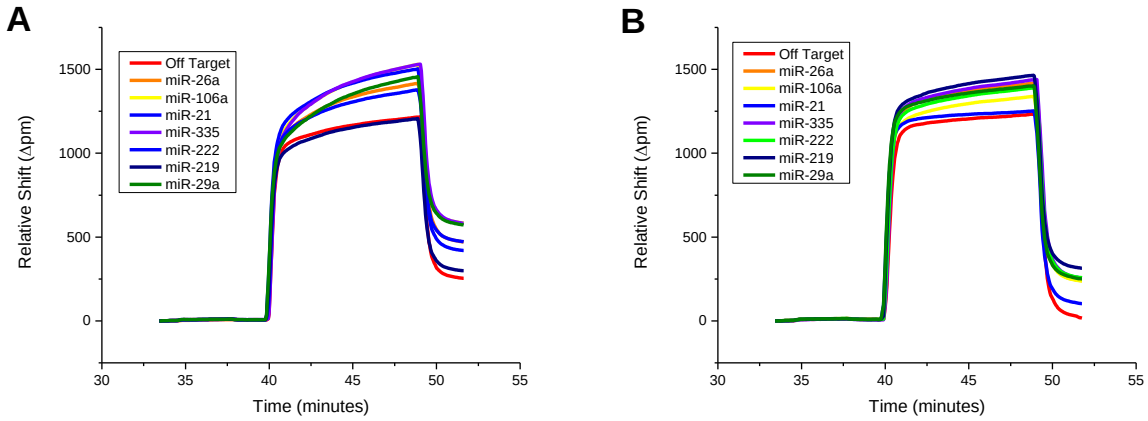

Figure 3.6: Microring sensor response of total RNA profiling from lung and brain tissue. Microrings previously functionalized with 8 different capture probes (7 complimentary to a specific miRNA target and one off target control) were subjected to the optimized assay. The resulting shifts were quantitated by taking the difference before and after 4-CN oxidation. (A) Binding curves obtained when using an input of 1 μg of total RNA isolated from lung tissue. (B) Binding curves obtained when using an input of 1 μg of total RNA isolated from brain tissue.

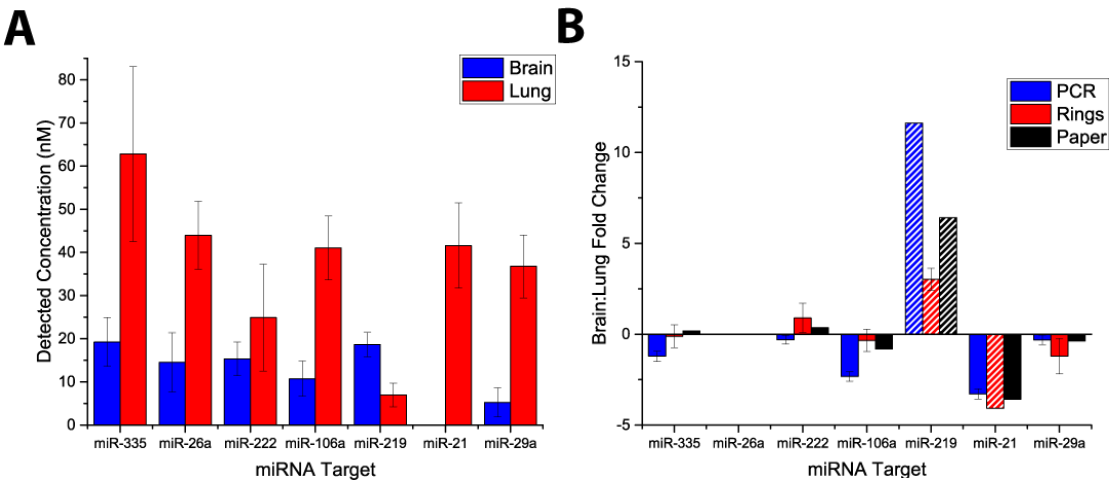

Figure 3.7: A) Comparison of the concentrations for each of the 7 targets (n=8-16 technical replicates). **B)** Comparison of miRNA expression profiles obtained using microrings and RT-qPCR normalized to miR-26a expression.

	Sequence
hsa miRNA-26a	UUC AAG UAA UCC AGG AUA GGC U
hsa miRNA-106a	AAA AGU GCU UAC AGU GCA GGU AG
hsa miRNA-21	UAG CUU AUC AGA CUG AUG UUG A
hsa miRNA-222	AGC UAC AUC UGG CUA CUG GGU CUC
hsa miRNA-335	UCA AGA GCA AUA ACG AAA AAU GU
hsa miRNA-219	UGA UUG UCC AAA CGC AAU UCU
hsa miRNA-29a	UAG CAC CAU CUG AAA UCG GUU A
Conserved region of stem loop primer	GTC GTA TCC AGT GCA GGG TCC GAG GTA TTC GCA CTT GGA TAC GAC … miRNA specific overhang
miR-26a SLP Overhang	AGCCTATCC
miR-106a SLP Overhang	CTACCTGCA
miR-21 SLP Overhang	TCAACATCAG
miR-222 SLP Overhang	GAGACCCAG
miR-335 SLP Overhang	ACATTTTTCG
miR-219 SLP Overhang	AGAATTGC
miR-29a SLP Overhang	TAACCGATTT
miR-26a Capture Probe	TTC AAG TAA TCC AGG ATA GGC TGT
miR-106a Capture Probe	AAA AGT GCT TAC AGT GCA GGT AGG
miR-21 Capture Probe	TAG CTT ATC AGA CTG ATG TTG AGT
miR-222 Capture Probe	AGC TAC ATC TGG CTA CTG GGT C
miR-335 Capture Probe	TC AAG AGC AAT AAC GAA AAA TGT GT
miR-219 Capture Probe	TGA TTG TCC AAA CGC AAT TCT GT
miR-29a Capture Probe	TAG CAC CAT CTG AAA TCG GT
Control Capture Probe	/5AmMC12/CTACAAGTGCCTTCACTGCAGT
Stem Loop Primer Compliment	5’-biotinTEG-ATACCTCGGACCCTGCACT-3’

Table 3.1: Summary of nucleic acid sequences

Target	Assay ID
miR-26a	000405
miR-106a	002169
miR-21	000397
miR-222	000525
miR-335	000546
miR-219	000522
miR-29a	002112

Table 3.2: RT-qPCR assay IDs for miRNA targets (sequences not provided by vendor)

Step	Flow Rate (μL/min)	Duration (min)
Hybridization Buffer	30	3
RT Product	15	14*
Hybridization Buffer	30	1
0.05% PBST	30	5
SA-HRP (4 μg/mL)	30	3
0.05% PBST	30	2
4-CN	30	9
0.05% PBST	30	3

*For total RNA profiling, the duration was increased to 25 minutes, which improved hybridization specificity.

Table 3.3: Details on fluid flow conditions used in the assay

Target	Brain Sample C(t)	Std. Dev.	Lung Sample C(t)	Std. Dev.
miR-26a	21.92	0.23	17.46	0.03
miR-106a	26.33	0.11	19.54	0.04
miR-21	24.78	0.13	17.04	0.05
miR-222	29.00	0.16	23.33	0.03
miR-335	24.78	0.05	20.01	0.03
miR-219	27.56	0.05	34.72	0.28
miR-29a	22.52	0.12	17.74	0.03

Table 3.4: The brain and lung RNA samples used in Figure S3 were subjected to RT-qPCR analysis. Each sample was reverse transcribed (100 ng input) and subjected to PCR in triplicate. Outlined in the table are the average C(t) values and the standard deviation of the measurements for individual miRNA targets.

3.6 References

(1)Wienholds, E.; Kloosterman, W.P.; Miska, E.; Alvarez-Saavedra, E.; Berezikov, E.; de Bruijn, E,; Horvitz, H.R.; Kauppinen, S.; Plasterk, R.H. *Science* **2005,** *309*, 310-311.

(2)Alvarez-Garcia, I.; Miska, E.A. *Development* **2005,** *132*, 4653-4662.

(3)Lu, J.; Getz, G.; Miska, E.A.; Alvarez-Saavedra, E.; Lamb, J.; Peck, D.; Sweet-Cordero, A.; Ebert, B.L.; Mak, R.H.; Ferrando, A.A.; Downing, J.R.; Jacks, T.; Horvitz, H.R.; Golub, T.R. *Nature* **2005,** *435*, 834-838.

(4)Rosenfeld, N.; Aharonov, R.; Meiri, E.; Rosenwald, S.; Spector, Y.; Zepeniuk, M.; Benjamin, H.; Shabes, N.; Tabak, S.; Levy, A.; Lebanony, D.; Goren, Y.; Silberschein, E.; Targan, N.; Ben-Ari, A.; Gilad, S.; Sion-Vardy, N.; Tobar, A.; Feinmesser, M.; Kharenko, O.; Nativ, O.; Nass, D.; Perelman, M.; Yosepovich, A.; Shalmon, B.; Polak-Charcon, S.; Fridman, E.; Avniel, A.; Bentwich, I.; Bentwich. Z.; Cohen, D.; Chajut, A.; Barshack, I. *Nat. Biotech.* **2008,** *26I, 462-469.*

(5)Graybill, R.M.; Bailey, R.C. *Anal. Chem.* **2016,** *88*, 431-450.

(6) Schultz, N. A.; Dehlendorff, C.; Jensen, B. V.; et al. *JAMA* **2014**, *311*, 392-404.

(7) Wade, J.H.; Bailey, R.C. *Ann. Rev. Anal. Chem.* **2016,** *9*, 1-25.

(8)Qavi, A.J.; Mysz, T.M.; Bailey, R.C. *Anal. Chem.* **2011,** *83*, 6827-6833.

(9)Luchansky, M.S.; Bailey, R.C. *J. Am. Chem. Soc.* **2011,** *133*, 20500-20506.

(10) Sloan, C.D.K.; Marty, M.T.; Sligar, S.G.; Bailey, R.C. *Anal. Chem.* **2013,** *85*, 2970-2976.

(11) Kindt, J.T.; Luchansky, M.S.; Qavi, A.J.; Lee, S.-H.; Bailey, R.C. *Anal. Chem.* **2013,** *85*, 10653-10657.

(12) Wade, J.H.; Alsop, A.T.; Vertin, N.R.; Yang, H.; Johnson, M.D.; Bailey, R.C. *ACS Central Science*, **2015,** *1*, 374-382.

(13) Valera, E.; Shia, W.W.; Bailey, R.C. *Clin. Biochem.* **2016,** *49*, 121-126.

(14) Vollmer, F.; Arnold, S. *Nat. Methods* **2008,** *5*, 591-596.

(15) Iqbal, M.; Gleeson, M.A.; Spaugh, B.; Tybor, F.; Gunn, W.G.; Hochberg, M.; Baehr-Jones, T.; Bailey, R.C.; Gunn, L.C. *J. Sel. Topics Quantum Electron.***2010,** *16*, 654-661.

(16) Qavi, A.J.; Bailey, R.C. *Angew. Chem. Intl. Ed.* **2010,** *49*, 4608-4611.

(17) Qavi, A.J.; Kindt, J.T.; Bailey, R.C. *Anal. Chem.* **2011,** *83*, 5949-5956.

(18) Liang, Y.; Ridzon, D.; Wong, L.; Chen, C. *BMC Genomics* **2007,** *8*, 166.

(19)Si, M-L. Zhu, S.; Wu, H.; Lu, Z.; Wu, F.; Mo, Y-Y. *Oncogene* **2007,** *26*, 2799-2803.

(20) Asangani, I.A.; Rasheed, S.A.K.; Nikolova, D.A.; Leupold, J.H.; Colburn, N.H.; Post, S.; Allgayer, H. *Oncogene* **2008,** *27*, 2128-2136.

Chapter 4

AN OPTICAL PLATFORM FOR THE LABEL-FREE DETECTION OF MULTIPLE MICRORNAS FROM TUMOR TISSUE ISOLATES

Acknowledgments:

This work was supported from the National Cancer Institute of the National Institutes of Health through Grant R33CA1774. Additionally, I acknowledge support from the National Cancer Institute Alliance for Nanotechnology in Cancer "Midwest Cancer Nanotechnology Training Center" Grant R25 CA154015A. This work also benefited from significant contributions from Maria C. Cardeonsa-Rubio and instrumental support provided through UIUC's Institute for Genomic Biology.

4.1 Introduction

The landscape of biomedical research is rapidly changing, and it is now well accepted that multiplexed diagnostics can significantly improve our understanding of disease onset and progression. One of the important consequences of multiplexed analysis is a better understanding of the role of microRNA (miRNA) molecules and their interconnectivity with proteins to regulate biological functions.[1] Dysregulation of these interactions has been shown to have profound implications in a wide range of pathological conditions.[2-6]

Unfortunately, current clinically relevant platforms suffer from technological gaps that have hindered the translation of miRNA-based diagnostics to the clinic.[7] Specifically, qRT-PCR methods are incredibly sensitive, relatively rapid, and cost effective; however they can only measure levels of one miRNA per assay, thus requiring multiple sample aliquots to profile a panel of targets. Microarrays, are well-suited for multiplexed analyses, but are typically slow, less sensitive, and more expensive. Next-generation sequencing is also amenable to multiplexed analyses and identifies known and unknown miRNA sequences, but requires complex processing steps and presents challenges with time-intensive data analysis. Given bioinformatic approaches that narrow down global expression profiles to reveal subsets of the most informative biomarkers,[8] the development of a meso-plex detection platform looms as an important goal for the clinical translation of miRNA diagnostics.

We believe that silicon photonic microring resonators, a class of high-Q optical sensors,[9] are a viable option to facilitate meso-plex diagnostics in the clinic. These sensors are a multiplexable, array-based technology that have been applied to a range of biomolecular detection applications.[10-13] While these sensors have been discussed in detail,[14] they rely on changes in refractive index near the surface of the sensor, which is induced by biomolecular

binding that displaces water. This change in refractive index causes a shift in the resonant wavelength of the sensor which is directly proportional to the amount of the surface bound biomolecules and the solution phase analyte concentration. These sensors have previously been used for detection of microRNAs in label-free,[15] capture-agent-enhanced,[16] and enzymatic-label-enhanced formats.[17] While these studies show the promise of multiplexed miRNA analysis, they suffer from large input requirements, lengthy processing steps, or sensitivity issues that preclude them from use in a clinical setting.

In this study, we improve upon these previously reported strategies. This assay leverages the abilities of asymmetric PCR (aPCR)[18,19] combined with silicon photonic microring resonators to make rapid and cost-effective measurements in a small footprint. When compared to previous efforts, we show this assay reduces the required sample amount from micrograms to nanograms, increases multiplexing capabilities, and provides a time to result within hours. Importantly, we are the first group to develop a robust miRNA detection platform using aPCR and show its utility by simultaneously profiling 9 miRNAs from multiple brain cancer patients.

4.2 Experimental

4.2.1 Materials

All nucleic acid sequences (stem loop primers, PCR primers, synthetic RNA, etc.) were synthesized from Integrated DNA Technologies (IDT; Coralville, IA) and are listed in Table 4.1. The TaqMan® microRNA Reverse Transcription Kit and the Platinum® Multiplex PCR Master Mix were purchased from Thermo Fisher. All buffers and dilutions were prepared in nuclease free Ultrapure distilled water (Invitrogen). 1X Phosphate Buffer Saline (PBS) buffer was obtained from Lonza and was used in the reconstitution of the DNA capture probes. For the

functionalization of the chips, 3-(Aminopropyl)triethoxysilane (APTES) and bis(sulfosuccinimidyl)suberate (BS3) were obtained from Thermo Fisher Scientific. For the hybridization steps, a high stringency hybridization buffer was made in 50 mL batches containing 15 mL of formamide (Fisher), 1 mL 10% sodium dodecyl sulfate (Fisher), 10 mL 20X saline-sodium phosphate buffer (Invitrogen), 6 mL 0.25 M ethylenediaminetetraacetic acid (Invitrogen) and 2.5 mL 50X Denhardt's solution (Invitrogen). RT-qPCR assays were purchased from Thermo Fisher, and target specific assay IDs are listed in Table 4.2.

4.2.2 Instrumentation

Microring sensor arrays and measurement equipment were purchased from Genalyte, Inc. (San Diego, CA). The chips were made using standard photolithography and etching techniques. After patterning, the wafers were covered by a polymer cladding and diced into individual chips containing 132 individual microring resonator sensors. After polymer removal, the surface is ready to be functionalized and used in hybridization experiments. To perform hybridization experiments, the ring array is covered with a microfluidic Mylar Gasket and Teflon lid. The Mylar Gasket directed fluid flow into two defined flow chambers. Integrated pumps were used to perform all liquid handling steps, and the specifics of those steps are listed in Table 4.3.

Resonant wavelengths for each microring were determined by coupling a tunable laser source into an adjacent linear waveguide via on-chip grating couplers. The laser output was then swept through an appropriate spectral window and the light intensity at the end of the linear waveguide was used to determine the resonance wavelength. This process was then serially repeated for each ring in the array, and the resultant shifts in resonance as a function of time were recorded.

The resonance condition that is supported by the microring resonators is governed by the following equation:

$$m\lambda = 2\pi r n_{eff}$$

where m equals a nonzero integer, λ is the wavelength of propagating light, r is the microring radius, and n_{eff} is the effective refractive index of the local microring environment. Boundary conditions of light propagating in linear waveguides via total internal reflectance result in an evanescent field extending into a region very close to the ring surface. Interactions between the evanescent field and the local environment cause a change in the resonant wavelength, which is then monitored by the optical scanning instrumentation. Therefore, the binding of higher refractive index biomolecules and accompanying displacement of water results in a resonance shift to longer wavelengths: a positive shift that is listed in units of Δ picometers (Δpm).

4.2.3 Surface Functionalization

Surface functionalization was performed using one of two protocols: spotting by hand or spotting with high-resolution instrumentation.

(1) Hand spotting was used to perform the validation experiments and calibration curves. Prior to chip functionalization, chips were cleaned with a Piranha solution (70% Sulphuric Acid/30% Hydrogen Peroxide) for 30 seconds at 60ºC. CAUTION: Piranha is a dangerous solution and needs to be handled with caution. Then, the chips were rinsed with water and dried with nitrogen. Once dried, chips were immersed in acetone for 2 minutes, followed by the surface silanization with a 5% APTES solution (diluted in acetone) for 4 minutes. After silanization, the chips were immersed in acetone and isopropanol for 2 minutes each. All steps were completed

with continued shaking. Chips were rinsed with water and nitrogen dried to complete the silanization process. Next, 20 μL of a freshly prepared BS3 solution (2.85 mg/mL in acetic acid) was placed on the microring array for 3 minutes. BS3 served as the linker between the amine groups of the silanized surface and the amino-functionalized nucleic acid capture probes. After BS3 incubation, the chips were dried with nitrogen, and the final step consisted of spotting approximately 260 nL of 200 μM 5'amino functionalized DNA captures probes onto discrete microring sensors. The chips were then left to incubate for at least 4 hours in a humidity chamber.

(2) Spotting using high resolution instrumentation was used to complete the cross reactivity studies and patient sample profiling. The only experimental difference when using this instrumentation was surface salinization with a 1% APTES solution, a lower concentration of BS3 (1 mg/mL), and a lower concentration of the DNA capture probes (100 μM). All incubation steps and times were identical.

4.2.4 Reverse Transcription - Asymmetric PCR Amplification

Reverse transcription reactions were conducted using the TaqMan microRNA Reverse Transcription Kit. Each 15 μL reaction volume contained 4.16 μL of nuclease free water, 1.5 μL of 10X RT buffer, 1 μL of Multiscribe™ RT enzyme (50 U/ μL), 0.19 μL of RNase inhibitor (20 U/ μL), 0.15 μL dNTP mix (100 mM), 5 μL of RNA sample and 3 μL of the reverse transcription primer. The concentration of the stem loop primer was 20 μM or all experiments, except for the data presented in Figure S1 where 200 μM was used. The thermal profile was completed following the manufactures protocol: 16º C (30 min), 42º C (30 min), and 85ºC (5 min).

Asymmetric PCR was performed using the Platinum® Multiplex PCR Master Mix. Each 50 μL reaction volume was composed of 14 μL nuclease free water, 25 μL of Platinum® Multiplex PCR Master Mix, 5 μL of each primer and 1 μL of the reversed transcribed product. The concentration of the forward primer (the limiting primer) was 2 μM while the concentration of the reverse primer was 200 μM. The reactions were incubated at 95 ºC for 2 min, followed by cycles of 95 ºC for 30 s, 56ºC for 1 min 30 s and 72 ºC for 1 min.

4.2.4 Data Analysis

Data was analyzed with Origin Pro 9.0 and completed in three steps: (1) calculation of the hybridization response, (2) determination of C(t) values, and (3) heat map compiling.

(1) Hybridization response calculation

Prior to plotting hybridization induced shifts, sensor traces were corrected for temperature and instrument drift by using a series of reference sensors. Afterwards, microring hybridization traces were plotted. Net shifts of the aPCR product hybridization were calculated by subtracting the signal of the buffer step after hybridization (22 minutes) from the baseline buffer signal at 5 minutes. After net shifts are calculated, the shift value of the miRNA target of interest is then subtracted from an off target control cluster.

(2) C(t) value determination

The calculated net shift induced by DNA binding was ploted versus the PCR cycle for every target. A linear trace was then used to connect the data points. The threshold cycle was calculated by determining where the linear trace crossed the threshold shift value, which was calculated by taking 40% of the maximum signal.

(3) Heat map

The heat map was produced by subtracting the C(t) value of the disease sample from the healthy sample. The resulting values are plotted in Table 4.4 using a log 2 scale. Positive numbers represent over expression in tumor tissue and negative numbers represent under expression in tumor tissue.

4.2.5 RT-qPCR

For RT-PCR validation experiments, 10 ng of total RNA was used. Reverse transcription was performed using the TaqMan microRNA Reverse Transcription Kit (Life Technologies) and miRNA-specific stem loop primers, listed in Table S2. Reverse Transcription was carried out using the following thermal profile: 16°C (30 min), 42°C for (30 min), and 85°C (5 min). RT products were subjected to quantitative PCR in triplicate using PCR primers from the same miRNA Assay Kit. The reaction was performed at 95°C (10 min), followed by 40 two-step cycles of (1) 95°C for 15 s and (2) 60°C for 1 min. All quantitative PCR work was done using an Applied Biosystems 7900HT Fast Real-Time PCR System. All procedures and reactions were carried out according to the protocols provided by the manufacturer.

4.3 Discussion

The schematic of the developed protocol is seen in Figure 4.1. First, total RNA is extracted from a sample of interest (i.e. cell culture, bodily fluids, tumor tissue, etc.). miRNA targets are then reverse transcribed (RT) using stem loop primers specific to each target.[20] Next, the RT products are amplified via asymmetric PCR since traditional PCR is not amenable to surface hybridization-based assays due to the fact that it produces double stranded DNA (dsDNA). Asymmetric PCR selectively produces single stranded DNA (ssDNA) products by

using an excess of the forward PCR primer.[18,19] Here, we use a 100 fold excess. As shown in Figure 4.1C, dsDNA is produced until the limiting PCR primer is exhausted; afterwards, ssDNA production occurs in subsequent thermal cycles by extension of the primer in excess. After thermal cycling is complete, the PCR product is diluted in a high stringency hybridization buffer and flowed across a microring array, where hybridization to complimentary, surface-bound capture probes occurs. As the hybridization takes place, it causes a shift in the resonant wavelength of the microring sensors.

To validate this approach, we first designed primer sets whose sequences are included in Table 4.1. Next, we show that this assay can detect varying input amounts of target miRNAs (Figure 4.2). As expected, an increase in the number of thermal cycles leads to lower amounts of RT being amplified to a detectable level. We mimicked qPCR quantitation protocols to determine the dynamic range and linear amplification profile of this assay. To complete these experiments, we reverse transcribed varying input concentrations of a synthetic let-7f RNA sequence. The reverse transcription products were thermally cycled, and samples were introduced to a microring surface after a varying number of cycles. The results are plotted in Figs. 4.2A and B. In Figure 4.2A, we used a logistic fit to produce binding curves for the respective input concentrations. We then took the second derivative of the binding curves and set the threshold value where the second derivative is equal to zero. In order simplify quantification, we also developed a protocol to manually determine the threshold value. As shown in Fig. 4.2B, we first determined a threshold shift value by calculating forty percent of the maximum shift value. After interpolating a line between all data points, we determine the cycle at which the interpolated lines cross the threshold relative shift value. Results for both quantitation methods are shown in Figure 4.2C and show linearity over 6 orders of magnitude.

We conducted similar experiments for all 9 miRNA targets with each one producing linear results (Fig. 4.3). Lastly, we show the target specificity of the platform in Figure 4.2D by combining all capture probes onto one sensor surface and introducing RT-aPCR products from individual target miRNA sequences. Each trace shows a specific response using a 200 nM sample that is thermally cycled for 20 cycles. Importantly, these results show limited non-specific response for all targets.

Next, we used the assay to profile 9 miRNAs extracted from tumor tissues and compared the expression profiles to that obtained from a commercially available pooled "healthy" total RNA sample. Representative data is shown in Figure 4.4A-B from the healthy reference sample and a glioblastoma (GBM) patient. C(t) values were calculated, using the manual method outlined above. To validate these results we profiled the same RNA samples using RT-qPCR and the correlation is shown in Figure 4.4C. While the overall correlation generally trends in the same direction, we attribute some of the inconsistencies to differing primer sets and PCR master mixes as well as other sample handling inconsistencies (i.e. pipetting and freeze-thaw cycles).

Lastly, the assay was used to profile miRNAs from 20 brain tumor patients (Fig. 4.4D). Patient specifics are listed in Table 4.5. After determining fold changes between the disease and healthy samples using the microring platform,[21] trends seen in this data can be confirmed with studies from the literature. The fold change values of the heat map are shown in Table 4.6. For example, miRs-10b, 155, and 222 are known to be upregulated in glioma tissue and the majority of patients show the same pattern.[22-24] Alternatively, miRs-34a and 29a have been shown to be downregulated in glioma tissue and a number of patients profiled here exhibit similar trends.[25,26]

4.4 Conclusions

In sum, we successfully developed a platform that enables the multiplexed detection of miRNAs. By leveraging the ability of asymmetric PCR to produce single stranded PCR products and silicon photonic microring resonators to detect the products in a highly-sensitive and label free fashion, we show that this platform can product linear calibration curves similar to those obtained using conventional qPCR and on the same time scale. This report provides the foundation that we aim to expand upon in the future. Future studies will aim to increase multiplexing capabilities, expand into different classes of RNA molecules, and improve automation capabilities.

4.5 Figures and Tables

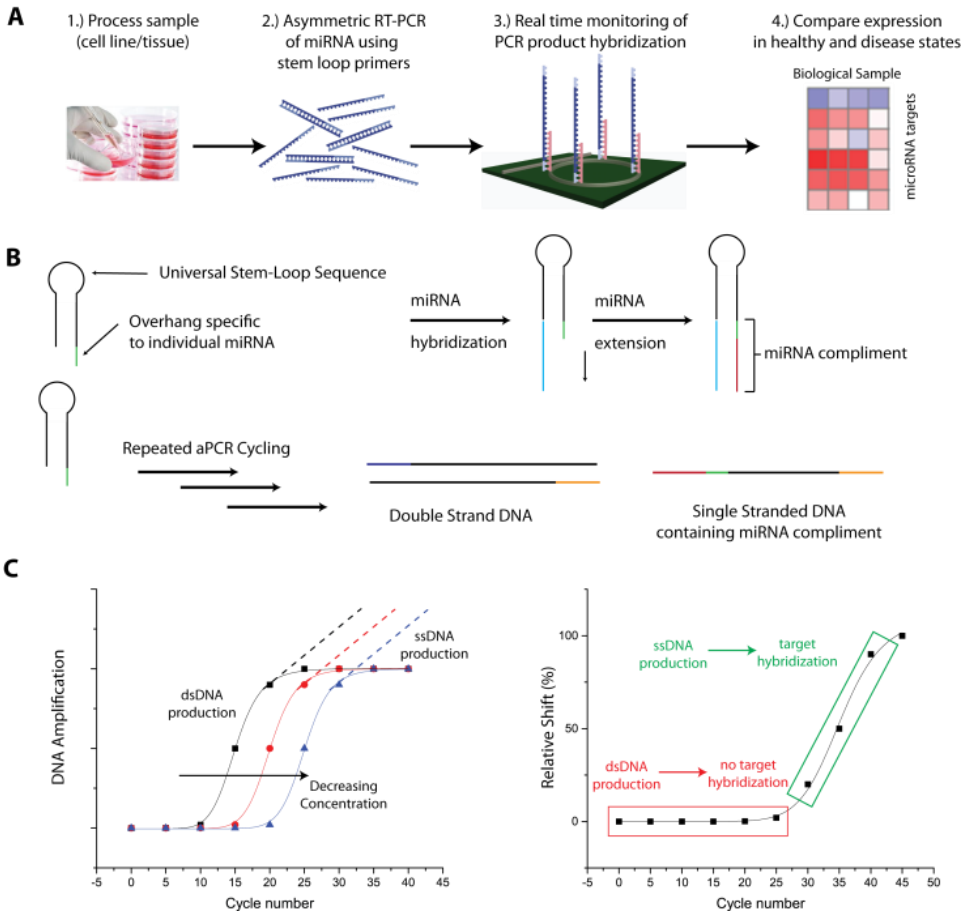

Figure 4.1: (A) Overview of aPCR-microring assay from RNA isolation to using miRNA profiles to make biological conclusions. (B) Mechanism of reverse transcription-asymmetric PCR amplification. (C) Schematic showing DNA amplification as cycle numbers increase. Importantly, there is a shift from double stranded DNA (dsDNA) production to ssDNA production when the limiting primer in the primer set is exhausted. Corresponding to this change is an increase in signal detected by the microring platform as these ssDNA amplicons hybridize to the sensor surface.

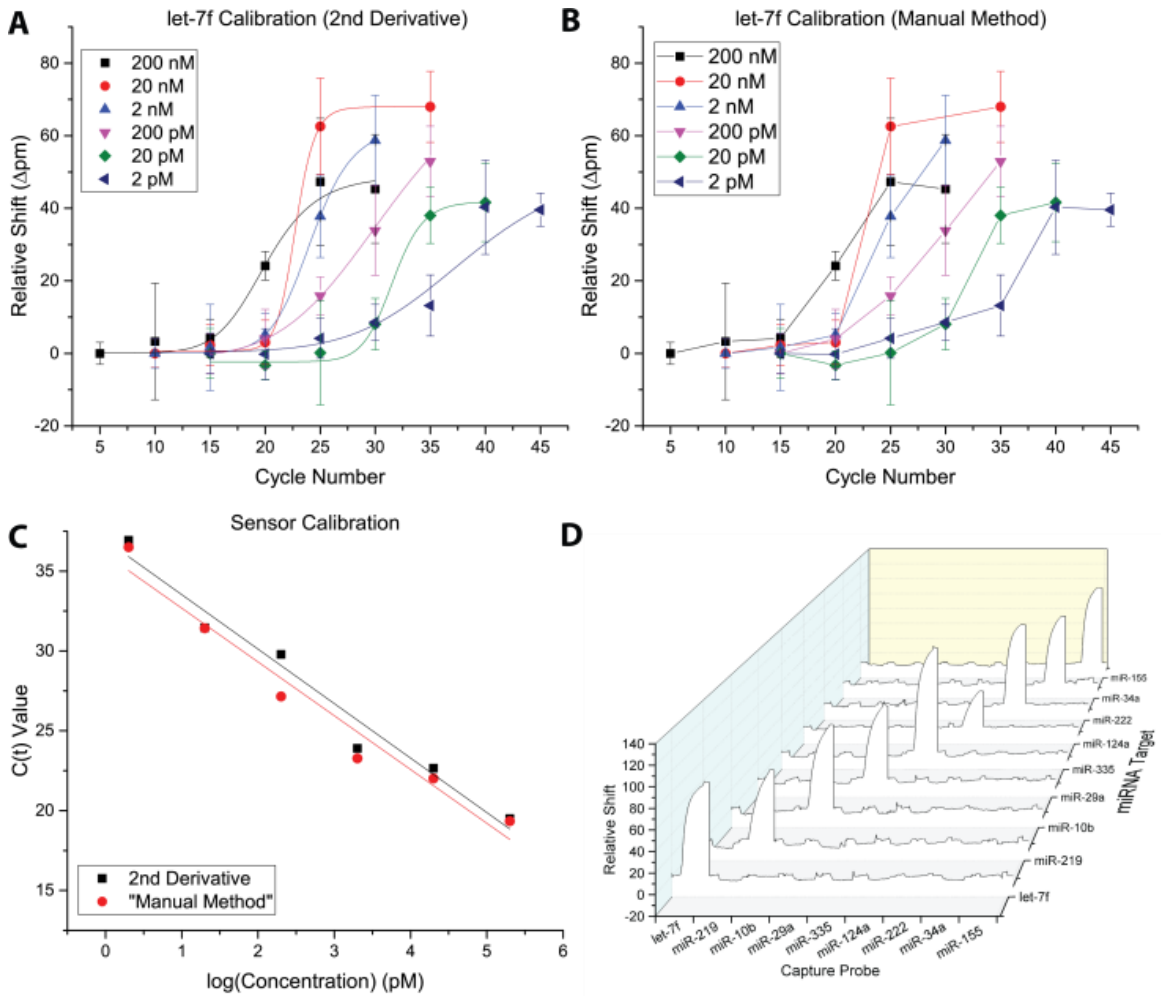

Figure 4.2: (A) Amplification plot used to quantitate let-7f using the second derivative method. (B) Amplification plot used to quantitate let-7f using the second manual method. (C) Calibration curve for each method (respectively, slope = -3.41 and -3.37 and R^2 values = 0.96 and 0.95, respectively). (D) Plot showing specificity of a capture probes on a single sensor array.

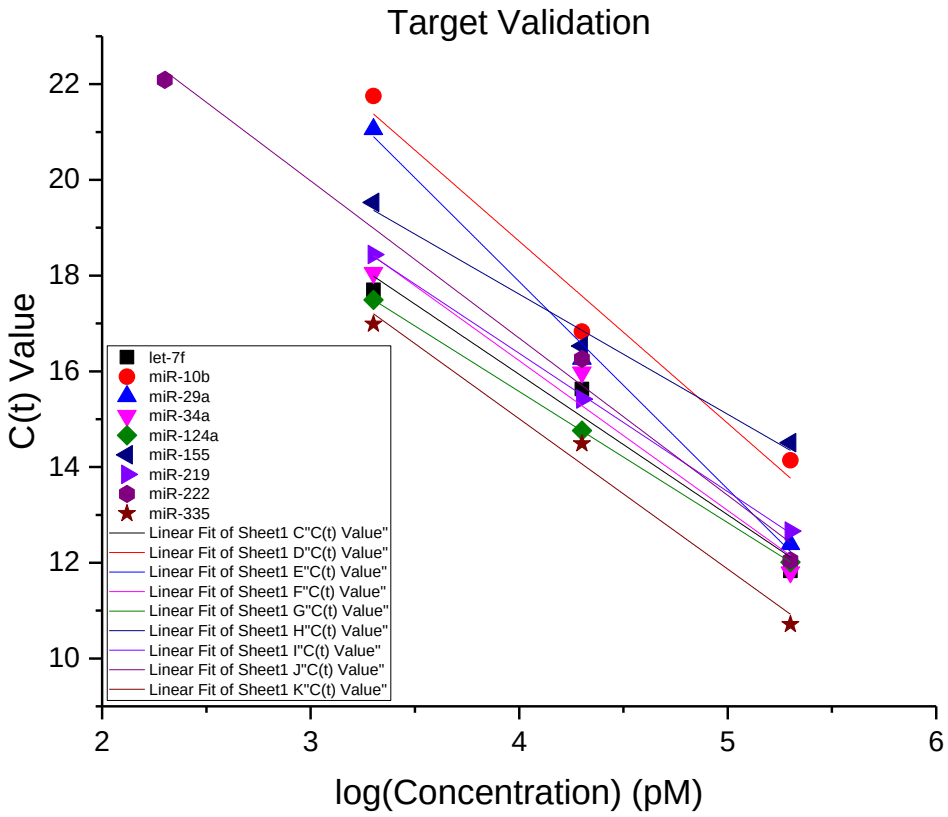

Figure 4.3: Amplification Validation of miRNA Targets. In order to prove linear amplification of all miRNA targets, 200 nM, 20 nM, and 2 nM samples of each target were subjected to the aPCR-microring assay using a stem loop primer concentration of 200 μM. The results validated the designed primer sets by displaying linear amplification profiles.

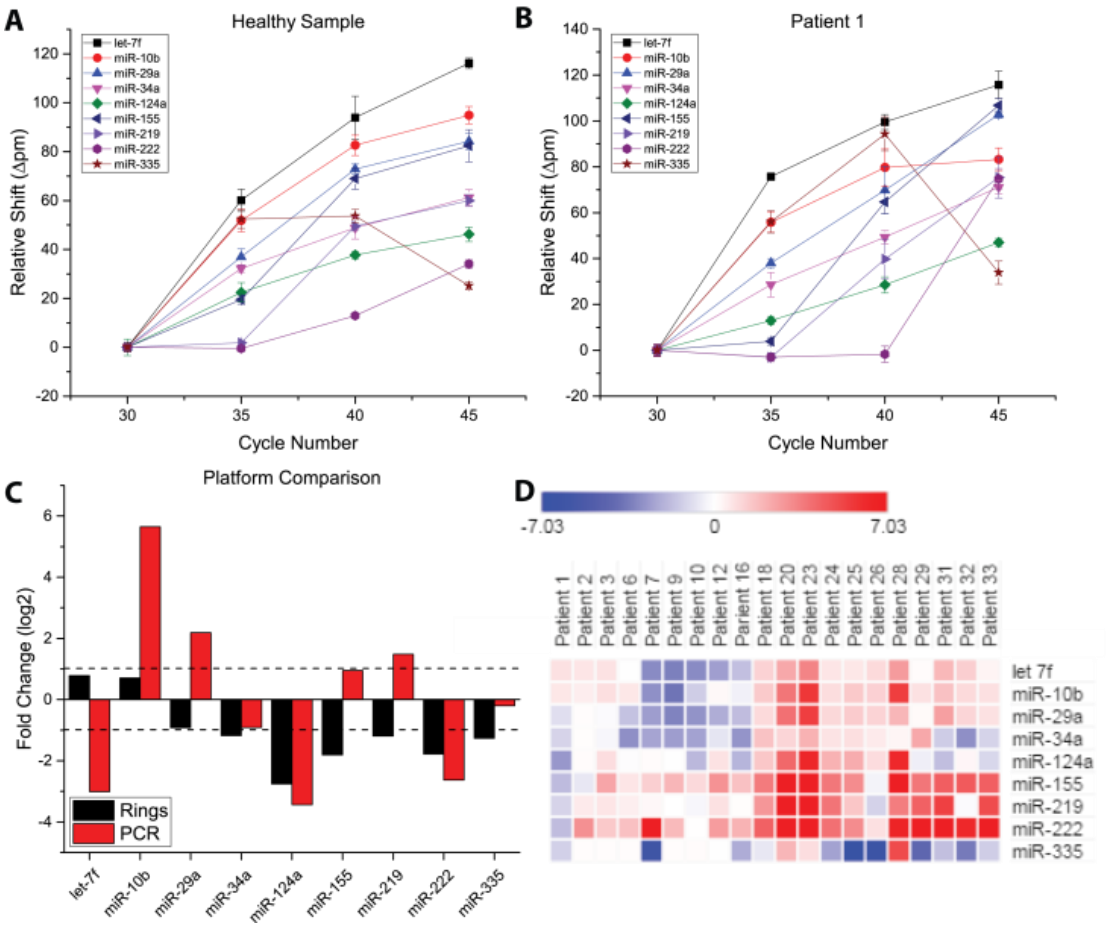

Figure 4.4: (A-B) Results obtained when using a 10 ng input of a healthy control and glioma grade IV total RNA sample, respectively, and subjecting it to varying cycles of the aPCR-microring assay. (C) Comparison of fold changes using the microring platform and qRT-PCR. (D) Heat map showing expression profiles from patient samples.

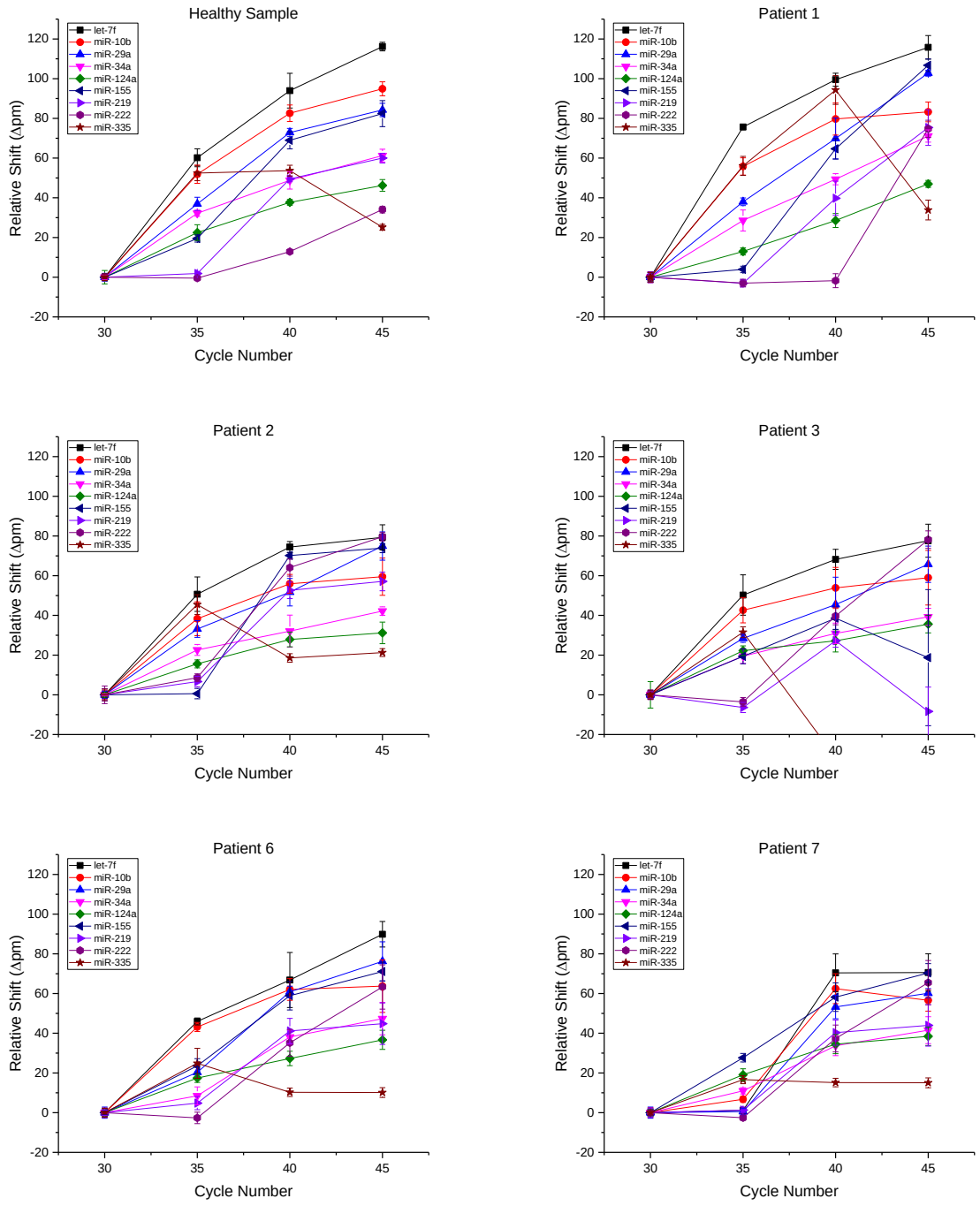

Figure 4.5: Plots used to calculate C(t) values for each sample of interest.

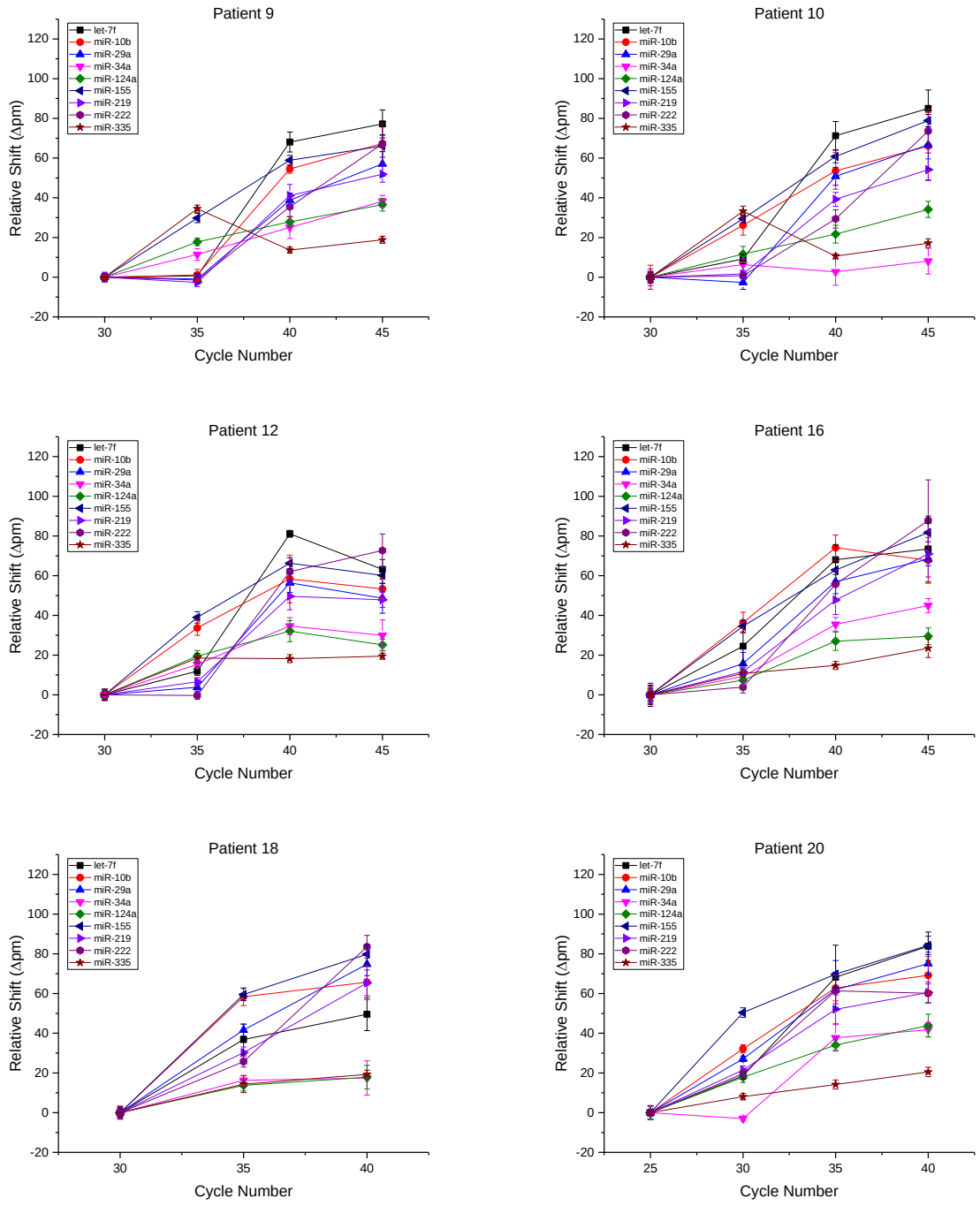

Figure 4.5 (cont.)

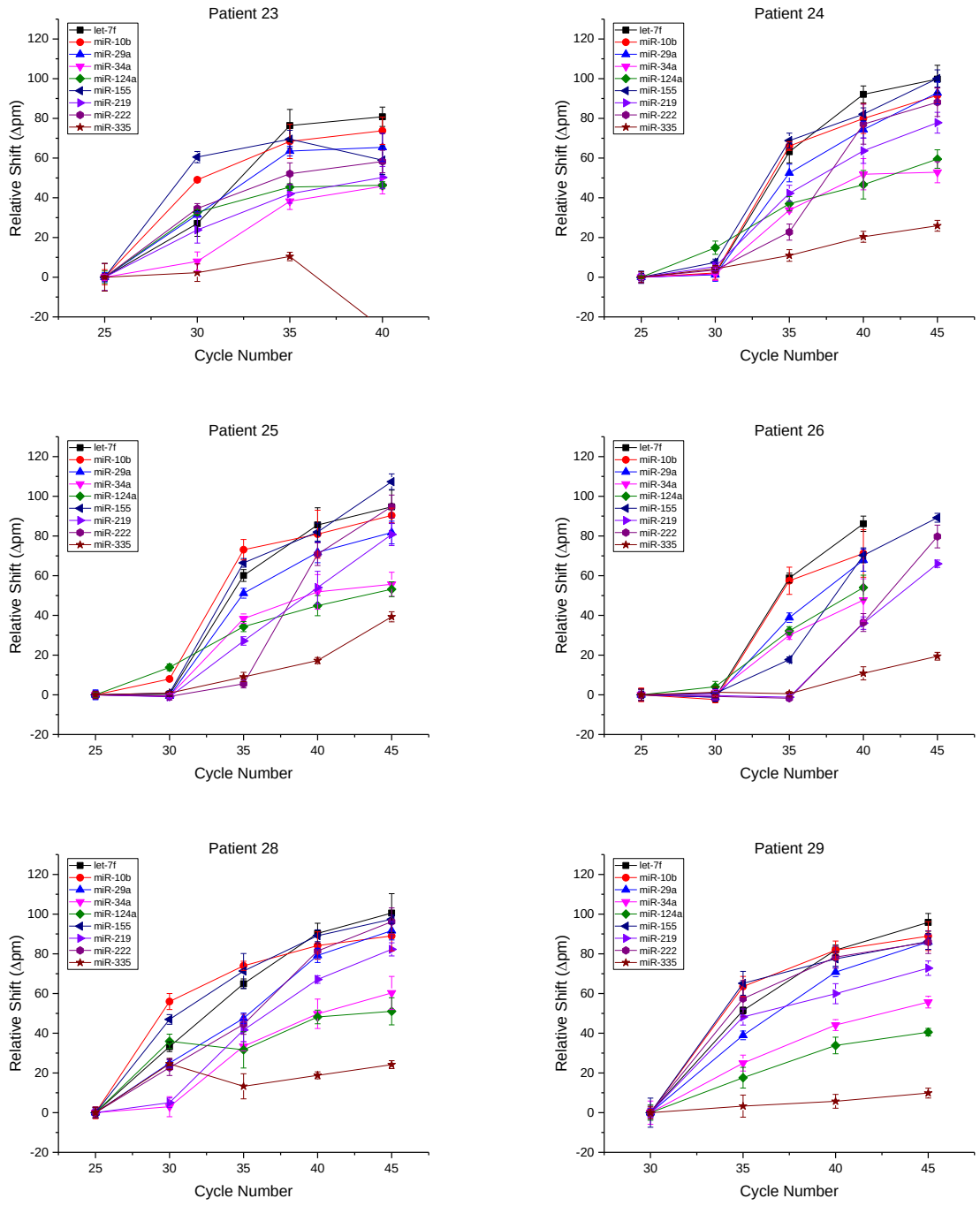

Figure 4.5 (cont.)

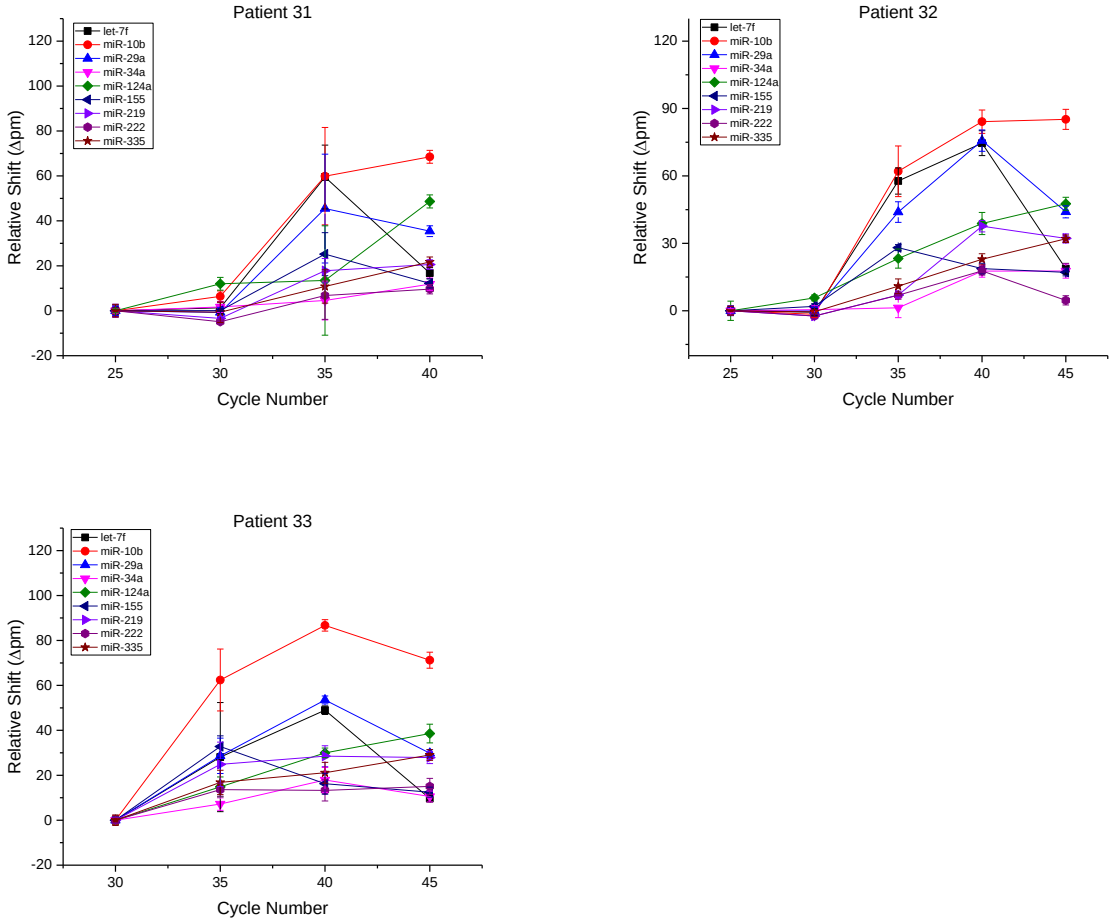

Figure 4.5 (cont.)

	Sequence
hsa miRNA-let7f	UGAGGUAGUAGAUUGUAUAGUU
hsa miRNA-219	UGAUUGUCCAAACGCAAUUCU
hsa miRNA-10b	UACCCUGUAGAACCGAAUUUGUG
hsa miRNA-29a	UAGCACCAUCUGAAAUCGGUUA
hsa miRNA-335	UCAAGAGCAAUAACGAAAAAUGU
hsa miRNA-124a	UAAGGCACGCGGUGAAUGCC
hsa miRNA-222	AGCUACAUCUGGCUACUGGGUCUC
hsa miRNA-34a	UGGCAGUGUCUUAGCUGGUUGU
hsa miRNA-155	UUAAUGCUAAUCGUGAUAGGGGU
Conserved Stem Loop Primer	GTCGTATCCAGTGCAGGGTCCGAGGTATTCGCACTGGA T…miRNA specific overhang
miR-let7f SLP overhang	AACTATAC
miR-219 SLP overhang	AGAATTG
miR-10b SLP overhang	CACAAATTC
miR-29a SLP overhang	TAACCG
miR-335 SLP overhang	ACATTTTT
miR-124a SLP overhang	GGCATTC
miR-222 SLP overhang	GAGACCC
miR-34a SLP overhang	ACAACCA
miR-155 SLP overhang	ACCCCT
Conserved reverse primer	GTGCAGGGTCCGAGGTATTCGCACTGGATACGAC
miR-let7f PCR forward primer	CGCGCTGAGGTAGTAGATT
miR-219 PCR forward primer	CGCGTGATTGTCCAAACG
miR-10b forward primer	GCGTACCCTGGTAGAACC
miR-29a forward primer	CGCTAGCACCATCTGAAAT
miR-335 forward primer	CGCGTCAAGAGCAATAACG
miR-124a forward primer	CGTAAGGCACGCGGT
miR-222 forward primer	CGAGCTACATCTGGCTACT
miR-34a forward primer	GCGTGGCAGTGTCTTAGC
miR-155 forward primer	CGCGTTAATGCTAATCGTGAT

Table 4.1: Summary of nucleic acid sequences

Target	Assay ID
miRNA-let7f	000382
miRNA-219	000522
miRNA-10b	002218
miRNA-29a	0022112
miRNA-335	000546
miRNA-124a	001182
miRNA-222	000525
miRNA-34a	000426
miRNA-155	002623

Table 4.2: Summary of RT-qPCR assay IDs

Step	Flow Rate (μL/min)	Duration (min)
Hybridization buffer	20	5
RT-PCR product	20	15
Hybridization buffer	20	5

Table 4.3: Details on fluid flow conditions

	Healthy Brain RNA sample C(t)	Standard Deviation	Patient 1 RNA sample C(t)	Standard deviation
let-7f	26.95	0.03	29.96	0.03
miRNA-219	28.89	0.04	28.14	0.02
miRNA-10b	33.79	0.16	20.56	0.05
miRNA-29a	22.75	0.02	27.87	0.03
miRNA-335	29.19	0.06	27.32	0.06
miRNA-124a	23.88	0.02	29.90	0.04
miRNA-222	24.69	0.03	27.42	0.02
miRNA-34a	26.95	0.02	27.33	0.06
miRNA-155	30.85	0.13	29.39	0.03

Table 4.4: Samples (10 ng) from the "healthy" pooled cohort and Patient 1 were subjected to qRT-PCR analysis as outlined above. This data provides the C(t) values used to compile fold change values.

Patient Sample	Gender	Age	Cancer type
1	M	62	Glioma – grade IV
2	M	42	Glioma – grade IV
3	M	47	Glioma – grade IV
6	F	52	Glioma – grade II
7	F	67	Glioma – grade IV
9	F	75	Glioma – grade IV
10	F	29	Glioma – grade III
12	F	48	Glioma – grade IV
16	F	37	Glioma – grade III
18	F	35	Glioma – grade III
20	M	26	Glioma – grade IV
23	M	38	Glioma – grade IV
24	F	67	Glioma – grade IV
25	M	25	Glioma – grade III
26	F	27	Glioma – grade II
28	M	30	Glioma – grade III
29	M	51	Glioma – grade IV
31	F	63	Meningioma – grade I
32	F	69	Glioma – grade IV
33	F	74	Meningioma – grade I

Table 4.5: Patient information

Patient	let 7f	miR-10b	miR-29a	miR-34a	miR-124a	miR-155	miR-219	miR-222	miR-335
1	0.83	0.68	-0.92	-1.18	-2.76	-1.81	-1.19	-1.78	-1.27
2	0.73	0.55	0.09	0.05	0.12	-0.7	0.61	3.02	0.08
3	0.8	0.88	-0.14	-0.27	0.91	2.42	0.71	1.45	0.07
6	-0.03	0.7	-1.65	-2.97	-0.08	0.73	0.53	1.7	0.07
7	-3.1	-2.95	-2.63	-2.44	0.11	1.29	0.27	8.05	-6.21
9	-3.38	-3.72	-3.31	-2.62	-0.02	1.96	-0.01	1.87	0.07
10	-3.09	-1.35	-2.89	-2.51	-1.89	1.03	-0.3	0.04	0.1
12	-2.6	0.23	-2.22	-0.74	0.81	2.98	0.84	2.67	-0.03
16	-1.71	-0.43	-1.8	-2.85	-2.02	1.68	0.05	2.07	-2.25
18	1.21	1.43	1	1.66	1.51	3.6	2.86	4.32	-0.68
20	2.35	3.76	3.9	1.15	4.17	8.02	6.86	9.44	1.95
23	3.36	5.68	5.42	2.1	6.3	9.08	8.14	11.67	0.91
24	0.73	0.94	1.08	0.76	2.09	3.7	3.79	3.9	-2.51
25	0.69	1.46	1.38	0.88	2.23	3.14	1.54	3.15	-7.03
26	0.99	1.23	1.19	0.61	0.97	-0.38	-1.24	0.86	-6.44
28	2.73	5.46	1.97	0.32	6.23	8.51	3.54	6.45	5.05
29	0.11	0.83	0.17	2.35	-0.51	3.73	4.32	7.05	-4.29
31	1.94	1.68	2.6	-1.37	-1.76	4.4	5.38	9.48	-1.73
32	1.33	0.98	1.16	-2.98	0.31	4.59	-0.13	6.27	-3.55
33	0.37	0.86	0.83	-1.21	-1.1	4.38	5.01	7.85	-1.36

Table 4.6: Fold changes presented in heat map (log2)

4.6 References

(1) Pritchard, C. C.; Cheng, H. H.; Tewari, M. *Nat Rev Genet* **2012**, *13*, 358-369.

(2) Calin, G. A.; Croce, C. M. *Cancer Research* **2006**, *66*, 7390.

(3) Madrigal-Matute, J.; Rotllan, N.; Aranda, J. F.; Fernández-Hernando, C. *Current Atherosclerosis Reports* **2013**, *15*, 322.

(4) Vickers, Kasey C.; Rye, K.-A.; Tabet, F. *Clinical Science* **2013**, *126*, 183.

(5) Zhu, S.; Pan, W.; Qian, Y. *Journal of Molecular Medicine* **2013**, *91*, 1039-1050.

(6) Abe, M.; Bonini, N. M. *Trends in Cell Biology* **2013**, *23*, 30-36.

(7) Graybill, R. M.; Bailey, R. C. *Analytical Chemistry* **2016**, *88*, 431-450.

(8) Henriksen, M.; Johnsen, K. B.; Andersen, H. H.; Pilgaard, L.; Duroux, M. *Molecular Neurobiology* **2014**, *50*, 896-913.

(9) Wade, J. H.; Bailey, R. C. *Annual Review of Analytical Chemistry* **2016**, *9*, 1-25.

(10) Wade, J. H.; Alsop, A. T.; Vertin, N. R.; Yang, H.; Johnson, M. D.; Bailey, R. C. *ACS Central Science* **2015**, *1*, 374-382.

(11) Sloan, C. D. K.; Marty, M. T.; Sligar, S. G.; Bailey, R. C. *Analytical Chemistry* **2013**, *85*, 2970-2976.

(12) Kindt, J. T.; Bailey, R. C. *Analytical Chemistry* **2012**, *84*, 8067-8074.

(13) Qavi, A. J.; Mysz, T. M.; Bailey, R. C. *Analytical Chemistry* **2011**, *83*, 6827-6833.

(14) Iqbal, M.; Gleeson, M. A.; Spaugh, B.; Tybor, F.; Gunn, W. G.; Hochberg, M.; Baehr-Jones, T.; Bailey, R. C.; Gunn, L. C. *IEEE Journal of Selected Topics in Quantum Electronics* **2010**, *16*, 654-661.

(15) Qavi, A. J.; Bailey, R. C. *Angewandte Chemie International Edition* **2010**, *49*, 4608-4611.

(16) Qavi, A. J.; Kindt, J. T.; Gleeson, M. A.; Bailey, R. C. *Analytical Chemistry* **2011**, *83*, 5949-5956.

(17) Graybill, R. M.; Para, C. S.; Bailey, R. C. *Analytical Chemistry* **2016**, *88*, 10347-10351.

(18) Gyllensten, U. B.; Erlich, H. A. *Proceedings of the National Academy of Sciences* **1988**, *85*, 7652-7656.

(19) Sanchez, J. A.; Pierce, K. E.; Rice, J. E.; Wangh, L. J. *Proceedings of the National Academy of Sciences* **2004**, *101*, 1933-1938.

(20) Chen, C.; Ridzon, D. A.; Broomer, A. J.; Zhou, Z.; Lee, D. H.; Nguyen, J. T.; Barbisin, M.; Xu, N. L.; Mahuvakar, V. R.; Andersen, M. R.; Lao, K. Q.; Livak, K. J.; Guegler, K. J. *Nucleic Acids Research* **2005**, *33*, e179.

(21) Schmittgen, T. D.; Livak, K. J. *Nat. Protocols* **2008**, *3*, 1101-1108.

(22) Lin, J.; Teo, S.; Lam, D. H.; Jeyaseelan, K.; Wang, S. *Cell Death Dis* **2012**, *3*, e398.

(23) Zhou, J.; Wang, W.; Gao, Z.; Peng, X.; Chen, X.; Chen, W.; Xu, W.; Xu, H.; Lin, M. C.; Jiang, S. *PLOS ONE* **2013**, *8*, e83055.

(24) Quintavalle, C.; Garofalo, M.; Zanca, C.; Romano, G.; Iaboni, M.; del Basso De Caro, M.; Martinez-Montero, J. C.; Incoronato, M.; Nuovo, G.; Croce, C. M.; Condorelli, G. *Oncogene* **2012**, *31*, 858-868.

(25) Yin, D.; Ogawa, S.; Kawamata, N.; Leiter, A.; Ham, M.; Li, D.; Doan, N. B.; Said, J. W.; Black, K. L.; Phillip Koeffler, H. *Oncogene* **2013**, *32*, 1155-1163.

(26) Aldaz, B.; Sagardoy, A.; Nogueira, L.; Guruceaga, E.; Grande, L.; Huse, J. T.; Aznar, M. A.; Díez-Valle, R.; Tejada-Solís, S.; Alonso, M. M.; Fernandez-Luna, J. L.; Martinez-Climent, J. A.; Malumbres, R. *PLOS ONE* **2013**, *8*, e77098.

Chapter 5

COMBINING PCR-BASED ENZYMATIC AMPLIFICATION WITH SILICON PHOTONIC MICRORING RESONATORS FOR THE DETECTION OF LNCRNAS FROM LOW INPUT HUMAN SAMPLES

Acknowledgements:

The authors gratefully acknowledge financial support from the National Cancer Institute of the National Institutes of Health through Grant R33CA1774. R.M.G. acknowledges support from the National Cancer Institute Alliance for Nanotechnology in Cancer "Midwest Cancer Nanotechnology Training Center" Grant R25CA154015A. M.C.R. acknowledges support from a la Caixa Banking Foundation Fellowship. We also appreciate the support provided through UM's DNA Sequencing Core.

5.1. Introduction

In recent years, the attention given to multiplexed biomolecular analysis has been increasing because of its potential to revolutionize areas of human health, such as diagnosis, prognosis and therapeutic selection. The discovery of potential biomarkers for different diseases has been one of the main drivers in the development of multiplexed diagnostic analysis. Among the different types of biomarkers, RNA molecules have risen in importance thanks to the use of next generation sequencing and the resulting insights in cell signaling regulation.[1] Furthermore, accumulating reports noting the differential expression of non-coding RNAs (ncRNAs) in disease suggest that they are potential candidates as biomarkers for the development of new diagnostic devices and therapies.[2]

ncRNAs can be defined as those transcripts that do not encode any protein. ncRNA can be divided into two major groups based on their length: small non coding RNAs (< 200 nucleotides), which include Piwi-interacting RNAs, small interfering RNAs and microRNAs (miRNAs) and long non coding RNAs, lncRNAs, those that are longer than 200 nucleotides.[3] Since the discovery of the first well studied imprinted lncRNA, H19,[4] there have been a plethora of studies identifying more of these transcripts, and these studies relate expression of lncRNAs to different biological functions.[5-7] Particularly in cancer, researchers have focused more of their effort in understanding how these transcripts have roles as drivers of tumor suppressive and oncogenic functions.[8,9]

As an illustration of the importance of using multiplexed lncRNA diagnostic panels, scientists have made progress connecting differential expression of these transcripts in cancers like glioma and glioblastoma with the objective of identifying different subtypes and malignant

behaviors in these tumors.[10,11] In the first study, microarrays were used to identify subtype and grade of glioma based on lncRNA signatures. Here, they were able to pare down their biopanels from around 2,000 potential lncRNA targets to around 25 to 50 targets. In the second study, based on *in silico* analysis, the researchers mined data from The Cancer Genome Atlas and developed a signature of six lncRNAs that allowed them to predict survival in glioblastoma.

To translate these panels into the clinic the main techniques for the detection of these transcripts, typically qRT-PCR, hybridization assay such as microarrays, and RNA sequencing,[12,13] need to be improved. These techniques are robust, sensitive and, in the case of RNA sequencing, allow the discovery of new lncRNAs in the genome. However, they either look at one target per sample, follow burdensome experimental protocols, or collect an unnecessary amount of data to analyze relevant RNA-based biopanels. One of the challenges for biosensor community is to develop multiplexed technologies to facilitate the detection of similar biopanels as those previously outlined in a sensitive, efficient, and affordable manner.

In response to this challenge, we have developed a silicon photonic microring resonator technology that enables the multiplexed detection of a host of biomolecules. The specifics of the instrumentation have been discussed in detail previously.[14,15]. The sensing principle is based on the change of refractive index near the surface of the rings, which occurs when biomolecules selectively bind to receptors on the microring surface. One of the advantages of this platform is the ability of sensing without the addition of fluorescent or enzymatic tags. Other advantages are the ability to fabricate sensing semiconductor chips in parallel arrays which enables multiplexed detection. The promise of these sensors have been used previously for the study of proteins[16-18] as well as nucleic acids, including mRNAs[19] and Bailey, 2012), tmRNAs[20] and miRNAs[21,22].

In this study, we develop an assay for the detection of long non coding RNAs. This assay relies on asymmetric PCR (aPCR) to selectively produce single stranded DNA (ssDNA) products by using an unequimolar primer ratio.[23,24] We then use microring arrays to detect these PCR process at different cycles, closely mimicking the process of qPCR. Compared to previous long RNA detection efforts from our lab,[19] we have decreased input amounts from micrograms to nanograms, incorporated an internal control mRNA sequence, and studied an important disease-relevant class of RNA molecules, lncRNA. We use this assay to study the expression of two lncRNA sequences and an internal control mRNA in reference samples from lung and brain as well as a glioblastoma cell line. We also compare the obtained expression profiles to previous literature findings and subject the same RNA samples to qRT-PCR analysis to validate this platform and demonstrate its potential to provide a new alternative for the detection of these transcripts in both clinical and research settings.

5.2. Experimental

5.2.1 Materials

All nucleic acid sequences (primers and capture probes) were synthesized from Integrated DNA Technologies (IDT; Coralville, IA). The TaqMan® microRNA Reverse Transcription Kit, the Platinum® Multiplex PCR Master Mix and the SYBR® Select Master Mix were purchased from Thermo Fisher. All buffers dilutions, DNA primer reconstitution and DNA primer dilutions were prepared in nuclease-free Ultrapure distilled water (Invitrogen). 1X Phosphate-Buffered Saline (PBS) was obtained from Lonza and was used in the reconstitution of the oligonucleotide capture probes. For the functionalization of the microring chips, 3-Aminopropyl)triethoxysilane (APTES) and bis(sulfosuccinimidyl)suberate (BS3) were obtained from Thermo Fisher Scientific. For all hybridization steps, a high stringency hybridization buffer

was made in 50 mL batches containing 15 mL of formamide (Fisher), 1 mL 10% sodium dodecyl sulfate (Fisher), 10 mL 20X saline-sodium phosphate buffer (Invitrogen), 6 mL 0.25 M ethylenediaminetetraacetic acid (Invitrogen) and 2.5 mL 50X Denhardt's solution (Invitrogen).

5.2.2 RNA Sample Preparation

Total RNA was extracted from GBM6 cell lines lysates with a miRNeasy® Mini kit (Quiagen) using manufacture's protocol. After extraction, total RNA was assessed for purity and quantity using a ThermoFisher Nanodrop UV−vis spectrometer and stored at −80°C until further use. The Brain and Lung Reference RNA samples were obtained commercially from Thermo Fisher Scientific and stored at -80°C until further use.

5.2.3 Amplification Primers and Capture Probe Design

Specific primers and capture probes for the amplification and detection of the human lncRNAs MALAT1 and KIAA0495 and the internal control β-actin were designed using sequence annotations from Genbank (NCBI) and the Primer-Blast platform (NCBI). In order to observe the secondary structure, we used the Dinamelt web server (Markham and Zuker, 2005). Sequences of the primers and capture probes can are listed in Table 5.1.

5.2.4 Silicon Photonic Microring Resonator Instrumentation

Microring sensor arrays and measurement equipment were purchased from Genalyte, Inc. (San Diego, CA), and the detection mechanism has been discussed in detail previously (Iqbal et al., 2010; Washburn et al., 2010). The chips were made on silicon on insulator wafers by photolithography and etching techniques. After patterning, the wafers were covered by a polymer cladding and diced into individual chips measuring 6 mm x 4 mm and containing 132 individual microring resonator sensors. After polymer removal, the surface is ready to be functionalized

and used in hybridization experiments. To perform hybridization experiments, the microring array is covered with a microfluidic Mylar gasket and Teflon lid. The Mylar gasket directs fluid flow into two defined flow channels. Integrated pumps were used to perform all liquid handling steps, and the specifics of those steps are listed in Table 5.2.

5.2.5 Surface Functionalization of the Microring Resonators

Sensor chips were immersed in acetone for 2 min, followed by the surface silanization with 5% APTES (diluted in acetone) for 4 min. After silanization, the chips were immersed in acetone and isopropanol for two minutes each. All steps were completed with continuous shaking. Chips were rinsed with water and nitrogen dried to complete the silanization process. Next, 20 uL of a freshly prepared BS3 solution (2.85 mg/mL in acetic acid) was placed on the microring array for 3 minutes. After BS3 incubation, the chips were dried with nitrogen, and the final step consisted of spotting approximately 260 nL of 200 μM 5'amino functionalized DNA captures probes onto discrete microring sensors. The chips were then left to incubate overnight in a humidity chamber.

5.2.6 Reverse Transcription – Asymmetric PCR

Reverse transcription reactions were conducted using the TaqMan microRNA Reverse Transcription Kit (ThermoFisher). Each 15 μL reaction volume contained 4.16 μL of nuclease free water, 1.5 μL of 10X RT buffer, 1 μL of Multiscribe™ RT enzyme (50 U/ μL), 0.19 μL of RNase inhibitor (20 U/ μL), 0.15 μL dNTP mix (100 mM), 5 μL of RNA sample (40 ng RNA total) and 3 μL of reverse transcription primer. The concentration of the reverse primer was 200 μM when only one transcript was reversed transcribed and 66 μM when three transcripts were

reverse transcribed. The thermal profile was completed following the manufactures protocol: 65º C (5 min), 4º C (2 min), 42º C (30 min), and 85ºC (5 min).

Asymmetric PCR was performed using the Platinum® Multiplex PCR Master Mix (Thermo Fisher). Each 50 μL reaction volume was composed of 14 μL nuclease free water, 25 μL of Platinum® Multiplex PCR Master Mix, 5 μL of each primer and 1 μL of the reversed transcription product. The concentration of the forward primer (the limiting primer) was 2 μM while the concentration of the reverse primer (the excess primer) was 200 μM. The reactions were incubated at 95 ºC for 2 min, followed by cycles of 95 ºC for 30 s, 58ºC for 45 s and 72 ºC for 30 s. To profile the amplification process, PCR samples were taken from the thermocycler at different cycle numbers (i.e. every two cycles or every 5 cycles).

5.2.7 Sensor Fluidics and Sample Introduction

PCR samples (50 μL) were diluted in 350 μL of the hybridization buffer described in the *Materials* section. The hybridization of the samples was carried out at room temperature, passing the fluids above the chip surface at a rate of 20 μL/min for 13 min. After the hybridization of each cycle sample, the chip was rinsed with the hybridization buffer for 2 min. The full hybridization assay protocol can be seen in the Table 5.2.

5.2.8 Quantitative PCR

Real time quantitative PCR was performed using a 7900HT Fast Real-Time PCR system (ThermoFisher). Reverse transcription protocols were identical to those listed in the *Reverse transcription - asymmetric PCR* section. Each reaction contained 5.6 μL of nuclease free water, 10 μL of SYBR® Select Master Mix, 2 μL of each primer (2 μM) and 0.4 μL of the reverse transcription product. The reaction was initiated at 95 ºC for 2 min, followed by 40 cycles at 95

ºC for 15 s followed by 58 ºC for 1 min. The threshold cycle (C_t) was automatically determined by the software provided with the instrument.

5.2.9 Data Analysis

The microring response was analyzed using OriginPro8 (OriginLab, Northampton, MA). The net shift signal from specific rings was corrected for temperature and instrument drift by subtracting the signal of control rings from the active rings functionalized with DNA capture probes. The data for every target in each sample was detected and averaged using 8 to 16 replicate measurements on a single chip.

5.3. Results and Discussion

In this study, we were able to detect and quantify the expression of two long non coding RNAs in three different RNA samples using a microrring resonator platform**.** The schematic of the assay can be visualized in Figure 5.1. In this assay, lncRNAs from different RNA samples were reversed transcribed using the target specific primers listed in Table 5.1. After reverse transcription, we use asymmetric PCR to selectively produce ssDNA at cycle values that are proportional to the initial concentration in the sample of interest. In asymmetric PCR, one of the primers is introduced in a limiting concentration and so, when all of the limiting primer is extended, only the primer in excess is extended and ssDNA is produced. This ssDNA product can then be detected using microring arrays when they hybridize with complimentary capture probes on the microring surface.

With this assay, we aimed to mimic the quantification process of qPCR, so we collected asymmetric PCR samples after varying amounts of thermal cycles. In the case of conventional qPCR, double stranded DNA is detected by the addition of SYBR dyes® and fluorescence

intensity increases upon double stranded DNA (dsDNA) accumulation. The fluorescent intensity is plotted against increasing PCR cycle number and expression profiles can be calculated based on the cycle at which fluorescent signal begins. With the aPCR-microring system, we quantitate ssDNA accumulation instead of dsDNA accumulation. The microring signal will increase upon hybridization of ssDNA targets to complimentary capture probes on the sensor surface. This will occur at increased number when compared to traditional qPCR (see Fig. 5.1B).

5.3.1 Optimization of PCR Amplification and Detection

An important step in the optimization of the protocol was the design of primer pairs and the resulting PCR product. For this purpose, Primer-BLAST was used.[25] This free online platform was very helpful in the designing of primers that contained the desired features and prevented the amplification of undesired regions. In addition to primer set design, the preferred amplified regions (PCR products) needed to have as little secondary DNA structures as possible in order to maximize hybridization to surface bound capture probes. Therefore, once we selected a pair of primers, we modeled the secondary structure of the amplified region using the Dinamelt web server to ensure that is linear.[26] An example of this process is included in Figures 5.2-5.3. First, this server was used to observe the folding of the molecules to assess secondary structure of the PCR product (Figure 5.2). The importance of minimizing secondary structure is shown in Figure 5.3. Primer sets for β-actin were designed with one set producing a PCR amplicon with a high degree of secondary structure and another set minimizing secondary structure. The microring signal response is much higher for the primer set minimizing secondary structure. After primer design optimization using computational tools, all of the primer pairs were validated using gel electrophoresis to ensure that they selectively produce a single band at the proper size range (Figure 5.4).

Once primer design was optimized, we proceeded to assess the selectivity of the capture probes arrayed on the sensor chip surface. In order to do so, we arrayed four capture probes per detection channel. A spotting layout and image of the arrayed captures are included in Figure 5.5. Next, RT-aPCR was carried out for each target using the healthy brain RNA reference sample. An initial input of 40 ng RNA was used for the RT, followed by 45 aPCR amplification cycles. Samples were individually introduced and allowed to hybridize on a sensor array that contained the capture probes for all studied transcripts. The results of these experiments are shown in Figure 5.6, where the aPCR products bind to the desired capture probes with limited non-specific response.

After validation of the primer sets and specificity of the microring sensor array, we developed a protocol to quantify the expression of target RNAs in a sample. To complete this, aPCR samples were collected after a varying number of thermal cycles. Then, they were sequentially introduced to a single microring array. An example sensorgram from this type of experiment can be seen in Figure 5.7A. Samples were collected between 25 and 45 cycles, because it was observed that there was no detectable signal at cycle numbers lower than 30 and further amplification after 45 cycles did not yield an increase in microring signal (data not shown). The trace signals observed in Figure 5.7A correspond to the average responses of 16 rings replicates on a single chip. After 13 min of hybridization at each cycle number, a 2 minute buffer step is added and is used to quantify Relative Shift values following hybridization. This is completed by subtracting the signal of control rings (Fig. 5.7A, blue trace) from the signal of target specific rings (Fig. 5.7A, red trace). The resulting calculated net shift induced by DNA binding is plotted versus the PCR cycle (Fig. 3B). In order to compare expression between samples, we follow similar qPCR quantification protocols and calculate a cycle threshold.[27] This

is completed by determining the Relative Shift corresponding to 40% of the maximum signal of the amplification trace. At this Relative Shift threshold, we then determine at what cycle number the amplification crosses that threshold. Forty percent of the maximum signal was chosen because it is significantly above the noise of the baseline and is not prone to any errors when the amplification trace plateaus. This method also corrects any experimental or fabrication variations between microring arrays by not relying on a set Relative Shift threshold value.

5.3.2 Demonstration in Clinically Relevant Samples

After completing the optimization steps of the assay, we move to show the clinical utility of this platform by profiling the expression of multiple RNA sequences from multiple human derived samples, two commercially available pooled healthy RNA samples and RNA extracted from a glioblastoma cell line (GBM6). To ensure biological relevance, we chose lncRNAs that play important roles in the development or progression of brain cancer. KIAA0495/PDAM has been shown to act as a tumor suppressor in oligrodendrioglioma because of its activity blocking the expression of a p53 inhibitor.[28] The other target, MALAT 1 (metastasis associated lung adenocarcinoma transcript 1), is a lncRNA that has been studied in different tumors.[29] MALAT 1 was first studied in NSCLC (non-small cell lung cancer cell) patients, and it was found that higher expression levels of MALAT1 occurred in those patients with metastasis.[30] However, it has also been seen that MALAT1 can act as a tumor suppressor in glioblastoma.[31] To correct from any sample processing variability we incorporate β-actin as an internal control.[32] When analyzing these biological samples, we first measured lncRNA expression in different human tissues where minimal expression differences are expected (EMBL-EBI Expression atlas: MALAT1; EMBL-EBI Expression Atlas: TP73-AS1 (KIAA)). After this validation step, we

aimed to analyze lncRNA expression in glioblastoma samples, where lncRNAs have been shown to be differentially expressed.[33]

The amplification plots obtained from the three samples using the previously described method are shown in Figure 5.8. Additionally, the raw data used to compile these amplification profiles are plotted in Figure 5.9. The C(t) values were calculated as described in the previous section and can be seen in Table 5.3. To validate the results obtained with the microring resonator platform, the same RNA samples were profiled using qRT-PCR. The C(t) values obtained from this method are also shown in Table 5.3. The correlation of the results can be seen in Figure 5.10. Figure 5.10 represents the fold change in the expression of the transcripts in the cell line, GBM6, compared to the healthy brain reference and the differential expression between the two healthy tissues, brain and lung. The internal control, β-actin, was used to normalize the results and correct for initial input of RNA and other variabilities. Both techniques showed trends in the same direction, proving the consistency of our method. Additionally, we can further validate these results upon comparison with previously published studies in the literature, such as the downregulation of MALAT1 in glioblastoma samples.[31]

5.4 Conclusions

With this study, we demonstrate a promising approach for the multiplexed detection of long non coding RNAs. We have shown that the microring resonator platform combined with reverse transcription and asymmetric PCR is able to produce similar results as those obtained using the gold standard in transcript quantification, qRT-PCR. Using the described protocol, we were able to detect the differential expression of two lncRNAs. The introduction of an internal control allowed us the compare the expression among different samples. Additionally, this

platform decreased input amounts to clinically relevant levels, provides results within hours, and has the potential to analyze 32 RNA targets per sample. Future directions will include expanding multiplexing capabilities in lncRNA analysis, interrogating multiple cell lines to study role lncRNAs play in various cancer types, and interfacing thermocycling with microring detection using a single device.

5.5 Figures and Tables

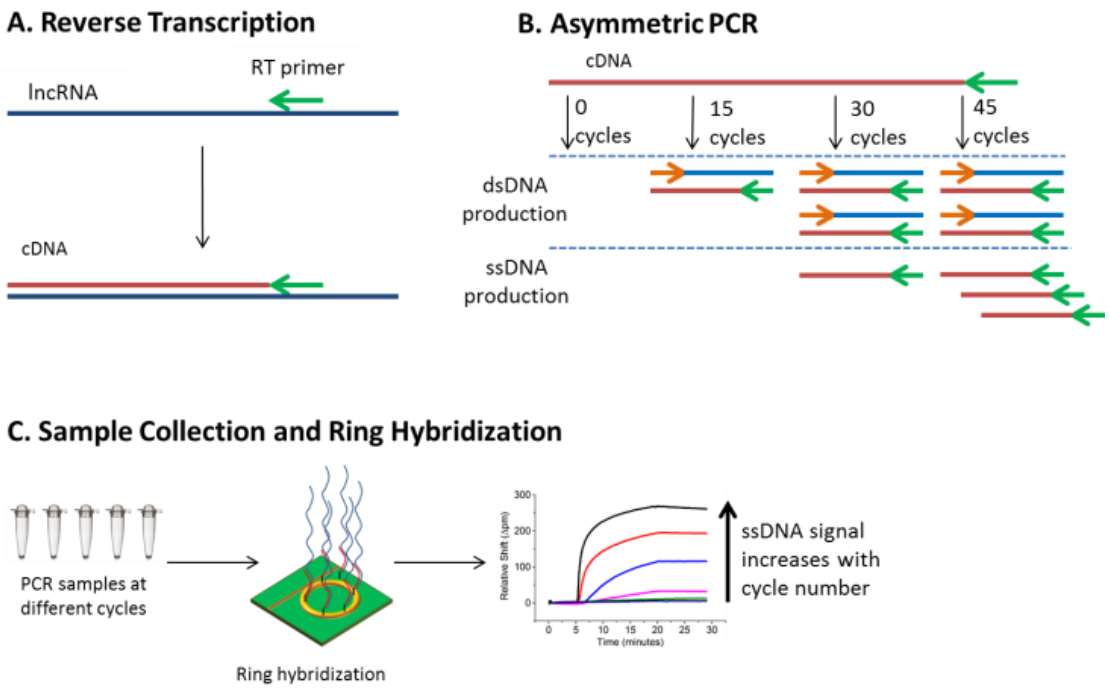

Figure 5.1: Assay schematic for microring resonator detection of long non coding RNAs.

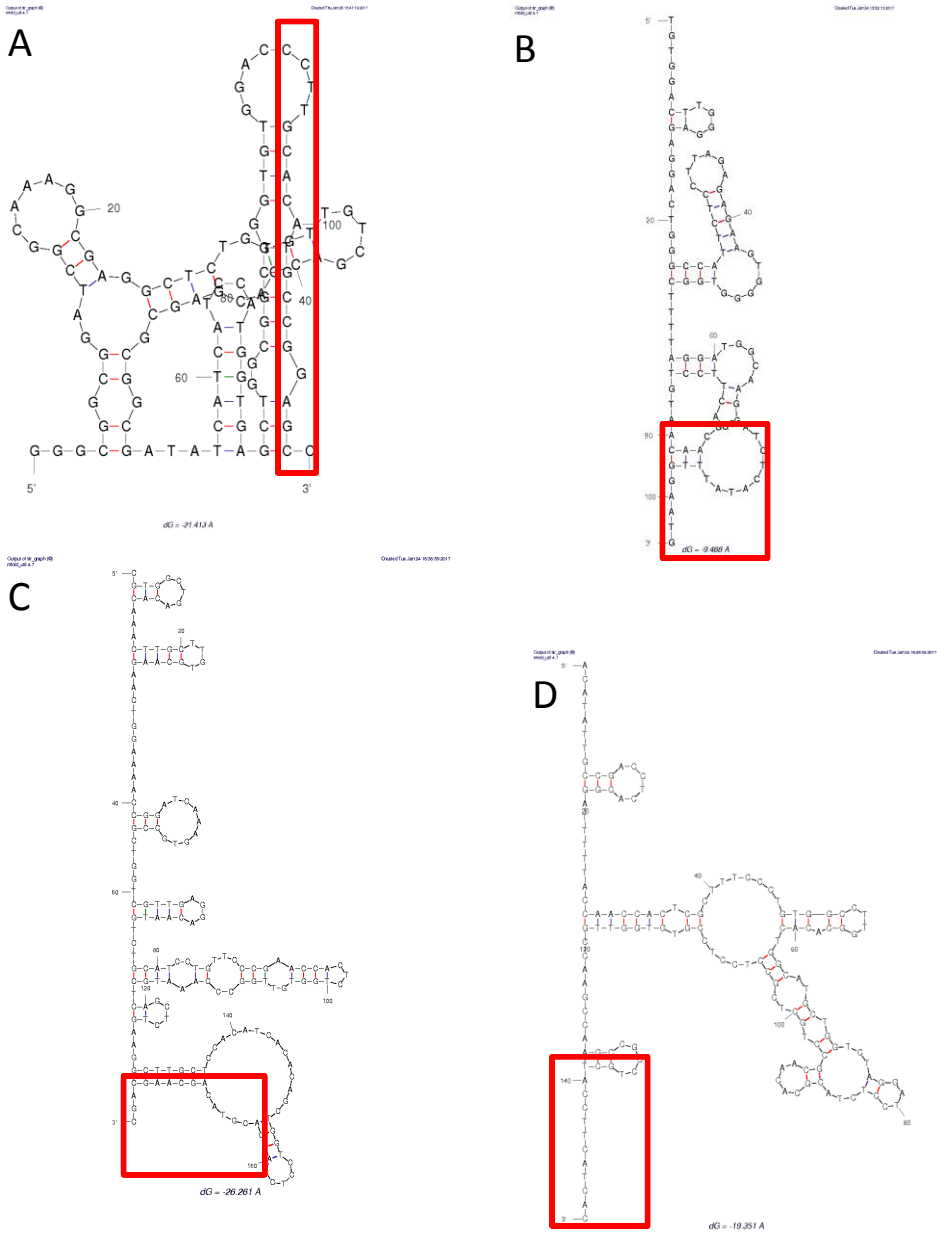

Figure 5.2: Secondary structures of amplified regions obtained using the DinaMelt Web Server. The region that binds to the capture probe is highlighted with a red square. (A) β-actin amplified region will not bind to complimentary capture probes due to excessive secondary structure. (B) β-actin amplified region after primer redesign that enables surface binding. (C) KIAA0495 amplified region with minimal secondary structure. (D) MALAT1 amplified region with minimal secondary structure.

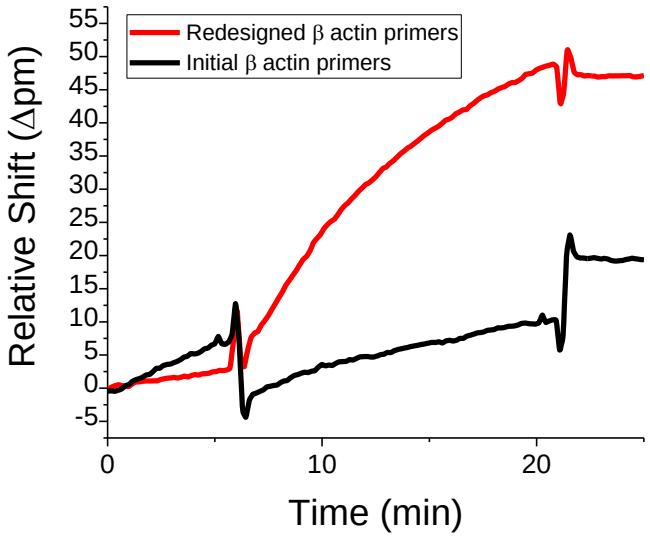

Figure 5.3: Comparison of β-actin PCR product binding with and without optimized primer design. The red trace shows improved binding when using the optimized primer sets (predicted structure shown in in Supplementary Figure 1B). The black trace shows data obtained using the PCR amplicon with a high degree of secondary structure (Supplementary Figure 1A).

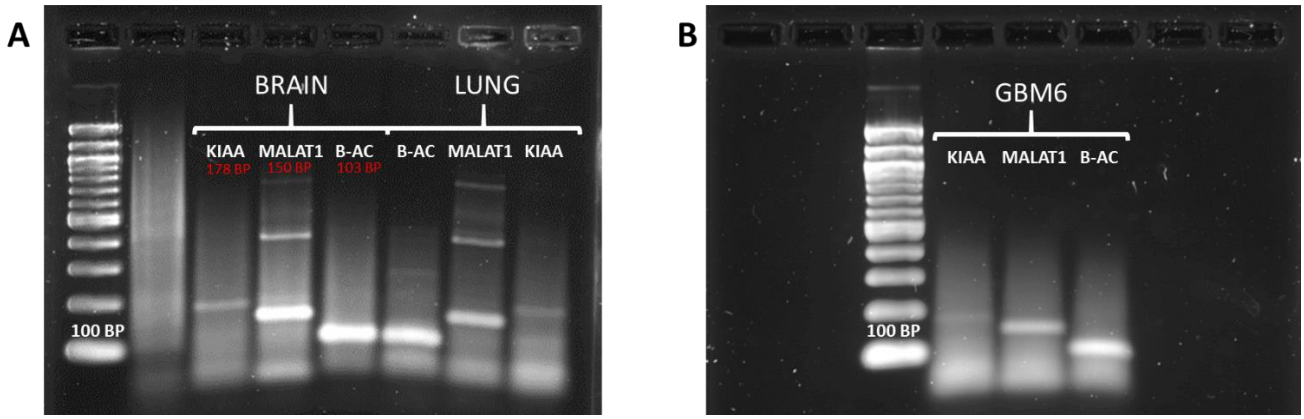

Figure 5.4: Agarose gel electrophoresis (2% agarose; SYBR Gold Stain) used to prove specific PCR amplification: (A) brain and lung RNA samples; (B) GBM6 cells RNA sample. Expected PCR product sizes are listed in red.

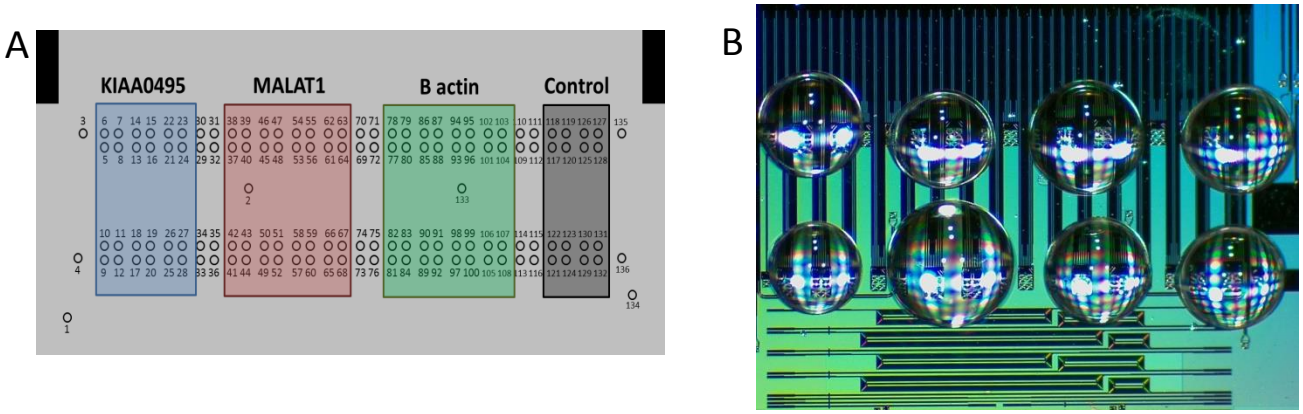

Figure 5.5: (A) Spotting layout of microring sensor chip. (B) Image of microring functionalization corresponding to the layout in Fig. 5.5A.

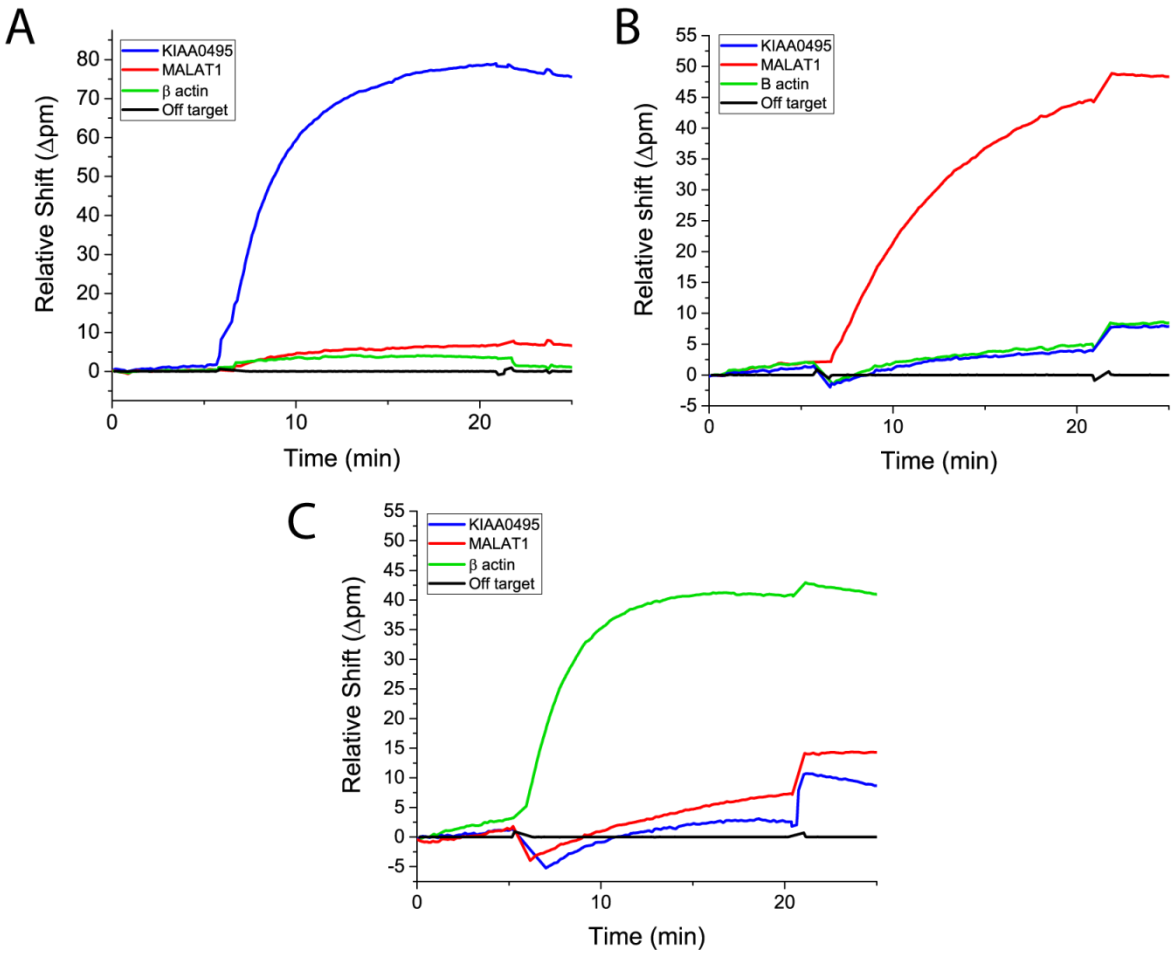

Figure 5.6: Cross-reactivity study used to determine the selectivity of the capture probes towards their specific target (A) KIAA0495, (B) MALAT1, and (C) β-actin.

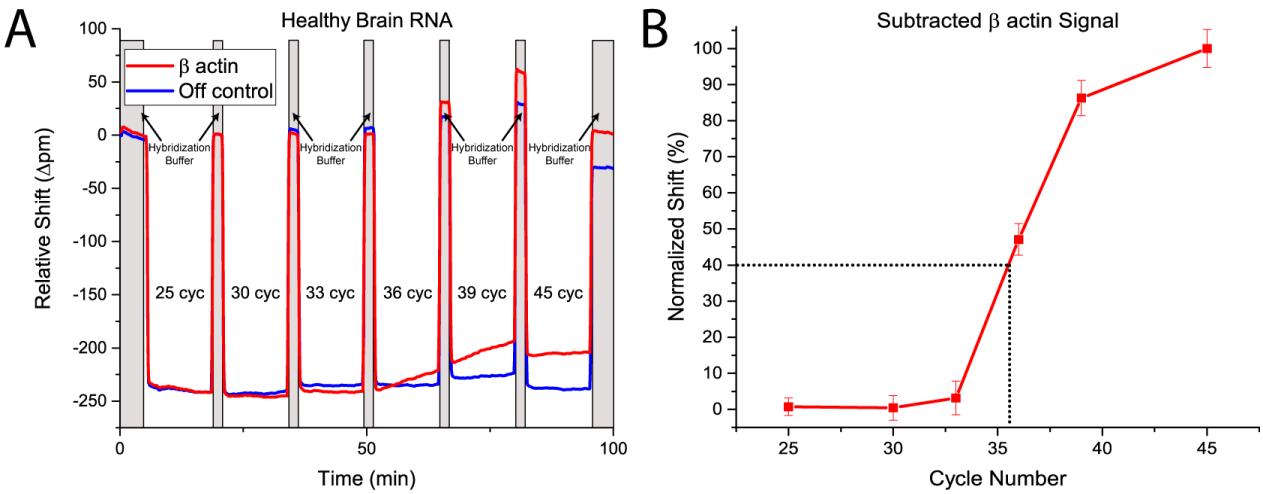

Figure 5.7: (A) Detection of the β-actin aPCR product at different cycles using one microring resonator array. The chip was functionalized with either the specific transcript (red) or an off target (blue) DNA oligonucleotide capture probes. (B) Amplification curve for β-actin in healthy brain reference RNA. The dotted lines outline the quantification process.

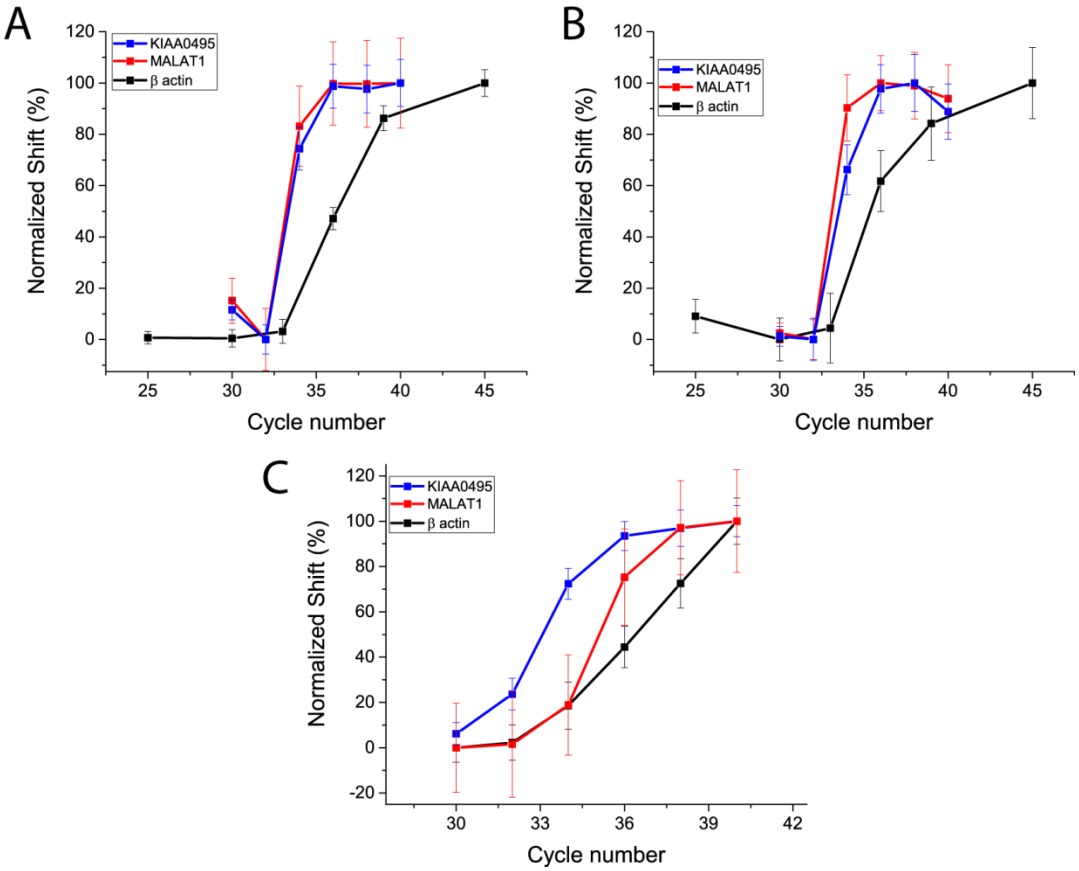

Figure 5.8: Amplification curves for the lncRNAs and internal control target (A) Healthy brain RNA, (B) Healthy Lung RNA, and (C) GBM 6 RNA

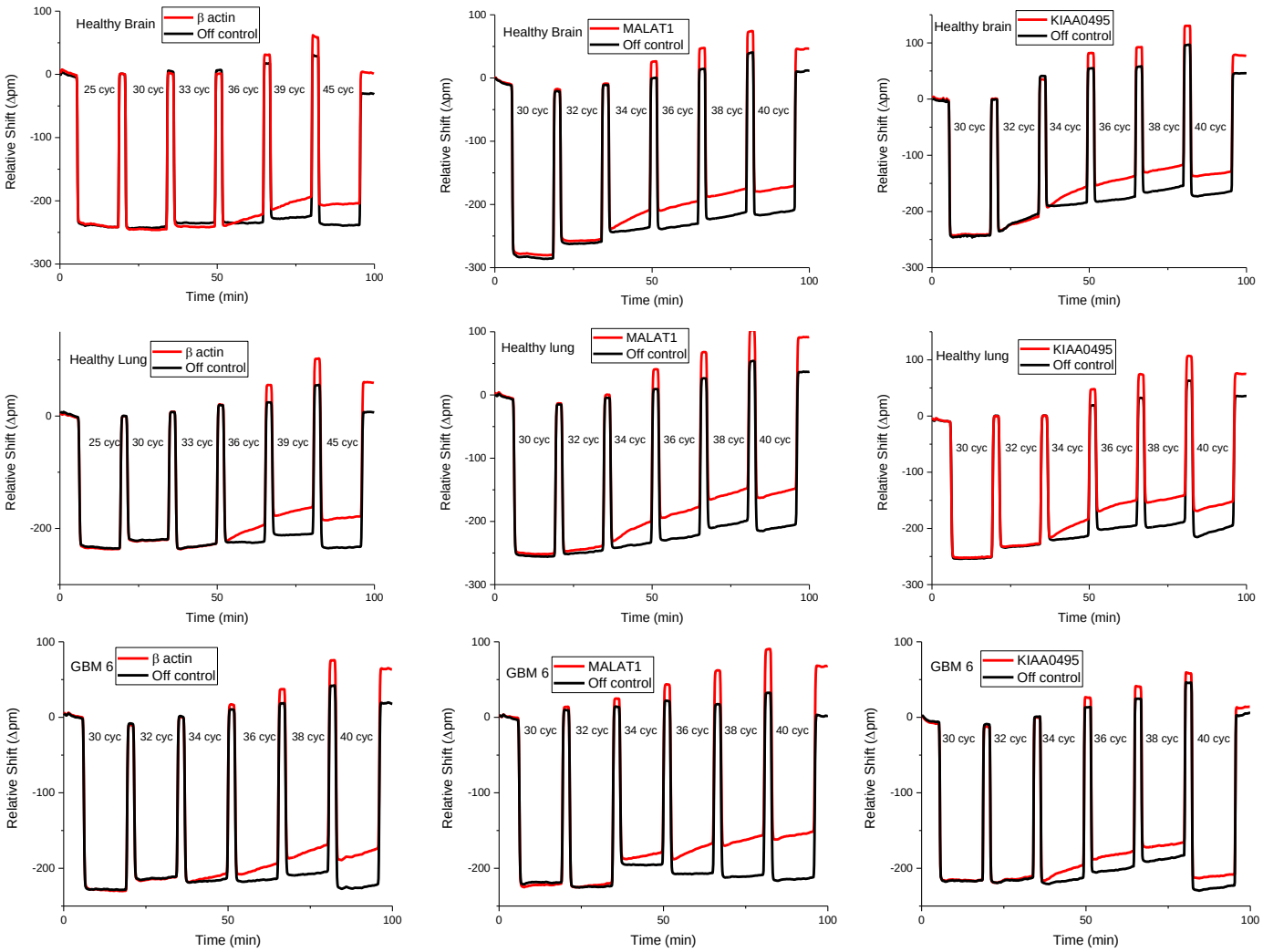

Figure 5.9: Microring traces used to calculate amplification plots in Figure 4. The trace signal represents the average from 8 – 16 ring replicates.

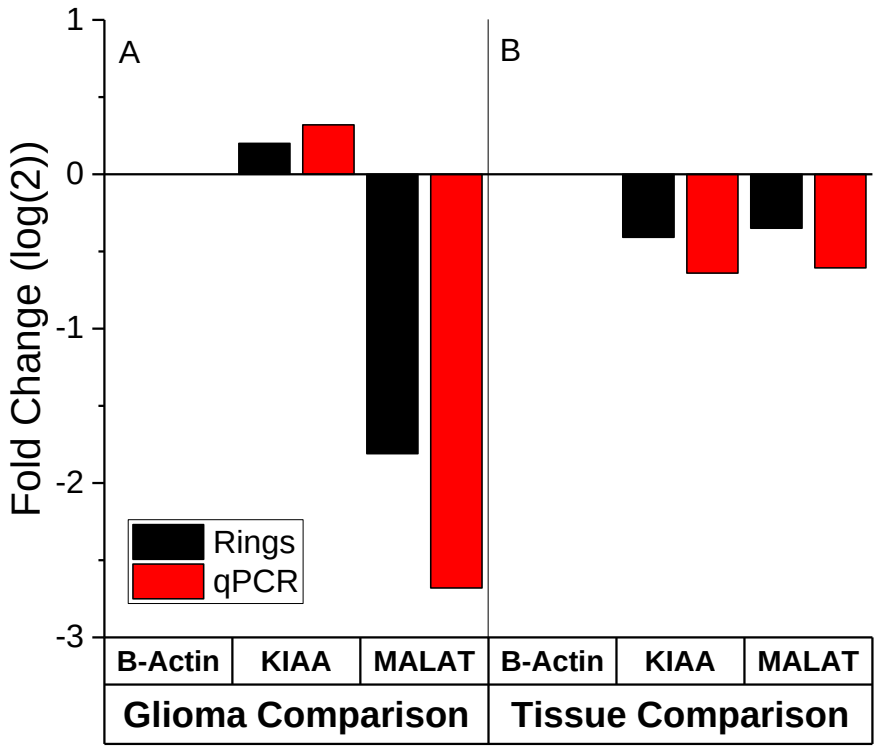

Figure 5.10: Comparison of fold changes using the microring resonator platform and quantitative PCR. Fold changes were calculated by normalizing to an internal control and comparing (A) lncRNA expression in GBM6 and healthy brain tissue and (B) the expression in lung and brain tissue.

Targeted transcript		Sequence (5' → 3')	Tm (° C)	Amplicon length
KIAA0495	RP (RT primer)	GCTGCTTGCTGTACGTGGTG	62.18	178 nt
	FP	CGTGGCTGACACAAACTTGC	60.59	
	CP	/5AmMC12/GCTGCTTGCTGTACGTGGTG		
MALAT1	RP (RT primer)	GTGATGAAGGTAGCAGGCGG	60.81	150 nt
	FP	ACATATTGCCGACCTCACGG	60.18	
	CP	/5AmMC12/GTGATGAAGGTAGCAGGCGG		
β-actin	RP (RT primer)	CATTCCAAATATGAGATGCGTTGT	58.18	103 nt
	FP	TGTGGACTTGGGAGAGGACT	59.81	
	CP	/5AmMC12/CATTCCAAATATGAGATGCGTTGT		
Off Target Control	CP	/5AmMC12/CTACAAGTGCCTTCACTGCAGT		

Table 5.1: Primers used in the experiments for reverse transcription, asymmetric PCR and qRT-PCR. Thermodynamic calculations were obtained from the Primer-Blast platform.

Step	Flow Rate (µL/min)	Duration (min)
Hybridization buffer	20	5
RT-PCR product cycle 30	20	13
Hybridization buffer	20	2
RT-PCR product cycle 32	20	13
Hybridization buffer	20	2
RT-PCR product cycle 34	20	13
Hybridization buffer	20	2
RT-PCR product cycle 36	20	13
Hybridization buffer	20	2
RT-PCR product cycle 38	20	13
Hybridization buffer	20	2
RT-PCR product cycle 40	20	13
Hybridization buffer	20	5

Table 5.2: Fluidic handling protocol for the ring hybridization steps

RNA	Target	qRT-PCR C(t)	Rings C(t)	qPCR Fold change (log(2))**	Rings Fold change (log(2))**
Brain	B actin	17.40	35.65	-	-
	KIAA0495	21.16	33.09	-	-
	MALAT1	17.77	33.04	-	-
Lung	B actin	17.40*	35.65*	0	0
	KIAA0495	21.57*	33.44*	- 0.41	- 0.64
	MALAT1	16.38*	33.68*	- 0.61	- 0.35
GBM 6	B actin	17.40*	35.65*	0	0
	KIAA0495	21.36*	32.72*	0.20	0.32
	MALAT1	19.05*	34.90*	-2.68	-1.81

* Corrected signal with internal control

** Healthy brain as reference; Fold Change = C(t)ref – C(t)sample

Table 5.3: Calculated qRT-PCR and microring C(t) values from healthy brain, healthy lung and GBM6 RNA samples. The RNA input for qRT-PCR experiments was 40 ng, and the qRT-PCR experiments were completed in triplicate.

5.6 References

(1) Byron, S. A.; Van Keuren-Jensen, K. R.; Engelthaler, D. M.; Carpten, J. D.; Craig, D. W. *Nat Rev Genet* **2016**, *17*, 257-271.

(2) Qi, P.; Du, X. *Mod Pathol* **2013**, *26*, 155-165.

(3) Mattick, J. S.; Makunin, I. V. *Human Molecular Genetics* **2006**, *15*, R17-R29.

(4) Bartolomei, M. S.; Zemel, S.; Tilghman, S. M. *Nature* **1991**, *351*, 153-155.

(5) Baker, M. *Nat Meth* **2011**, *8*, 379-383.

(6) *Annual Review of Biochemistry* **2012**, *81*, 145-166.

(7) Fatica, A.; Bozzoni, I. *Nat Rev Genet* **2014**, *15*, 7-21.

(8) Gibb, E. A.; Brown, C. J.; Lam, W. L. *Molecular Cancer* **2011**, *10*, 38.

(9) Prensner, J. R.; Chinnaiyan, A. M. *Cancer Discovery* **2011**, *1*, 391.

(10) Zhang, X.; Sun, S.; Pu, J. K. S.; Tsang, A. C. O.; Lee, D.; Man, V. O. Y.; Lui, W. M.; Wong, S. T. S.; Leung, G. K. K. *Neurobiology of Disease* **2012**, *48*, 1-8.

(11) Zhang, X.-Q.; Sun, S.; Lam, K.-F.; Kiang, K. M.-Y.; Pu, J. K.-S.; Ho, A. S.-W.; Lui, W.-M.; Fung, C.-F.; Wong, T.-S.; Leung, G. K.-K. *Neurobiology of Disease* **2013**, *58*, 123-131.

(12) Pritchard, C. C.; Cheng, H. H.; Tewari, M. *Nat Rev Genet* **2012**, *13*, 358-369.

(13) Graybill, R. M.; Bailey, R. C. *Analytical Chemistry* **2016**, *88*, 431-450.

(14) Iqbal, M.; Gleeson, M. A.; Spaugh, B.; Tybor, F.; Gunn, W. G.; Hochberg, M.; Baehr-Jones, T.; Bailey, R. C.; Gunn, L. C. *IEEE Journal of Selected Topics in Quantum Electronics* **2010**, *16*, 654-661.

(15) Qavi, A. J.; Bailey, R. C. *Angewandte Chemie International Edition* **2010**, *49*, 4608-4611.

(16) Washburn, A. L.; Luchansky, M. S.; Bowman, A. L.; Bailey, R. C. *Analytical Chemistry* **2010**, *82*, 69-72.

(17) Luchansky, M. S.; Washburn, A. L.; McClellan, M. S.; Bailey, R. C. *Lab on a Chip* **2011**, *11*, 2042-2044.

(18) Wade, J. H.; Alsop, A. T.; Vertin, N. R.; Yang, H.; Johnson, M. D.; Bailey, R. C. *ACS Central Science* **2015**, *1*, 374-382.

(19) Kindt, J. T.; Bailey, R. C. *Analytical Chemistry* **2012**, *84*, 8067-8074.

(20) Scheler, O.; Kindt, J. T.; Qavi, A. J.; Kaplinski, L.; Glynn, B.; Barry, T.; Kurg, A.; Bailey, R. C. *Biosensors and Bioelectronics* **2012**, *36*, 56-61.

(21) Qavi, A. J.; Kindt, J. T.; Gleeson, M. A.; Bailey, R. C. *Analytical Chemistry* **2011**, *83*, 5949-5956.

(22) Graybill, R. M.; Para, C. S.; Bailey, R. C. *Analytical Chemistry* **2016**, *88*, 10347-10351.

(23) Gyllensten, U. B.; Erlich, H. A. *Proceedings of the National Academy of Sciences* **1988**, *85*, 7652-7656.

(24) Sanchez, J. A.; Pierce, K. E.; Rice, J. E.; Wangh, L. J. *Proceedings of the National Academy of Sciences* **2004**, *101*, 1933-1938.

(25) Ye, J.; Coulouris, G.; Zaretskaya, I.; Cutcutache, I.; Rozen, S.; Madden, T. L. *BMC Bioinformatics* **2012**, *13*, 134.

(26) Markham, N. R.; Zuker, M. *Nucleic Acids Research* **2005**, *33*, W577-W581.

(27) Schmittgen, T. D.; Livak, K. J. *Nat Protoc* **2008**, *3*.

(28) Pang, J. C.-S.; Li, K. K.-W.; Lau, K.-M.; Ng, Y. L.; Wong, J.; Chung, N. Y.-F.; Li, H.-M.; Chui, Y.-L.; Lui, V. W. Y.; Chen, Z.-p.; Chan, D. T.-M.; Poon, W. S.; Wang, Y.; Mao, Y.; Zhou, L.; Ng, H.-K. *Brain Pathology* **2010**, *20*, 1021-1032.

(29) Yuting, W.; Cheng, H.; Xiaoming, M.; Jun, L. *Current Pharmaceutical Design* **2015**, *21*, 5017-5028.

(30) Ji, P.; Diederichs, S.; Wang, W.; Boing, S.; Metzger, R.; Schneider, P. M.; Tidow, N.; Brandt, B.; Buerger, H.; Bulk, E.; Thomas, M.; Berdel, W. E.; Serve, H.; Muller-Tidow, C. *Oncogene* **0000**, *22*, 8031-8041.

(31) Han, Y.; Wu, Z.; Wu, T.; Huang, Y.; Cheng, Z.; Li, X.; Sun, T.; Xie, X.; Zhou, Y.; Du, Z. *Cell Death Dis* **2016**, *7*, e2123.

(32) Thellin, O.; Zorzi, W.; Lakaye, B.; De Borman, B.; Coumans, B.; Hennen, G.; Grisar, T.; Igout, A.; Heinen, E. *Journal of Biotechnology* **1999**, *75*, 291-295.

(33) Kiang, M. K.; Zhang, X.-Q.; Leung, K. G. *Cancers* **2015**, *7*.

Chapter 6

ADDITIONAL RESEARCH EFFORTS AND FUTURE DIRECTIONS

Acknowledgements:

The canine osteosarcoma work discussed here was in collaboration with Prof. Timothy Fan in the Department of Veterinary Medicine at UIUC. I would like to acknowledge the work your lab has done to collect and bank the canine blood samples as well as your insights along the way to help frame this study and interpret the results. I also would like to acknowledge support from the National Cancer Institute Alliance for Nanotechnology in Cancer "Midwest Cancer Nanotechnology Training Center" Grant R25CA154015A.

The initial studies regarding the pathogen work presented in this Chapter are in collaboration with Prof. Douglas Mitchell. In addition, I would like to acknowledge Graham Hudson who performed the bacteria culture and RNA isolation.

6.1 Additional Research Effort: Profiling Circulating miRNA Targets in Canine Osteosarcoma

Canine osteosarcoma (OSA) patients have many biological and clinical similarities to human OSA patients, where it develops predominantly in children. Like children, OSA is the most common primary bone malignancy in dogs.[1] While advances in treatment over the last several decades have pushed five year survival rates above 70%, pulmonary metastases are typically the cause of death in both humans and dogs.[2] This, in combination with variable survival rates, suggests that OSA in both humans and canines exhibits variable metastatic capability, rate and/or resistance to chemotherapy.[3] Additionally, these similarities have shown that canine patients serve as good models for human osteosarcoma,[4-6] and that identifying biomarkers linking patients with likelihood of metastasis would help identify therapeutic decisions.

Recent studies have identified miRNA panels that are associated with OSA progression,[7,8] prognosis,[9] and chemotherapeutic response.[10] However, a diagnostic test that determines the likelihood of metastasis is lacking in the clinic. Given the success of miRNA panels to determine clinical outcomes, we have applied a similar assay to that listed in Chapters 4-5 in an attempt to analyze profiles of circulating microRNAs found in patient's blood that are predictive of OSA metastasis. Circulating miRNAs are a promising class of miRNA that can be detected by a simple blood test. This makes the resulting diagnostic test non-invasive and provides the ability to perform multiple blood draws to continuously monitor patients and determine the chance of metastasis in real time.

To complete this, a panel was developed using circulating miRNAs linked to OSA diagnosis[8] as well as additional miRNA targets that have been linked to cancer metastasis.[9,10] The microRNA targets are listed in Table 6.1. Next, blood samples were obtained from Prof.

Tim Fan (UIUC Veterinary Medicine). Blood samples were collected every four weeks during the course of treatment. This allowed for the longitudinal study of circulating biomarkers in the patient's bloodstream. Analysis of the time scale at which miRNA expression panels change and linking the changes of specific miRNA to metastasis onset could provide the missing link in OSA diagnostics.

The blood samples were split into three cohorts, poor responders, good responders and healthy canine patients. The poor responder cohort lived a maximum of 130 days after treatment started; whereas, the good responder cohort lived at least 237 days. Healthy patient samples were profiled in an attempt to understand the underlying biomolecular signatures of canines. It is important to note that both the poor responders and good responders eventually passed away due to metastasis to various tissues in the body.

In order to detect circulating miRNA in these patient samples, we followed the following experimental protocol. The miRNeasy Serum/Plasma Kit (Qiagen) was used to isolate circulating RNAs from blood samples. It is important to avoid heparinized samples, as heparin is a PCR inhibitor. After using UV-Vis spectroscopy, concentrations and RNA integrity were determined. RNA samples were then diluted in RNase-free water to 1 nanogram per microliter. Reverse transcription products were prepared using the TaqMan microRNA reverse Transcription Kit, and the recommended experimental protocol from the manufacturer was followed. The final volume of all stem loop primers in the SLP mix was 200 μM. After reverse transcription, asymmetric PCR was performed using the Platinum® Multiplex PCR Master Mix. Each 50 μL reaction volume was composed of 14 μL nuclease free water, 25 μL of Platinum® Multiplex PCR Master Mix, 5 μL of each primer and 1 μL of the reversed transcribed product. The concentration of the forward primer (the limiting primer) was 2 μM while the concentration

of the reverse primer was 200 μM. The reactions were incubated at 95 ºC for 2 min, followed by 50 cycles of 95 ºC for 30 s, 56ºC for 1 min 30 s and 72 ºC for 1 min.

The resulting PCR product was introduced to the microring chip at 20 μL per minute using the fluidic handling protocol listed in Table 6.2. For this project, a new generation of the Maverick silicon photonic microring resonator platform was used. This featured arrays of 12 sensor chips that could be run sequentially and eliminates the needs to fabricate sensor cartridges for every experiment. We incorporated an internal control, cel-39, to correct for any differences between runs. This was completed by adding a fixed amount of the miR sequence before RNA extraction. Since this should yield identical Relative Shift values upon ring quantification, any differences in this signal used to normalize the rest of the miRNA target Relative Shift values.

In order to quantitate the data, a modified protocol to that presented in Chapters 4-5 was followed. First, a calibration curve was prepared by preparing varying concentrations of miR-21 and subjecting it through a fixed number of aPCR cycles. This calibration curve was then used to determine the concentration of miRNA in the sample of interest, after normalizing to cel-39. This quantification protocol was followed before the updated version was developed. It would be interesting to recollect this data using the updated quantification method.

The preliminary results for all patients can be seen in Figures 6.1-3. Figure 6.1 shows the underlying biological variability in the RNA signatures of healthy patients. It is apparent that there is some patient to patient variability, as Patients 1 and 2 have much higher expression levels compared to the others. Figure 2 and 3 shows the comparison between data collected using the microring resonator platform and qRT-PCR for the poor and good responding cohorts, respectively. Given the differing quantification protocols between the platforms, it is hard to directly compare the results, which is why overall magnitude and expression trajectories deviate

in some cases. Additionally, there were no readily apparent expression changes that corresponded to cancer metastasis.

These results show the possibility to profile blood-based biomolecular profiles. It also shows that there is a need for better predictive algorithms that can deconvolute changes in expression over time to aid in clinical decisions. Additionally, there are improvements that can be made to the experimental design to help correct for underlying biological variability. First, some of the miRNA targets were based on studies relating miRNA expression to OSA outcome in human samples. We assumed that these findings would still be relevant in canines as well but this assumption has not yet been validated. Second, using the improved quantitation protocol will increase the dynamic range of the sensing platform by effectively removing the baseline and plateau of the calibration curve. This would allow for the direct comparison between qRT-PCR and the microring platform. Third, there is no correction for canine breed or at what time point they are in disease progression. Lastly, instead of just profiling multiple healthy patients at one time point, it would be interesting to first understand the temporal dynamics of circulating miRNA expression in healthy individuals before moving to diseased patients to see what moves are statistically significant.

6.2 Conclusions and Future Work

The work presented in this dissertation lays the foundation to make multiplexed RNA measurements in clinical samples. Moving forward, additional milestones will need to be reached. Chapters 3-5 discussed the development and application of enzymatic processing strategies for RNA detection that provided lower sample input requirements, expanded dynamic ranges, and reduced assay times compared to previous lab attempts. The aPCR assay presented in Chapters 4 and 5 provided better figures of merit, which makes it the scheme of choice for

future studies. Future iterations of this this assay will need to focus on further automation, decreasing PCR reaction volume, and decreased time to result. Additionally, after these assay improvements are made, further clinical utility will need to be determined.

While Chapter 4 laid the foundation for the development of the aPCR assay for short RNA sequences, Chapter 5 not only translated this to longer RNAs but also lowered the aPCR processing time from over three minutes per cycle to under two minutes. Further progress can be made here by further automating the system. The main limitation currently is the PCR volume. The current instrumentation needs approximately 300 microliters of solution to be able to flow long enough to get consistent hybridization curves. Future efforts should aim to integrate microfluidic thermal cycling with the microring resonator array chip. This will allow for the sample volumes to decrease as well as allow for the repeated cycling of the PCR product. This will prevent the need for multiple aliquots of PCR samples, which makes the assay more cost effective and user friendly. Second, by using a microfluidic approach, the thermal cycling speed can go much faster since less material needs to be heated and cooled. This will then allow for the automated analysis of RNA molecules and make the transition to studying a higher number of samples more feasible.

After device optimization is completed, different biological systems can be probed both in clinical and research settings. In a clinical setting, we have started to make progress in diagnosing pathogenic infections based on RNA analysis. This is a unique problem because sepsis is a leading cause of death in hospitals. Diagnosis is of utmost importance to begin antibiotic therapy, as every hour of delay in administration of antibiotics is associated with an 8% decrease in survival rate.[11] Additionally, continuous reassessment is important, because inappropriate therapy deteriorates patient prognosis.[12]

Given the importance of making rapid diagnosis and the need to continuously reassess patient biomolecular profiles, current clinical gold standards have their own shortcomings. Bacterial culture and biochemical staining have long procedural times (24-72 hours) and limitations in identifying certain species. Likewise, sequencing techniques are too expensive and time consuming for an everyday clinical setting.[13] qPCR has sown particular promise in determining the pathogenic material based on unique 16S RNA sequences. Using the asymmetric PCR-microring platform, initial studies have validated primer sets to detect specific pathogen species based on differences in the 16S RNA sequence of each pathogen. The results are shown in Figure 6.4. Future work will aim to expand out this panel to determine antibiotic resistance in these samples. It is well documented that antibiotic resistant bacteria have evolved to obtain additional genes that lead to resistance of specific antibiotic therapies. In response to treatments, drug-resistant pathogens upregulate these genes, and yield the possibility to develop a biosensor to predict resistance.[14-16] After validation of antibiotic resistance determination, experiments in whole blood should be completed before profiling clinical samples. This finished product will be a two tier detection scheme where (1) infection determination based on 16S RNA target sequences and (2) antibiotic resistance determination based on dynamic changes to select genes.

6.3 Figures and Tables

	Overhang	Forward Primer	Sequence
miR-21	tcaacatca	CGCGCTAGCTTATCAGAC	UAGCUUAUCAGACUGAUGUUGA
miR-143	gagctacag	GCGCGTGAGATGAAGCA	UGAGAUGAAGCACUGUAGCUC
miR-34a	acaaccag	CGTGGCAGTGTCTTAGC	UGGCAGUGUCUUAGCUGGUUGU
miR-150	cactggtac	GCGTCTCCCAACCCTT	UCUCCCAACCCUUGUACCAGUG
miR-335	acatttttcg	CGCGTCAAGAGCAATAACG	UCAAGAGCAAUAACGAAAAAUGU
miR-340	aatcagtct	GCGCGCTTATAAAGCAATG	UUAUAAAGCAAUGAGACUGAUU
miR-544	gaacttgc	GCGCGATTCTGCATTTTTA	AUUCUGCAUUUUUAGCAAGUUC
miR-199-3p	aaccaatgt	GCGCACAGTAGTCTGC	ACAGUAGUCUGCACAUUGGUU
miR-140	tccgtgg	GCGACCACAGGGTAGAA	ACCACAGGGUAGAACCACGGA
miR-132	gcgacca	CGCTAACAGTCTACAGCCA	UAACAGUCUACAGCCAUGGUCGC
miR-34b	caatcagc	CGCGAGGCAGTGTAATTA	AGGCAGUGUAAUUAGCUGAUUG
miR-382	aaagtgttg	CGCGAATCATTCACGGA	AAUCAUUCACGGACAACACUUU
cel-39	caagctga	GCTCACCGGGTG TAAAT	UCACCGGGUGUAAAUCAGCUUG

Primer	Sequence
Reverse Primer	GTGCAGGGTCCGAGGT
Stem Loop Primer	GTC GTA TCC AGT GCA GGG TCC GAG GTA TTC GCA CTG GAT ACG AC...overhang
Capture Probes	Identical sequence to forward primers with 5’ amino group modification

Table 6.1: Table listing nucleic acid sequences used in the canine osteosarcoma study.

Step	Flow Rate (µL/min)	Duration (min)
Hybridization buffer	20	5
RT-PCR product	20	15
Hybridization buffer	20	5

Table 6.2: Summary of liquid handling steps

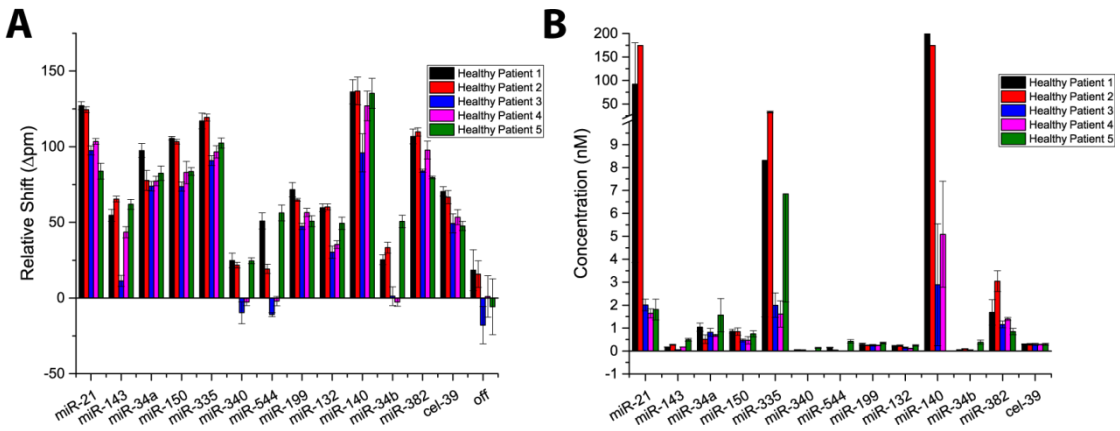

Figure 6.1: (A) Relative shifts obtained when profiling miRNA expression in the healthy patient cohort. (B) Calculated concentrations obtained after normalizing to cel-39.

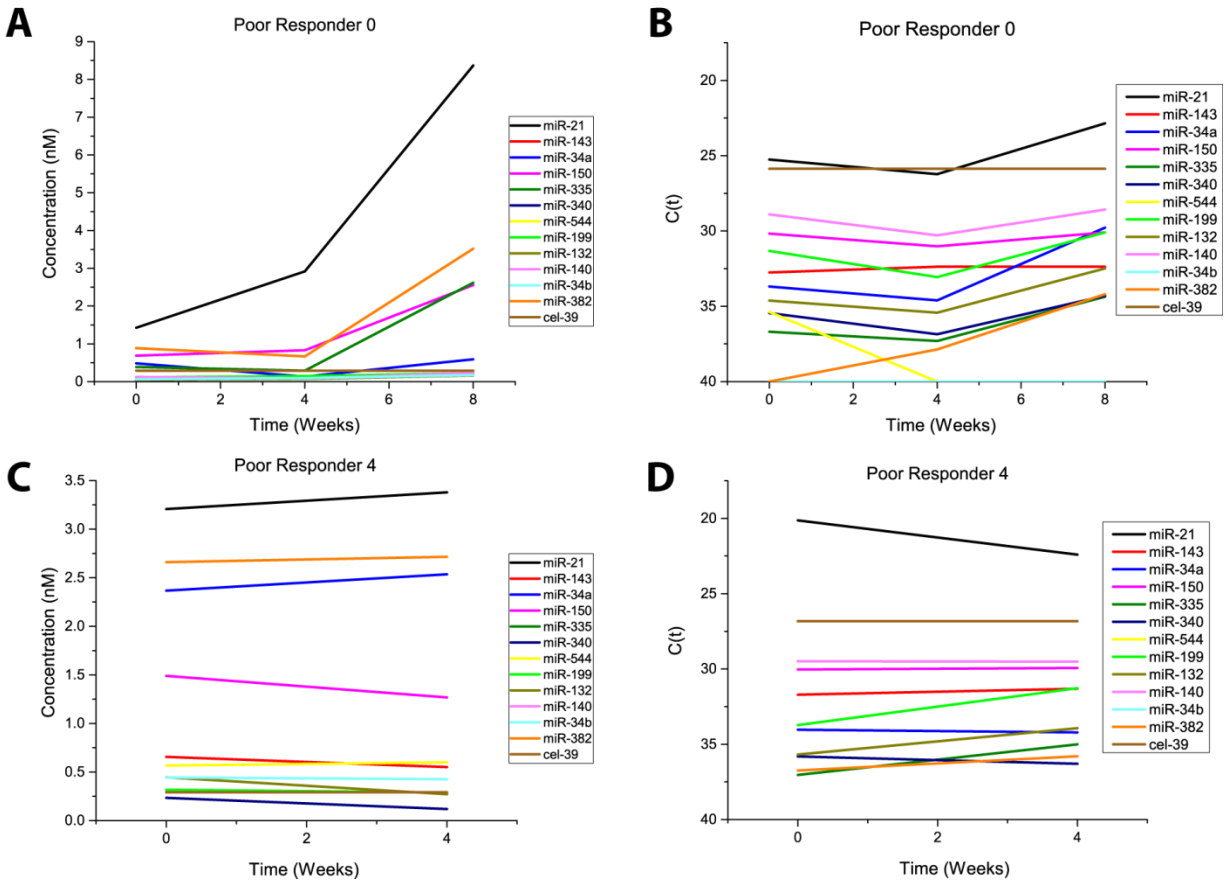

Figure 6.2: (A and B) Comparison of Poor Responder 0 results obtained using the microring platform (A) and qRT-PCR (B). (C and D) Comparison of Poor Responder 4 results obtained using the microring platform (C) and qRT-PCR (D).

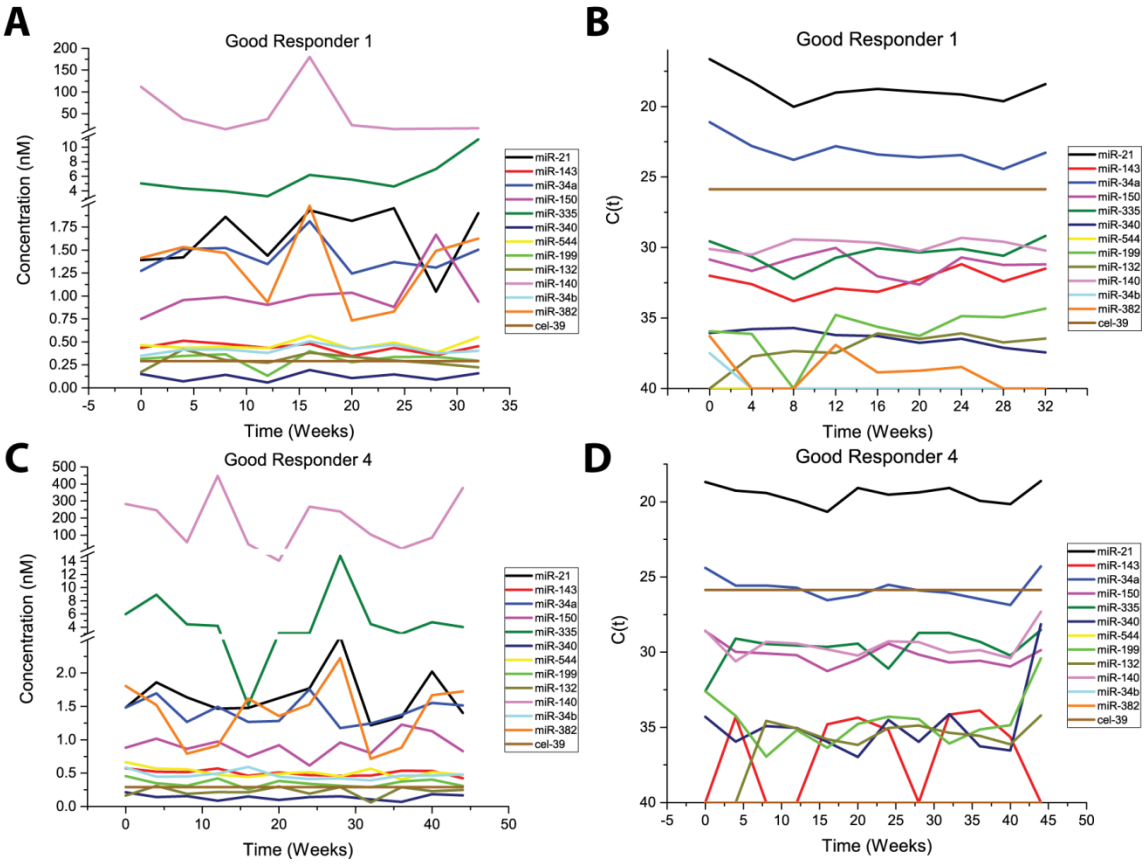

Figure 6.3: (A and B) Comparison of Good Responder 1 results obtained using the microring platform (A) and qRT-PCR (B). (C and D) Comparison of Good Responder 1 results obtained using the microring platform (C) and qRT-PCR (D).

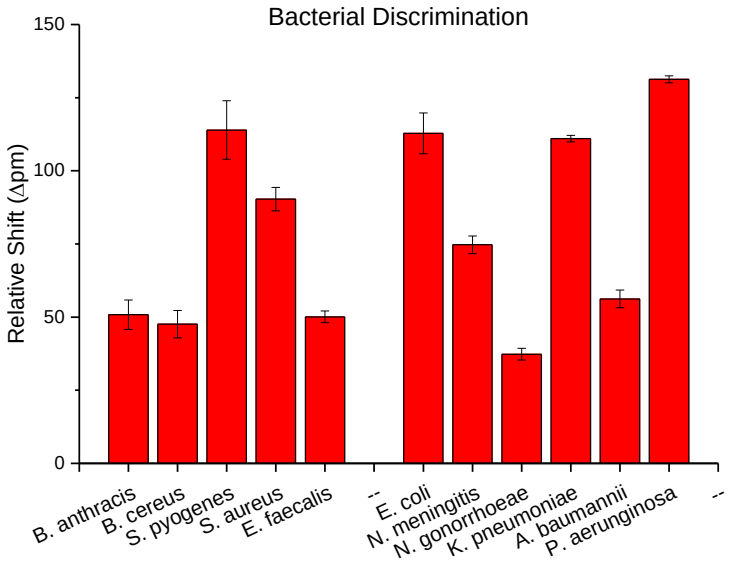

Figure 6.4: Maximum signal achieved when determining specific pathogen types using the aPCR-microring platform. This is an area of future work to be continued.

6.3 References

(1) O'Donoghue, L. E.; Ptitsyn, A. A.; Kamstock, D. A.; Siebert, J.; Thomas, R. S.; Duval, D. L. *BMC Cancer* **2010**, *10*, 506.

(2) Jaffe, N. In *Pediatric and Adolescent Osteosarcoma, Cancer Treatment and Research*, Jaffe, N.; Bielack, S. S.; Bruland, O. S., Eds.; Springer: New York, 2009.

(3) Bacon, N. J.; Ehrhart, N. P.; Dernell, W. S.; Lafferty, M.; Withrow, S. J. *JAVMA* **2008**, *232*.

(4) Karlsson, E. K.; Sigurdsson, S.; Ivansson, E.; Thomas, R.; Elvers, I.; Wright, J.; Howald, C.; Tonomura, N.; Perloski, M.; Swofford, R.; Biagi, T.; Fryc, S.; Anderson, N.; Courtay-Cahen, C.; Youell, L.; Ricketts, S. L.; Mandlebaum, S.; Rivera, P.; von Euler, H.; Kisseberth, W. C.; London, C. A.; Lander, E. S.; Couto, G.; Comstock, K.; Starkey, M. P.; Modiano, J. F.; Breen, M.; Lindblad-Toh, K. *Genome Biology* **2013**, *14*, R132.

(5) Paoloni, M.; Davis, S.; Lana, S.; Withrow, S.; Sangiorgi, L.; Picci, P.; Hewitt, S.; Triche, T.; Meltzer, P.; Khanna, C. *BMC Genomics* **2009**, *10*.

(6) Scott, M. C.; Sarver, A. L.; Gavin, K. J.; Thayanithy, V.; Getzy, D. M.; Newman, R. A.; Cutter, G. R.; Lindblad-Toh, K.; Kisseberth, W. C.; Hunter, L. E.; Subramanian, S.; Breen, M.; Modiano, J. F. *Bone* **2011**, *49*, 356-367.

(7) Nugent, M. *Cancer Management and Research* **2014**, *6*, 15-25.

(8) Ouyang, L.; Liu, P.; Yang, S.; Ye, S.; Xu, W.; Liu, X. *Medical Oncology* **2012**, *30*, 340.

(9) Sarver, A. L.; Thayanithy, V.; Scott, M. C.; Cleton-Jansen, A.-M.; Hogendoorn, P. C. W.; Modiano, J. F.; Subramanian, S. *Orphanet Journal of Rare Diseases* **2013**, *8*, 7.

(10) Gougelet, A.; Pissaloux, D.; Besse, A.; Perez, J.; Duc, A.; Dutour, A.; Blay, J.-Y.; Alberti, L. *International Journal of Cancer* **2011**, *129*, 680-690.

(11) Kumar, A.; Roberts, D.; Wood, K. E.; Light, B.; Parrillo, J. E.; Sharma, S.; Suppes, R.; Feinstein, D.; Zanotti, S.; Taiberg, L.; Gurka, D.; Kumar, A.; Cheang, M. *Critical care medicine* **2006**, *34*, 1589-1596.

(12) Harbarth, S.; Nobre, V.; Pittet, D. *Clinical infectious diseases : an official publication of the Infectious Diseases Society of America* **2007**, *44*, 87-93.

(13) Chung, H. J.; Castro, C. M.; Im, H.; Lee, H.; Weissleder, R. *Nat Nano* **2013**, *8*, 369-375.

(14) Brazas, M. D.; Hancock, R. E. *Drug discovery today* **2005**, *10*, 1245-1252.

(15) Wecke, T.; Mascher, T. *The Journal of antimicrobial chemotherapy* **2011**, *66*, 2689-2704.

(16) Hiramatsu, K.; Ito, T.; Tsubakishita, S.; Sasaki, T.; Takeuchi, F.; Morimoto, Y.; Katayama, Y.; Matsuo, M.; Kuwahara-Arai, K.; Hishinuma, T.; Baba, T. *Infection & Chemotherapy* **2013**, *45*, 117-136.